

Carnegie Mellon University

CARNEGIE INSTITUTE OF TECHNOLOGY

THESIS

SUBMITTED IN PARTIAL FULFILLMENT OF THE REQUIREMENTS

FOR THE DEGREE OF Doctor of Philosophy

TITLE Utilization of As-Is Building Information Models
Obtained from Laser Scan Data for Evaluation of
Earthquake Damaged Reinforced Concrete Buildings

PRESENTED BY Engin Anil

ACCEPTED BY THE DEPARTMENTS OF
Civil and Environmental Engineering

Burcu Akinci February 23, 2015
CO-ADVISOR, MAJOR PROFESSOR DATE

James H. Garrett February 23, 2015
CO-ADVISOR, MAJOR PROFESSOR DATE

David A. Dzombak February 23, 2015
DEPARTMENT HEAD DATE

APPROVED BY THE COLLEGE COUNCIL
Vijayakumar Bhagavatula February 24, 2015
DEAN DATE

Utilization of As-is Building Information Models Obtained from Laser Scan Data for Evaluation of Earthquake Damaged Reinforced Concrete Buildings

Engin Burak Anil

Submitted in Partial Fulfillment of the
Requirement for the Degree of
Doctor of Philosophy

Committee Members

Prof. Burcu Akinci

Prof. James H. Garrett

Prof. Semiha Ergan

Prof. Matteo Pozzi

Prof. Ozgur Kurc

Civil and Environmental Engineering Department
Carnegie Mellon University
Pittsburgh, Pennsylvania, 15213

Monday, February 23 2015

© Copyright by Engin Burak Anil 2015

All Rights Reserved

Abstract

Objective, accurate, and fast assessment of damage to buildings after an earthquake is crucial for timely remediation of material losses and safety of occupants of buildings. Currently, visual inspection of buildings for damage and manual identification of damage severity are the primary evaluation methods. However, visual inspections have a number of shortcomings. In different research studies, visual observations and inspector judgment have been shown to differ amongst different inspectors in terms of thoroughness and reliability of inspection, details included in inspection reports, and results of the damage assessment.

Automatic damage assessment could help in evaluating damaged buildings by reducing the dependency on subjective data collection and evaluation of the damage observations. Laser scanning is a promising tool for field data collection for post-earthquake damage assessment as laser scanners are able to produce accurate and dense 3D measurements of the environment. Laser scan data can be processed to extract damage indicators.

Identifying the damage severity requires the damage indicators be related to the building components in 3D space, as well as the structural configuration of the building, details of the reinforcement, and actual material properties. A Building Information Model (BIM) within which a structural system and damage are represented can serve as the underlying information source for damage assessment and post-earthquake seismic performance evaluation. However, further research is required for utilizing laser scan data and as-is BIMs generated from laser scan data for storing and reasoning about damaged buildings.

In order to address the challenges and needs stated above, (1) the unique characteristics of laser scan data, which can potentially limit the reliability of the scanner data for crack identification under certain scenarios were investigated; (2) the information requirements for representing and reasoning about damage conditions were formalized; (3) a representation schema for damaged conditions was developed; and (4) reasoning mechanisms were studied for identifying the damage modes and severities of components using the identified damage parameters and structural properties.

The research methods involved experiments to identify the characteristics of laser scanners for damage detection, investigation of damage assessment guidelines, and investigation and analysis of Building Information Modeling standards. The results of the investigation on damage assessment standards were used for identifying the information requirements for the representation of damage and for developing the representation schema. Validation studies include: (1) validation of the information requirements by an analysis to quantify the sensitivity of damage assessment to the identified damage parameters; (2) validation of generality of the representation schema to masonry components; (3) validation of the reasoning mechanisms with a user study.

The contributions include: (1) characterization of two laser scanner for detecting earthquake induced cracks; (2) identification of information requirements for visual assessment of earthquake damage on reinforced concrete shear walls; (3) a schema for representing the earthquake damage for supporting the visual assessment; and (4) approach for identifying the damage mode and severity of reinforced concrete walls.

Acknowledgements

I feel fortunate to have had the privilege of being a PhD student and a research assistant at Carnegie Mellon University. The past five years broadened my knowledge and perspective and nurtured my growth both professionally and personally. I would like to express my gratitude to everyone who contributed to the completion of this thesis.

First and foremost, I would like to acknowledge my deepest appreciation to my academic advisors Professor Burcu Akinci, Professor James H. Garrett, Jr, and Professor Ozgur Kurc (Civil Engineering, METU, Turkey).

I would like to express my sincere appreciation to my PhD committee members, Prof. Semiha Ergan (Civil and Environmental Engineering, CMU) and Prof. Matteo Pozzi (Civil and Environmental Engineering, CMU) for their constructive feedback and invaluable suggestions.

I gratefully acknowledge the financial support from the National Science Foundation (NSF) and the General Services Administration (GSA). I am also grateful and proud for receiving the Bertucci Graduate Fellowship that supported my PhD work.

I am thankful to Mosaic research team members, Guzide Atasoy, Xuesong (Pine) Liu, Saurabh Taneja, Te Gao, Asli Akcamete, Matineh Eyb Poosh, Eui Jae Jin, Xue (Sheryl) Yang, Merthan Koc, Bo Gu, Raghuram Sunnam for the helpful criticisms and discussions, as well as their company.

I would also like to thank all of the Civil and Environmental Engineering community, which has become my family, and departmental staff, especially Maxine Leffard who have always been kind and helpful.

to Uzay and Mine

Table of Contents

| | |
|---|-------------|
| Utilization of As-is Building Information Models Obtained from Laser Scan Data for Evaluation of Earthquake Damaged Reinforced Concrete Buildings..... | i |
| Table of Contents | v |
| List of Figures..... | viii |
| List of Tables | xii |
| Chapter 1 Introduction | 1 |
| 1.1. Introduction | 1 |
| 1.2. Problem Statement | 3 |
| 1.3. Research Vision..... | 6 |
| 1.4. Research Questions | 8 |
| 1.5. Research Method | 11 |
| Chapter 2 Experimental Characterization of Performance of Laser Scanners for Post-Earthquake Crack Detection | 15 |
| 2.1. Introduction | 15 |
| 2.2. Research Background | 18 |
| 2.2.1. Crack Properties | 18 |
| 2.2.2. Image-Based Crack Detection..... | 19 |
| 2.2.3. Laser Scanners for Crack Detection | 21 |
| 2.3. Testbed | 24 |
| 2.3.1. Properties of Artificial Cracks on the Hydrostone Blocks | 25 |
| 2.3.2. Scanning Parameters..... | 26 |
| 2.3.3. Automated Detection Algorithm | 29 |
| 2.4. Results..... | 32 |
| 2.4.1. Effects of Sampling Interval on Minimum Detected Crack Width and Measured Crack Depth..... | 32 |
| 2.4.2. Effect of Range on the Minimum Detected Crack Width and Measured Crack Depth | 38 |
| 2.4.3. Effect of Crack Orientation on the Smallest Detected Crack Width | 41 |
| 2.4.4. Effect of Incidence Angle on the Smallest Detected Crack Width | 46 |
| 2.5. Evaluation of the results on a real case..... | 49 |
| 2.6. False Detection | 52 |
| 2.7. Conclusions..... | 54 |
| Chapter 3 Information Requirements for Earthquake Damage Assessment of Reinforced Concrete Walls | 57 |
| 3.1. Introduction | 57 |
| 3.2. Damage Assessment Procedures Based on FEMA 306..... | 58 |
| 3.3. Background Research | 63 |
| 3.3.1. Methods for Identification of Information Requirements..... | 63 |
| 3.3.2. Exhaustive listing | 63 |
| 3.3.3. Affinity Diagramming Method..... | 64 |
| 3.4. Approach | 65 |

| | |
|--|------------|
| 3.5. Results and Discussion | 69 |
| 3.6. Validation..... | 74 |
| 3.7. Conclusions..... | 85 |
| Chapter 4 Representation of Earthquake Damage for Reinforced Concrete Buildings using Building Information Models | 87 |
| 4.1. Introduction | 87 |
| 4.2. Information Requirements of Visual Damage Assessment..... | 88 |
| 4.3. Background research | 89 |
| 4.3.1. Representation of Damaged Conditions | 90 |
| 4.3.2. Building Information Modeling for Damaged Condition Representation | 91 |
| 4.4. Development of the Schema for Representing Damage Information | 92 |
| 4.5. Validation..... | 97 |
| 4.5.1. Coverage of the parameter space for a damaged RC building | 97 |
| 4.5.1.1. Rule-based System for Visual Assessment..... | 98 |
| 4.5.1.2. The Results | 100 |
| 4.5.2. Generality | 101 |
| 4.6. Conclusions..... | 105 |
| Chapter 5 Building Information Modeling Based Earthquake Damage Assessment for Reinforced Concrete Walls..... | 107 |
| 5.1. Introduction | 107 |
| 5.2. FEMA 306, Damage Assessment Procedures | 108 |
| 5.3. Information Requirements of Strength Analysis..... | 110 |
| 5.4. Background Research | 113 |
| 5.4.1. Representation of Structural Information | 113 |
| 5.4.1.1. Structural Analysis Models..... | 113 |
| 5.4.1.2. Building Information Modeling..... | 114 |
| 5.4.2. Transformation Mechanisms | 115 |
| 5.5. Approach | 115 |
| 5.6. Representation of the Components for Damage Assessment..... | 118 |
| 5.6.1. Identification of Piers and Spandrels | 122 |
| 5.6.2. Generation of the Strength Analysis Model | 125 |
| 5.6.3. Determination of the Damage Mode..... | 127 |
| 5.6.4. Generate the Damaged Model..... | 129 |
| 5.6.5. Determination of the Damage Severities | 130 |
| 5.7. Validation Case Study..... | 132 |
| 5.8. Conclusions..... | 140 |
| Chapter 6 Conclusions and Contributions | 142 |
| 6.1. Introduction | 142 |
| 6.2. Summary of Contributions | 144 |
| 6.2.1. Contribution 1: Characterization of two laser scanners for detecting earthquake induced cracks | 144 |
| 6.2.2. Contribution 2: Identification of information requirements for visual assessment earthquake damage on reinforced concrete shear walls | 145 |
| 6.2.3. Contribution 3: A schema for representing the earthquake damage for supporting the visual assessment | 146 |
| 6.2.4. Contribution 4: An approach for identifying the damage mode and severity of reinforced concrete walls | 147 |

| | |
|---|-----|
| 6.2.5. Compare and contrast existing crack detection algorithms on 3D point cloud data | 148 |
| 6.2.6. Test more materials for evaluate the applicability of the results of the experiments | 149 |
| 6.2.7. Applicability of the damage representation schema to other construction types | 149 |
| 6.2.8. Research on developing metrics for quantifying the severity of spalling, crushing, and displacement type of damage | 150 |

List of Figures

| | |
|---|----|
| Figure 1-1 The envisioned process involves three steps. The first step detects damage from laser scan data and optionally from other sources. The second step updates an as-is BIM with the damage information. The last step performs the damage assessment tasks. The output of the overall process is the damage mode and severity of the components..... | 8 |
| Figure 2-1 The blocks have 10 cm (left block) and 5 cm (right block) depth and various crack sizes. The 5 cm block has a moveable piece that allows adjustment of crack size. The blocks are shown in 45° orientations. Six targets were placed on each block. These targets were used to establish a reference coordinate system to be used by the algorithm for crack measurement. | 25 |
| Figure 2-2 Laser scan points are analyzed on a slice of points extracted across the surface of the blocks (highlighted in red) (a). Every point is classified as being a crack point or a surface point by analyzing the spread of the local neighborhoods (b). The transition between crack points and surface points is marked as an edge. | 30 |
| Figure 2-3 Smallest crack widths that were measured for different sampling intervals. 1.25 mm crack is detected using a sampling interval denser than 1.5 mm for the PTOF scanner or 6.3 mm for the AMCW scanner..... | 33 |
| Figure 2-4 Cross section of scan points and detected edges for AMCW and PTOF scanners. AMCW scanner was able to produce points inside the 1.25 mm crack (a), whereas PTOF scanner returned no points that can be classified as crack points at the same location (b). Please note the crack at $x = -.05$ cm. That particular crack is an extra crack, which is an artifact of the block construction, and is not used..... | 35 |
| Figure 2-5 Smallest crack widths that were detected at different crack orientations. The AMCW scanner is able to consistently detect the smallest crack of 1.25 mm regardless of the crack orientation (a). On the other hand, the PTOF scanner is able to detect the 1.25 mm crack only at 0° and 90° orientations using 0.5 mm sampling interval, and at 0° using 3.1 mm sampling interval. | 43 |
| Figure 2-6 Smallest detected crack width as a function of the incidence angle of the laser beam with the surface..... | 47 |
| Figure 2-7 The infill wall has several cracks ranging from less than a millimeter upto several centimeters. Figure presents the intensity image of the scan with 0.5 mm sampling interval at 3.8 m range. The wall is located at the mid bay on the first story of a three-story three-bay reinforced concrete frame. The frame was loaded to failure using a real earthquake record. | 50 |
| Figure 4-1 The final schema is developed by integrating the requirements of each damage parameter..... | 94 |
| Figure 4-2 The assembly of components, which resists the earthquake forces can contain a variety of structural components, such as piers, slabs, columns, beams | |

| | |
|--|-----|
| (a). For the damage assessment, the component assemblies are divided into segments based on their type of contribution into the non-linear mechanism (e.g., coupled pier mechanism). The DamagedElement entity represents these segments with a 2D slice across the main wall axis (b). The DamagedElementRegion entity is placed on the same plane with the DamagedElement and represents the regions on the components. | 97 |
| Figure 4-3 The CrackPattern and CrackPath entities enable representing complex cracking on the components (a). Continuity of cracks across occlusions or cracks, which should be evaluated together (e.g., X-shaped cracks) were represented using the CrackPattern entity. For the visual assessment, the regions, which contain the damages were represented using the DamageElementRegion entity (b)..... | 101 |
| Figure 5-1 FEMA 306 process for determining the damage modes and severities of wall components..... | 109 |
| Figure 5-2 In the damage assessment context, an element entails an assembly of components, which resist lateral forces together. A component entails individual piers and spandrels, which make up an element. (RC1: Strong pier, RC2: Weak pier, RC3: weak spandrel, RC4: strong spandrel) [2]..... | 111 |
| Figure 5-3 In order to determine the damage modes of components, the moment, shear, web crushing, and sliding shear strengths of the components should be calculated. The table shows a breakdown of the capacity equations [2, 4, 5]. The calculations require a large set of information including expected material strengths, component geometries, reinforcement sizes and locations, and forces on the sections..... | 112 |
| Figure 5-4 The proposed approach takes a BIM and damage records as input. Two analyses, a strength analysis and a visual assessment are performed to determine the damage modes and severities of components. | 116 |
| Figure 5-5 A structural wall system can be modeled in a number of ways in a BIM. Components may or may not be divided at floor levels and can contain openings. For a strength analysis of the wall sections, the wall elements should be divided into pier and spandrel components. | 117 |
| Figure 5-6 The engineering analysis is supported through the integration of two models. A damaged model represents the damaged conditions of the components. A strength analysis model supports the calculation of strengths for damage modes. A model entity, which replaces the IfcBuildingElement entity for the easiness of computations in the prototype implementation, integrates the two models for building elements..... | 120 |
| Figure 5-7 The transformation for generating the components for damage assessment first divides the building elements, if they have openings and creates the ModelEntities for each piece. Then, the relationships are established between the connected components in order to form the flanged sections and maintain the connection relationship between the divided components..... | 123 |
| Figure 5-8 The first steps of the assessment procedure are the division of elements into components and determining the connected components. For the wall under consideration (yellow) (a), the connected walls and boundary elements | |

| | |
|--|-----|
| are determined (MEw, highlighted in blue) (c). If a wall has openings, it is divided into piers (MElp, MErp) and spandrels (MEb_0, MEb_1) (c and d). | 124 |
| Figure 5-9 A critical section represents a cross-section through a component and spans the web and flanges of the component. The reinforcing bars and the structural analysis model elements at the section are calculated by finding the intersection of the section and the bars and the elements. | 125 |
| Figure 5-10 Effective flange widths and effective reinforcement within the effective flanges are computed for the compression and tension of the flanges. The effective reinforcing bars for tension (a) and compression (b) are computed separately. The distance of the bars from the center of the main wall determines, whether the bars will be considered for tension or compression. For the wall in the given figure, the critical section is at the bottom of the wall. | 126 |
| Figure 5-11 In the final state, the assembly of components are divided in to piers (blue) and spandrels (red) (if any), the damaged schema is generated and the damage indicators are superimposed on to the divided components. The figure also shows the reinforcing bars and the critical sections (highlighted in blue) on which the capacity analyses will be performed. The green cross-sections are temporarily used for calculating the shear area of the transverse bars. | 130 |
| Figure 5-12 A 3D rendering of the building model. The rendered model was used in the user studies (next section). The IFC model of the building contained the building components. The IFC model was extended using the damage and strength analysis schema for the damage assessment. | 133 |
| Figure 5-13 A snapshot of the prototype. The window on the right is used for guidance through the steps of the procedure. The building is analyzed one wall at a time. The other walls are hidden from view for easy visualization. | 137 |
| Figure 5-14 In total 18 wall elements, which contain 42 piers and spandrels were assessed visually and by performing strength analyses. Six of the elements containing various crack patterns and spalling are shown. Reinforcing bars, which were used for calculating the strengths are also shown. | 138 |
| Figure 6-1 The users were given a virtual environment, where they can walk around a damaged building. The example was adopted from the example application in Chapter 7 of FEMA 307 (1999). | 166 |
| Figure 6-2 The snapshot of the user interaction window. The window first presents the 18 damage parameters without showing the values to the user and asks the user to select exactly three parameters. Upon selection, the values of the parameters are shown and the user is asked to make a decision about the severity of the damage. The user keeps asking for parameters, three at a time, until he/she is satisfied. The parameters, which affected the decision are recorded. | 169 |
| Figure 6-3 Users have been given a sketch of the damages on a solid wall and asked to determine the severities of the potential damage modes. | 172 |
| Figure 6-4 The users have been given the damage sketches on a wall with openings and asked to assess the severities of potential damage modes of the piers and the coupling beams. | 175 |

List of Tables

| | |
|---|----|
| Table 2-1 Crack parameters used in the experiments are crack width, crack orientation, and crack depth. | 26 |
| Table 2-2 Sampling intervals used for the two scanners at 10 m range. The reference sampling intervals are used at other ranges. Values in parenthesis for the AMCW scanner represent the sampling interval in angular units..... | 27 |
| Table 2-3 Experiment parameters were tested one at a time, by changing one by one while keeping the others fixed at the reference values. This way four test cases were obtained. Shaded cells show the fixed parameters in each test case, while unshaded cells show the varied parameter..... | 29 |
| Table 2-4 Mean and standard deviation of crack width measurements of the smallest detected cracks at 10 meters using varying sampling intervals (all units in mm). The orientation of the cracks is set to vertical and incidence angle of the laser beam is fixed to 0°. The mean and standard deviations are calculated for 5 repeated scans using the same configuration. Note that only three sampling intervals are available for the AMCW scanner. | 36 |
| Table 2-5 Mean depth measurements at fixed range, crack orientation, and angle of incidence. Depth measurements show a decreasing trend with increasing sampling interval or decreasing actual crack width..... | 38 |
| Table 2-6 Mean and standard deviation of crack width measurements of the smallest detected cracks using fixed sampling intervals at varying ranges (all measurement units are in millimeters). The orientations of the cracks are fixed to vertical and incidence angle of the laser beam is 0°..... | 40 |
| Table 2-7 Mean depth measurements at fixed crack orientation, sampling intervals, and angle of incidence. Measured depths have a decreasing trend with range. | 41 |
| Table 2-8 Mean and standard deviation of crack width measurements of the smallest detected cracks using fixed sampling intervals at varying crack orientations (all measurement units are in millimeters). The range is fixed to 10 m and incidence angle of the laser beam is 0°. Crack orientation is defined as the angle between the crack and the horizontal axis. With the PTOF scanner two sampling intervals were used: 0.5 mm and 3.1 mm at 10 meters range. With the AMCW scanner only 3.1 mm sampling interval was tested..... | 44 |
| Table 2-9 Mean depth measurements at fixed range, sampling interval, and angle of incidence. Crack orientation has a less of an effect on crack depth measurement compared to range and sampling interval. | 46 |
| Table 2-10 Mean and standard deviation of crack width measurements of the smallest detected cracks using fixed sampling intervals at varying beam incidence angles (all measurement units are in millimeters). The range is fixed to 10 m and the cracks are vertically aligned. Incidence angle is defined as the angle between the laser beam hitting the surface and the normal of the surface. With the PTOF scanner two sampling intervals were used: 0.5 mm and 3.1 mm | |

| | |
|--|----|
| at 10 meters range. With the AMCW scanner only 3.1 mm sampling interval was tested. | 49 |
| Table 2-11 Minimum crack sizes that were recognized on the real wall are larger than the results obtained for the hydrostone blocks..... | 51 |
| Table 3-1 A selected subset of statements about crack types and widths. The statements contain crack types and crack widths. | 68 |
| Table 3-2 Other statements extracted from the guideline about cracking..... | 69 |
| Table 3-3 The affinity diagram for reinforced concrete components. Level 1 contains the individual statements extracted from the FEMA 306 guideline and is hidden for brevity. Cracking and crack properties emerge as the most important feature in the diagram, followed by the location and quantity of the other damage indicators..... | 71 |
| Table 3-4 Cracking is the main damage indicator in masonry, similar to reinforced concrete. The affinity diagram shows other features in addition to size and type of cracks, such as opening of head joints and sliding of bed joints..... | 72 |
| Table 3-5 Affinity diagram for additional modes of infilled frames. Due to the low number of statements, only three levels were considered. | 73 |
| Table 3-6 The damage modes and severities for every damage mode was implemented according to the descriptions in FEMA 306. Table shows the rules as given in FEMA 306 and the corresponding damage parameters for the Insignificant severity of the ductile flexure mode (A). In order to avoid false positives, damage parameters, which do not belong to the insignificant A damage, have been set accordingly. | 76 |
| Table 3-7 Eighteen parameters have been identified based on the affinity diagrams and the damage descriptions, that help determine the damage mode and severity. | 78 |
| Table 3-8 The assessment results for the base configuration of insignificant ductile flexural damage (RC1A). The base configuration is checked against all damage modes and severities. It can be seen that the base configuration also conforms insignificant D and E type of damage. | 79 |
| Table 3-9 Base configurations used in the simulations for ductile flexure (A)..... | 80 |
| Table 3-10 For every variation in the configuration, the change in the results are recorded in a results vector. Zero indicates no change in severity from the base configuration as a result of the variation..... | 81 |
| Table 3-11 Sensitivity of the damage modes to errors in the damage parameters. Higher the number, higher the sensitivity of the damage mode to misclassification of the damage parameter. The analysis shows that maximum vertical crack width has no effect on the classification of the damage and severity. The other parameters have varying degree of impact on the classification..... | 83 |
| Table 3-12 By averaging the change of damage age assessment across all of the damage modes, the mean effect of each damage parameter on the assessment can be obtained..... | 84 |
| Table 4-1 The affinity diagram for reinforced concrete wall components. Statements were extracted from the FEMA 306 guideline and grouped into four levels in increasing generality. Level 1 contains the individual statements and is hidden | |

| | |
|---|-----|
| for brevity. In the diagram, cracking and crack properties emerge as the most important feature in the diagram, followed by the location and quantity of the other damage indicators. | 89 |
| Table 4-2 Seventeen parameters have been identified based on the affinity diagrams and the damage descriptions, that help determine the damage mode and severity. | 99 |
| Table 4-3 The affinity diagram for masonry components show similar patterns at Level 3 and Level 4. In addition to the Level 3 groups in reinforced concrete, masonry requires representing the movement modes. The table also shows the number of statements extracted from the FEMA 306 guideline for masonry damage. | 103 |
| Table 5-1 The strength against the potential damage modes are calculated using strength equations given in standards. | 128 |
| Table 5-2 Seventeen damage parameters define the damage state of a component. | 131 |
| Table 5-3 The case study contained four basic configurations of buildings, which required different approaches to transformation and representation. | 135 |
| Table 5-4 The representation schema and the reasoning mechanisms facilitated analyzing various forms of complex damages. Damages could be analyzed both individually, as in the case of cracks, and also in relation to another (e.g., spalling along cracks). | 139 |
| Table 6-1 Reinforced concrete visual damage assessment affinity diagram. Level 1 presents the statements, which were extracted from the Chapter 5 of the FEMA 306 (1999) guideline. | 151 |
| Table 6-2 Unreinforced masonry visual damage assessment affinity diagram. Level 1 presents the statements, which were extracted from the Chapter 7 of the FEMA 306 (1999) guideline. | 155 |
| Table 6-3 Infilled frame visual damage assessment affinity diagram. Level 1 presents the statements, which were extracted from the Chapter 8 of the FEMA 306 (1999) guideline. | 161 |
| Table 6-4 The table shows the order in which the users asked to see the damage parameters. For example, 1 means that the corresponding parameter was seen first and 0 means that the parameter was never seen before deciding on the damage severity. The last column shows if the user changed his/her decision after seeing a certain parameter. | 170 |

Chapter 1 Introduction

1.1. Introduction

The earthquake regions around the world contain a large stock of reinforced concrete (RC) buildings. For example, only in Los Angeles, CA, there is a stock of estimated 40,000 particularly vulnerable RC buildings, due to old design practices [59, 60]. The total number of buildings, which will need to be assessed following a future earthquake is much higher given that it would be necessary to assess not just vulnerable RC buildings, but all RC buildings and other types of buildings that are impacted from the earthquake. Historical evidence and research studies show that there is a pressing need to assess the damage severities of RC buildings objectively, accurately, and rapidly, and quantify the effects of the earthquake on the structural properties of the components [61, 62].

Current methods for damage assessment are manual and rely heavily on the structural engineering expertise of the inspectors and their engineering judgment [63]. Inspectors are expected to have a good level of understanding and experience in assessing the effects of the ground motion on the seismic performance of components by observing the indications of damage, performing structural computations, and synthesizing the structural properties and construction details of a building [63].

Manual approaches for evaluating structures have been criticized for being error-prone, slow, and subjective [5, 6, 26, 38]. Therefore, several researchers have been studying ways to automate the damage assessment process [8, 9, 11, 27, 31-36, 38, 39, 46, 52, 64-69]. Studies on computer vision techniques show promising advancements for capturing

and identifying damage indicators, such as cracking, spalling, and displacements, using machine vision methods [12, 27, 28, 31, 32, 34-36, 38, 46, 57, 58, 66, 68, 70]. On the other hand, automation of the actual damage assessment procedures using the captured damage indicators is not a well-studied subject. The studies on automating the damage assessment procedures include using augmented reality along with the residual story drift as the damage metric, and using damage indicators (e.g., cracking, spalling) in a fragility analysis to identify the aftershock vulnerability of buildings [39, 64]. However, none of the previous studies address the automation of the engineering analyses for damage assessment, based on the FEMA 306 guideline, which practicing engineers have to follow [1].

This research mainly focuses on the engineering analysis of reinforced concrete structures using the standards FEMA 306 manual for “Evaluation of Earthquake Damaged Concrete and Masonry Wall Buildings: Basic Procedures”. This study focused on FEMA 306 for three reasons. First, it is the standard document, which the engineers have to follow when assessing the performance of damaged buildings in the US [1]. Second, the guideline builds on a thorough investigation of existing body of research and presents a procedure that can be used for a wide variety of damage modes and component types [1]. Finally, it is being adopted by other countries, such as New Zealand, thus reaching wider application [2].

According to FEMA 306, engineering analyses are performed on those earthquake damaged buildings, which are tagged for further analysis after a rapid assessment [1]. The commonality amongst damage assessment standards of different countries, such as United States and Japan, is that the pre-event performance of a given structure is

compared to the damaged performance of the same structure through engineering analyses [1-3]. Thus, accurate quantification of the degrading effects (e.g., reduction in the stiffness, strength, and displacement capacity) of the earthquake on the structural components is critical in all established procedures.

The degrading effects of the earthquake motion on the components are quantified by first determining the damage modes of the components. A damage mode is the type of failure a component sustains under lateral loads. For example, the lateral strength of an RC wall can be such that the flexural strength is reached before reaching all other possible failure modes, such as shear or boundary compression, thus allowing the wall to fail under ductile flexure. Previous research has found seven common damage modes for reinforced concrete wall components (i.e., piers and spandrels), including ductile flexure, preemptive shear, diagonal compression, boundary compression, sliding shear, and pier rocking [1]. Reinforced concrete frames generally exhibit either flexure or shear type of failure. Compared to RC frames, distinguishing between damage modes can be especially challenging for wall components, considering that the damage modes can look alike at low severities and calculations are required to determine the governing mode [1]. This study develops an approach for streamlining the objective and accurate collection of damage data and processing of building information and the damage data for the engineering analysis of damaged reinforced concrete walls.

1.2. Problem Statement

The current practice of data collection and engineering analyses is a largely manual process, which requires extensive engineering judgment and experience to correctly identify the damage modes and severities of components [1-3]. On the other hand,

manual procedures for collecting and analyzing the data have been criticized for being subjective, error-prone, and slow [4-6].

Laser scanners have several potential benefits for collecting data for damage assessment. First, laser scanning technology has been shown to be effective for identifying damage indicators, such as cracks, displacements, deflected shapes, spalling, crushing, and reinforcement damage [7-9]. Second, once point cloud data is collected from multiple view angles and locations inside and outside of a structure, the scans can be registered to generate a 3D representation of a structure [10]. Such a holistic representation of the actual conditions of a building presents opportunities for analyzing damage information at system level from a damage assessment perspective. Third, point cloud data and detected damage can be used to generate Building Information Models (BIM), which represent the actual damaged conditions of buildings to support reasoning for damage assessment [11, 12]. BIMs can be used to perform topological queries to extract required damage and connectivity information for system level reasoning and they can support information, such as reinforcement details for capacity calculations [13, 14]. Fourth, laser scanners are light independent and long range [7]. Light independence is an advantage especially when working in the interiors of damaged buildings, where there may be no power after an earthquake to properly illuminate the scene. Long range makes it easier to reach upper floors and distant objects.

Laser scanners also have limitations and unique challenges for imaging cracks [15]. The phenomenon called mixed pixels results in incorrect measurements [16, 17]. Mixed pixels occur due to the fact that the laser beams have a finite size (generally a couple of millimeters) and captured coordinates of the points are functions of the returned signal

over the entire beam area [17]. Geometric discontinuities, such as when the laser beam partially hits a wall edge and a portion of the beam hits on the wall and the remaining portion of the beam hits a background surface, are prone to mixed pixels [17]. Depending on the distances of the foreground surface (e.g., surface of a component) and the background surface (e.g., inside of the crack), and the scanner technology, the returned range can be erroneous [17]. Mixed pixels also occur when the imaged object is smaller than the beam itself or when the beam partially falls on the object [15]. Additionally, the actual resolutions achieved by laser scanners is also dependent not only on the sampling interval, but also on overlapping of laser beams [18]. All these factors impact whether cracks will be detectable with laser scanners. So far, these effects have not been fully studied from crack detection perspective.

In order to support the engineering analysis of damaged structures, we need accurate information about the existing conditions of the structures, including the configuration, reinforcement details, expected material properties, and structural analysis models, previous damages to structural components, and the current damaged conditions. Building Information Models (BIM) can potentially support representing and reasoning about the damaged conditions of the buildings and the building information, such as the configuration, reinforcement details, and structural analysis models [11, 13, 19-22]. BIMs can be used to support the engineering analyses for the damage assessment tasks, such as those for strength analysis [13, 19]. However, current BIMs are not developed to represent existing conditions of the buildings [11, 12, 23]. Therefore, in order to utilize BIMs in damage assessment, representing the damage information needs to be researched.

Developing a representation for damage assessment requires identifying the information items, which need to be represented.

On the other hand, the current BIMs can support the representation of structural information including component sizes, reinforcement details, and material properties. Since, they are developed for conveying design information to the construction stage, the exact information requirements of the engineering analysis for damage assessment might not be satisfied directly. When a model is used for a purpose other than the original intent transformation may need to occur [24]. For example, in order to compute the strength of components the locations of reinforcing bars in the sections need to be known. In order to utilize the current BIMs for damage assessment, such transformation mechanisms should be formalized.

Utilizing BIMs for determining the damage mode and severity for structural components requires specific reasoning mechanisms for assessing the damage. Current damage assessment methods are formulated to use nodal displacements or accelerations recorded during the earthquake. However, it is possible that the damage will be quantified after the earthquake and a computerized approach could use the damage indicators measured using the laser scanner after the earthquake. Therefore, damage assessment approaches that can process an information model, which contains the damage information and building information should be researched.

1.3. Research Vision

The discussions in the previous sections indicate that it is necessary to: (1) Characterize the performance of laser scanners to detect cracks, (2) Identify the information requirements for representing and processing visual damage information, (3) Develop a

schema for representing earthquake damage and supporting the engineering analysis, (3) Formalize and develop the product model transformation mechanisms to extract the necessary information for the engineering analysis, and (4) Formalize a reasoning mechanism for processing the developed schema to accurately identify the damage modes and severities of building components.

It is envisioned that the automated damage assessment method for the engineering analysis will have three main steps (Figure 1-1). The first step is the detection of the damage from various input sources, such as laser scanned point clouds, photographs, hand sketches of reports. The detection of the damage can be semi- or fully-automated. Hand sketches or verbal descriptions can be interpreted manually. This thesis primarily focused on laser scanned point clouds as the input source for their long range, light independence, and being able to construct 3D representation of the building accurately [7]. The outputs of the damage detection stage are the damage parameters, which are required for updating the BIM and performing a visual assessment per the requirements of FEMA 306.

The model updating stage takes an as-is BIM and the damage parameters and generates a damage model by transforming the existing model and associating the damage information with the model. It was assumed that the as-is BIM contains the accurate reinforcement amounts, locations and details, material properties, and building configuration.

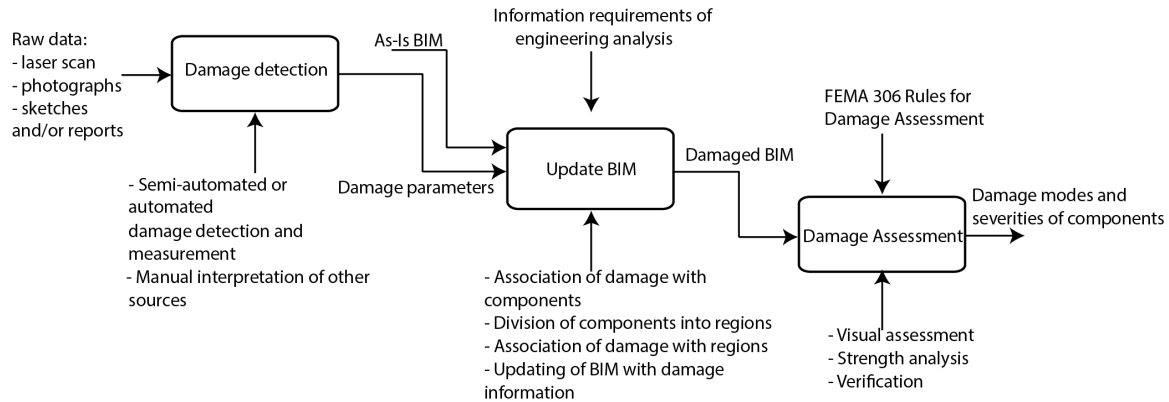


Figure 1-1 The envisioned process involves three steps. The first step detects damage from laser scan data and optionally from other sources. The second step updates an as-is BIM with the damage information. The last step performs the damage assessment tasks. The output of the overall process is the damage mode and severity of the components.

In the damage assessment stage, two analyses are performed. A strength analysis, which calculates the lateral forces to initiate the common damage modes, identifies the governing damage mode. The visual assessment identifies the damage severity for the governing damage mode. The verification involves checking whether the strength and visual assessment agree on the governing mode. If the visual assessment has eliminated the governing damage mode, then the potential sources of discrepancies should be checked and corrected, if necessary. The outputs of the overall process are the damage modes and the damage severities of the reinforced concrete walls.

1.4. Research Questions

In order to automate the engineering analysis tasks, it is necessary to understand the characteristics of the laser scanners for damage detection, formalize the information requirements of the engineering analysis, develop a representation schema for the damage information, and develop reasoning mechanisms to perform the analysis tasks. In order to address these, three research questions were posed:

1. How do the characteristics of 3D terrestrial laser scanners impact the detection of cracks?
2. What representation enables performing the visual assessment tasks for detection of damage modes and severities of reinforced concrete walls?
3. What reasoning mechanisms enable performing the engineering analysis of earthquake damage assessment?

Below is a detailed description of these research questions.

Research Question 1: How do the characteristics of 3D terrestrial laser scanners impact the detection of cracks?

This research question focuses on understanding the limitations of using laser scanners for damage detection tasks. The previous studies on crack detection using laser scanners are limited in the chosen crack parameters, the laser scanner parameters tested, or use non-repeatable manual methods for analyzing the results. In order to fully understand the characteristics of laser scanners for detecting earthquake induced cracks on reinforced concrete components a thorough experimental study was designed and executed. Artificial blocks were cast and scanned using two different laser scanners, which represent the state of the technology.

An algorithm was implemented and parameters were tuned using a variety of scans to obtain the least false positives and high detection rates. The scans were repeated at least five times on the artificial blocks. The scans were analyzed to identify the smallest crack widths, which can be identified at different ranges, resolution, incidence angles, and

crack alignments. Then, for a selected set of parameters the results were compared to the results obtained from a real wall. Chapter 2 describes the research question in detail.

Research Question 2: What representation approach enables performing the visual assessment tasks for detection of damage modes and severities of reinforced concrete walls?

The second research question focuses on the development of a schema for supporting the visual assessment for earthquake damage assessment. Two sub-questions were addressed.

1) What are the information requirements of the visual assessment? 2) What general representation enables the representation of the damage parameters?

The first sub-question focuses on identifying the damage parameters, which need to be represented. This task was performed primarily based on the FEMA 306 guideline. Based on the findings of the first sub-question, a representation schema was developed. Chapter 3 describes the information requirements in detail. Chapter 4 describes the developed representation schema and validates the schema for the coverage of the damage parameter space based on a real case.

Research Question 3: What reasoning mechanisms enable performing the engineering analysis of earthquake damage assessment?

This research question focuses on processing a damaged BIM for performing the visual assessment as well as the strength analysis for determining the damage severities and damage modes of structural components. As discussed in the previous section, the damaged BIM is composed of an as-is BIM updated with the damage information.

Two sub-questions were addressed. 1) What transformation mechanisms are required to extract the necessary information from the damaged BIM to perform the strength analysis? 2) What approach enables performing the visual and strength analyses on a damaged BIM?

The research question was validated by comparing the precision and recall of the results obtained from the automated method and the manual method. Chapter 5 describes the details of the research activities related to this research question.

1.5. Research Method

The research method has three aspects. The first aspect requires understanding the laser scanning technology from a feature detection perspective and developing the knowledge, which is required for designing and executing experiments using laser scanners. The first aspect is independent from the other two aspects. The second aspect involves capturing the qualitative and quantitative knowledge about the damage assessment procedures. This aspect requires processing the traditional structural engineering problem from an information modeling and processing perspective. The third aspect involves applying the knowledge on the damage assessment procedures for developing an approach for representing and reasoning about the damaged structures.

The following tasks were performed:

- Investigate the imaging related background research for detecting thin features, and specifically cracks: a wide range of studies was reviewed in order to understand the imaging and image processing techniques. The literature ranged from computer vision focused studies to civil engineering applications of imaging

techniques and covered both 2D imaging and 3D imaging. Quantitative techniques for modeling imaging device characteristics and experimental studies for characterizing imaging devices were covered.

- Investigate different countries' damage assessment guidelines: various countries' damage codes were studied to understand the commonalities between different applications. The review not only covered the engineering analysis stage, but also covered the rapid assessment procedures and important standards, which the main damage assessment guidelines refer to, in order to develop an in depth understanding of the domain.
- Develop and execute experiments: a series of experiments were designed to characterize the performance of laser scanners for detecting cracks. Two hydrostone blocks were cast to be used in the experiments. In total, the experiments resulted in hundreds of individual scans. The results were analyzed and tabulated using a crack edge detection algorithm.
- Study the FEMA 306 guideline in depth: the FEMA guideline for three aspects. First, in order to conduct the laser scanner characterization experiments, the guideline was studied for the important crack parameters and the ranges of parameter values. Second, the guideline was studied to identify the information items, which are required to develop a representation for visual damage assessment. This step was performed using structured systems design techniques. Finally, the guideline was studied for identifying the requirements of the strength analysis. This aspect also required studying the related design and evaluation

standards and various research reports to capture the requirements of the equations and the thought process of the analyses.

- Investigate the damage assessment automation studies: a wide range of studies was studied, which aim at the automation of the rapid assessment and engineering analysis. This task also ties to the first task of investigating the imaging related literature for detecting damages.
- Investigate BIM development approaches and product model transformation methods: the literature was reviewed for developing representations as well as integrating models. These studies helped develop the representation schema for the damage information. In addition the studies on product model evolution and transformation were reviewed.
- Develop an approach for streamlining the damage assessment procedure and implement a prototype: Based on the findings on damage assessment procedures, information requirements identification, and information modeling practices, an approach was developed, which puts together the visual assessment and strength analysis procedures. A prototype was implemented, which consists of a damage digitization script, damage information processing program, and a damage assessment program. The damage digitization script was used to convert the hand sketches of the damages in the validation case into the representation schema. The damage information processing program was used to manually input some of the damage parameters, which cannot be directly digitized. The damage assessment program performs the damage assessment tasks on a given BIM by walking the user through the steps of the damage assessment process.

The following sections discuss the research questions and tasks in detail. Chapter 2 discusses the experimental study to characterize laser scanners for damage detection. The identification of information requirements will be detailed in Chapter 3. Chapter 4 develops the schema for representing damage information. Chapter 5 builds on the damage representation schema and develops the reasoning mechanisms to perform a complete analysis including strength analysis and visual assessment using a Building Information Model. Chapter 6 summarizes the conclusions and the contributions of this research.

Chapter 2 Experimental Characterization of Performance of Laser Scanners for Post-Earthquake Crack Detection

2.1. Introduction

Earthquake damaged buildings must be inspected to determine the nature and severity of the damage, to assess the safety of the structure, and to design strengthening measures. Currently, accepted practices of damage assessment of reinforced concrete buildings rely mainly on visual observation of damage and manual interpretation of reports and sketches prepared by the inspectors in the field to identify the damage modes (also called the failure modes) of components and damage severities [1]. Typically, buildings are inspected by structural engineers and trained building inspectors, and building inspection requires experience and extensive knowledge about structural behavior [1, 25, 26].

Visual inspection has been criticized for being subjective, error-prone, and slow [27, 28]. Important details can be missed, misinterpreted, or field measurements and calculations can be incorrect [4, 5, 26]. Moreover, visual inspections and reports may not cover all the details required by inspection guidelines. Finally, interpretation of the reports and overall results of the inspection can vary greatly from inspector to inspector [5].

For these reasons, researchers have been studying automation methods using vision sensors for detection and interpretation of various types of structural damage for better coverage, higher detection rates and accuracy [7-9, 27-39]. Another motivation for automating the damage detection is the unavailability of qualified engineers to be employed after disasters [38]. Besides damage detection purposes, vision sensors can also

help in supporting a growing interest in capturing and modeling the existing conditions of facilities accurately to be used in future analysis [10, 23].

Damage often initiates as cracks in reinforced concrete buildings. Other damage indicators appear as the damage progresses. Which of these indicators will occur and their order depend on many factors, such as relative strengths of infill and frame, system and reinforcement configuration, strengths of materials, and loading [1, 40]. All of the damage modes contain cracks, however the other damage indicators do not occur in every case [1]. Cracking is the main quantified damage indicator. Width of the cracks, orientation of cracks, and whether a crack penetrates through the entire depth or is only a surface crack are related properties of cracks for damage detection. For the other damage indicators, inspectors mostly look for whether those indicators exist or not, such as whether there is rebar damage or not. In summary, cracking has been identified as the most important damage indicator; hence, identification of cracks is the main focus of this chapter.

Laser scanners have several potential benefits for such detailed damage assessment tasks. First, laser scanning technology has been shown to be effective for identifying damage indicators, such as cracks, displacements, deflected shapes, spalling, crushing, and reinforcement damage [7-9]. Second, after point cloud data is collected from multiple view angles and locations inside and outside a structure, the scans can be registered to generate a 3D representation of a structure [10]. Such a holistic representation of the actual conditions of a building presents opportunities for analyzing damage information at system level from a damage assessment perspective. Third, point cloud data and detected damage can be used to generate Building Information Models (BIM), which

represent the actual damaged conditions of buildings to support reasoning for damage assessment [11, 12]. BIMs can be used to perform topological queries to extract required damage and connectivity information for system level reasoning and they can support information such as reinforcement details for capacity calculations [13, 14]. Fourth, laser scanners are light independent and long range [7]. Light independence is an advantage especially when working in the interiors of damaged buildings, where there may be no power after an earthquake to properly illuminate the scene. Long range makes it easier to reach upper floors and distant objects.

Laser scanners also have limitations and unique challenges for imaging cracks [15]. The phenomenon called mixed pixels results in incorrect measurements [16, 17]. Mixed pixels occur due to the fact that the laser beams have a finite size (generally a couple of millimeters) and captured coordinates of the points are functions of the returned signal over the entire beam area [17]. Geometric discontinuities, such as when the laser beam partially hits a wall edge and a portion of the beam hits on the wall and the remaining portion of the beam hits a background surface, are prone to mixed pixels [17]. Depending on the distances of the foreground surface (e.g., surface of a component) and the background surface (e.g., inside of the crack), and the scanner technology, the returned range can be erroneous [17]. Mixed pixels also occur when the imaged object is smaller than the beam itself [15]. Additionally, the actual resolutions achieved by laser scanners is also dependent not only on the sampling interval but also on overlapping of laser beams [18]. All these factors impact whether cracks will be detectable with laser scanners. To the best knowledge of the authors, these effects have not been fully studied from crack detection perspective.

This chapter presents the results of an experimental study on the performance of laser scanners for imaging cracks. The main goal of the experiments is to identify widths, orientations, and depths of cracks that can be detected from point cloud data given the scanning parameters. The scan data was also evaluated in terms of loss of continuity of cracks. For these purposes, experiments on artificial cracks were performed to test the interaction of the crack parameters and laser scanner parameters on crack detection. In addition to the experiments on artificial blocks, an actual earthquake damaged wall was scanned and results obtained from the real case were compared to the artificial blocks to evaluate the applicability of obtained results in real cases.

2.2. Research Background

2.2.1. Crack Properties

Ultimately, the overall objective for this study is to determine what damage severities it would be possible to identify from point cloud data, given the configuration of the scanner. In order to test the capability of the scanners, it is necessary to determine the crack parameters that mark the boundaries between different damage severities and those that help in defining different damage modes. For this purpose, FEMA's "Evaluation of earthquake damaged concrete and masonry wall buildings" documents (FEMA 306 and FEMA 307) were studied, which present a comprehensive assessment of behavior of reinforced concrete structures to identify the important crack parameters for damage assessment [1, 25]. The investigation of damage modes defined in FEMA 306 revealed that three properties of cracks are relevant to this study. These are: width of cracks, orientation of cracks, and whether a crack is a surface crack or penetrates through the entire component.

The type of cracks (e.g., shear or flexure) is manifested by the orientation of the cracks with respect to the axis of the component, since concrete cracks in the direction of the principal tension. For example, on a vertical column diagonal cracks indicate shear cracking. Vertical cracks near the edge of a column may indicate lap-splice splitting. For more complex damage modes, different types of cracks may appear together. For example, some flexural cracking may be observed along with extensive shear cracking for a pre-emptive shear failure, but the flexural cracks will generally be narrower than shear cracks [1].

Once the damage mode is identified, damage severity is mainly related to the widths of cracks. In different failure modes, the same crack width can correspond to different damage severities. For example, a shear crack is generally corresponds to a more severe damage level compared to a flexural crack with the same width [1]. Therefore, there is no generic list of crack widths that can apply to all of the damage modes. In this study, we generated a list of crack widths according to FEMA 306 [1].

For damage assessment, changes to the load bearing properties of components are important. Therefore, it is important to know whether a crack is a surface crack (e.g., plaster crack) or penetrates through the core concrete to the other side of the component. Cracks that penetrate into the concrete core are more critical.

2.2.2. Image-Based Crack Detection

Digital imaging has certain advantages as well as challenges and shortcomings as field data collection and damage detection devices. Some of the advantages are that cameras are cheap, light, and high resolutions can be achieved [34]. Imaging and damage

detection using images can be investigated from hardware, operation, and algorithm perspectives [41-46]

Spatial resolution, noise level, color and tone reproduction performances, optical distortions, operational settings of the camera (e.g., aperture size and exposure), and lighting conditions characterize the quality of images for damage detection [43]. Besides internal factors, such as electronics of the camera, operation of the camera by the inspector and external lighting conditions plays an important role on the quality of images [43]. For example, signal-to-noise ratio (SNR) can be affected by the aperture settings and lighting. The noise level affects whether damage will be detectable by automated algorithms [43]. Suboptimal selection of aperture and exposure coupled with bad lighting conditions can lead to poor damage detection rates [43].

Damage detection algorithms, on the other hand, aim at identifying as many cracks as possible, while minimizing false positives with minimal loss of information (e.g., continuity of cracks) from a given image [44, 46]. Crack detection algorithms based on edge detection techniques, wavelet analysis, frequency-domain analysis, segmentation methods, percolation based methods and other computational techniques have been proposed [45, 46]. Using a semi-automated method, crack width measurement accuracies up-to 0.35 mm have been reported [47]. Challenges affecting the crack detection algorithms have been reported as false detection due to surface stains or texture and losing the continuity of cracks due to hardware limitations, operation of the device, and algorithm limitations [44, 48, 49].

For detailed damage assessment of structures, detected damage should be mapped to actual dimensions to reason about the properties of damage indicators, which is an

additional processing step. An alternative approach to processing damage at component level is detecting the components in the images and rectifying dimensions using known component dimensions to locate the damage and compute damage properties [49]. Zhu et al. developed an approach to aid in safety evaluation of buildings immediately after disasters [49]. Detailed performance evaluation requires much more complex reasoning than safety assessment, including reasoning about damage levels on connected components. It is not clear how such approaches developed for component-based assessment can be applied at the system level to evaluate assemblies of components together.

Images can potentially be used in conjunction with laser scan data for damage assessment. For example, images can complement laser-scan data for better visualization or in cases where laser scanners may fail, but images may perform better. This can potentially be realized by registering images with 3D point clouds [50]. While this is a promising approach, the first towards that is to understand under what conditions laser scanners perform better in crack detection and assessment – which is the focus of the research described in this paper.

2.2.3. Laser Scanners for Crack Detection

Several studies have investigated the accuracy and resolution of laser scanners [18, 30, 51, 52]. Previous studies can be grouped into two groups: (1) experimental studies that scan a target object using several scanners and compare the errors of the scanners, and (2) theoretical studies that attempt to develop formal mathematical models to quantify the performance of scanners.

Detecting and measuring the dimensions of thin structures, such as cracks, have been found to be especially challenging due to mixed pixels and high accuracy needs [15, 33, 34]. In a particularly related study, the crack widths measured manually show that crack widths can be overestimated up to four times of the original crack width [33]. The mentioned study highlights, the effects of angle of incidence of the laser beam and crack orientation on the detection of cracks and the accuracy of the width measurements.

The laser scanner accuracy has been shown to degrade as a result of the interaction of the scanner characteristics and environment. This is caused by the mixed response captured by the scanner when a laser beam illuminates two surfaces with different ranges, or two surfaces at the same range, but with different reflectivity [16]. As a result, range errors occur. Such range errors can cause losses around the edges of objects making them seem smaller [17]. For geometric discontinuities, the edge losses can be predicted using the size of the actual beam footprint on the target object and the measurement method used by the scanner [17]. The model assumes that the laser beam will hit two surfaces (i.e, a background and a foreground). However, studies on mixed pixel behavior do not account for cases within which only the mid portion of the laser beam illuminates the background (e.g., interior of the crack), and there is centimeter or millimeter level geometric discontinuity between the surfaces, which exists when scanning cracks. Studies on mixed pixels point to two important crack parameters for crack detection: width and depth of cracks. The width of crack determines the distribution of the laser beam hitting the surface and the interior of the crack for a given range and angle of incidence. The depth determines the amount of geometric discontinuity captured by the scanner.

Application of Modulation Transfer Function (MTF) analysis to laser scanners is one of the quantitative modeling approaches [18, 51]. MTFs of imaging systems can be obtained either experimentally or theoretically by making certain assumptions about the behavior of the system. Lichti and Jamtsho's (2006) model for determining the angular resolution of laser scanners using MTF approach considers laser beam size, sampling interval, and quantization errors and shows the importance of these parameters in characterizing the effective resolution of laser scanners [18]. Being sampled imaging devices, laser scanners have anisotropic character, which means the alignment angle of the feature being scanned (e.g., crack) with the sampling grid formed by the laser spots falling on the surface determines whether the feature will be captured or not [41]. In terms of crack detection, this translates to crack orientation.

It has been reported that range errors can be affected by the reflectivity of surfaces [16]. Although, building materials can come in a variety of colors, textures, and compositions, we did not consider different materials in the experiments for two reasons. First, previous research on range errors due to different materials did not identify significant range errors [53]. Experiments on various material types, including common construction materials, such as concrete and brick, found the range errors to be at the order of individual point standard deviations [53]. The study concluded that the observed errors can be due to accidental incidence angle instead of the effects of target object material [53]. The results of the mentioned study point to the potential insignificance of the effects of surface reflectivity on measurements when construction materials are scanned. Second, large variety of surface colors can be observed in a building. To keep this research focused on

most prominent parameters, studying the effects of different materials for crack detection were left for future research.

In the light of the previous research, this chapter focuses on three important scanners parameters: Sampling interval, angle of incidence, and range. Additionally, crack width, depth, and orientation are other important parameters as discussed in Section 2.1. In order to evaluate all of the affecting parameters of laser scanners and the interaction of the crack properties with the laser scanner measurements, a new experimental setup was designed. The details of the testbed and the algorithm used for measuring cracks are introduced in the following section.

2.3. Testbed

A testbed was developed in order to objectively and consistently evaluate the capabilities of laser scanners for detecting thin cracks. The testbed consists of two hydrostone blocks onto which slots representing cracks were opened using a water jet. Two laser scanners representative of the current laser scanner technologies were used. The first one is a pulsed time-of-flight (PTOF) scanner [54]. The second one is an amplitude modulated waveform (AMCW) scanner [55]. Two hydrostone blocks were prepared to represent three important parameters of cracks, as discussed in Section 2.1: crack width, orientation, and depth (Figure 2-1). The values of the crack parameters were determined based on FEMA 306, since it presents an assessment of behavior modes of building components under earthquake loads [1].

Based on prior work discussed in Section 2.2, we identified the important scanning parameters as: sampling interval, range, and angle of incidence. Beam size was implicitly considered, since beam size is a function of range. The values of the scanning parameters

were identified according to prior work [16, 18, 41]. The values of crack and scanning parameters and the experimental setup will be discussed in the following sub-sections.

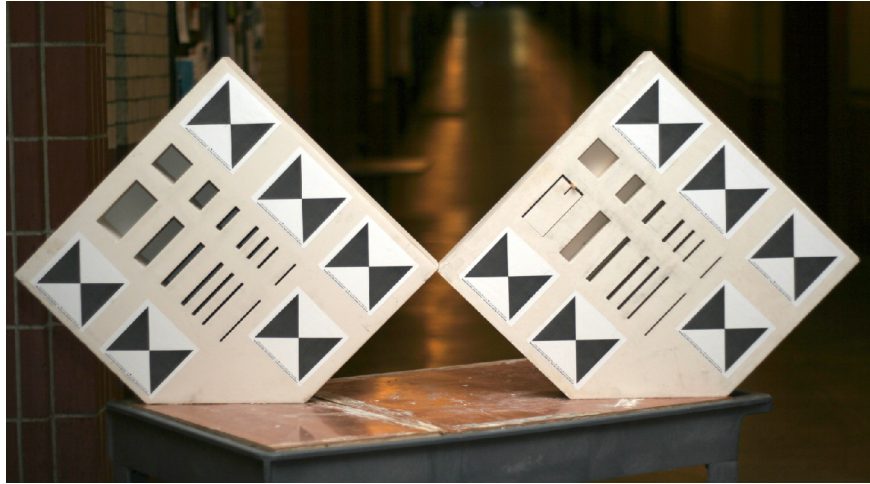


Figure 2-1 The blocks have 10 cm (left block) and 5 cm (right block) depth and various crack sizes. The 5 cm block has a moveable piece that allows adjustment of crack size. The blocks are shown in 45° orientations. Six targets were placed on each block. These targets were used to establish a reference coordinate system to be used by the algorithm for crack measurement.

2.3.1. Properties of Artificial Cracks on the Hydrostone Blocks

Hydrostone blocks were cut using a waterjet to open slots, which represent cracks. One corner of each block was cut at 45° angle so that the cracks can be oriented diagonally. Six laser scanner targets were placed on each block. The targets were used for registration and setting local coordinate systems during edge detection. After opening the slots using a waterjet, the actual crack sizes were measured with a digital caliper to determine the ground truth.

The set crack widths were determined based on FEMA 306 [1] (Table 2-1). Due to the limitations of the waterjet in adjusting the width of the slots, the actual crack widths came up to be slightly different than the planned crack widths. For a typical concrete member, the concrete cover is generally around 3-5 cm. Adding the thickness of the reinforcement,

the depth to which a crack needs to penetrate to reach the concrete core becomes larger than 5 cm. Therefore, 5 cm was selected as the limiting crack depth in this experiment. In addition, 10 cm was used as a second crack depth, to identify the performance of laser scanners for deeper cracks. Block 1 has a depth of 10 cm, whereas block 2 has a depth of 5 cm.

Table 2-1 Crack parameters used in the experiments are crack width, crack orientation, and crack depth.

| Parameter | Block 1 | Block 2 |
|----------------------|--|--|
| Planned crack widths | 0.8, 1.6, 3.2, 4.8, 6.4, 9.5, 25, 50 mm | |
| Actual widths | 3.50, 4.60, 6.40, 10.80, 27.00, 52.50 mm | 1.25, 3.50, 4.60, 6.40, 10.80, 27.00, 52.50 mm |
| Crack orientation | 0°, 45°, 90° | |
| Planned crack depth | 10 cm | 5 cm |
| Actual crack depth | 10.5 cm | 5.8 cm |

2.3.2. Scanning Parameters

The main parameters that control the resolution of laser scanners are sampling interval, which is the distance between laser beams when they hit a surface, and beam width [18]. Unlike sampling interval, beam width typically cannot be controlled by the user and is a function of range, beam divergence angle, and angle of incidence of the laser beam with the object surface [17, 33]. Therefore, range, angle of incidence, and sampling interval were selected as variables. The effects of beam width were implicitly considered through range and angle of incidence.

Sampling interval values were selected to represent the values used in practice and also theoretical studies performed for characterizing the resolution of laser scanners. An approach applicable to discrete sampling of data suggests that the best resolution can be achieved if a sampling interval smaller than half the minimum crack size is used [18]. This sampling interval corresponds to the Nyquist frequency. Applying the Modulation Transfer Function (MTF) analysis concept, it was theoretically shown that best angular resolution can be achieved by setting the sampling interval equal to 86% of the beam

width [18]. Both of these approaches were incorporated into the design of the experiment (Table 2-2).

In order to set a sampling interval that agrees with the Nyquist theorem, 0.5 mm was used as the smallest sampling interval. The second sampling interval was selected as 86% of the beam width. Third, a sampling interval that is twice the beam width was selected as the high value to constitute an upper bound. Finally, an intermediate value between the smallest value (0.5 mm) and the 86% value was selected. Because the beam width varies with range, these values were calculated for the selected range values. One of the limitations was that the waveform scanner neither has the capability of adjusting sampling interval in millimeters nor the sampling interval can be set as small as 0.5 mm [55]. Therefore, the waveform scanner was evaluated using the three pre-defined settings of the scanner, which are 0.0018°, 0.0036°, and 0.0072° (Table 2-2). At 10 meters, these angular sampling intervals correspond to 3.1 mm, 6.3 mm, and 12.6 mm, respectively. Additional configurations were used with the time of flight scanner to match those of the waveform scanner for comparison.

Table 2-2 Sampling intervals used for the two scanners at 10 m range. The reference sampling intervals are used at other ranges. Values in parenthesis for the AMCW scanner represent the sampling interval in angular units.

| Scanner | Sampling intervals (mm) | | | | | | | |
|---------|-------------------------|-----|------------------|-----|------------------|----|-------------------|----|
| PTOF | 0.5 | 1.5 | 3.1 | 4.3 | 6.3 | 10 | 12.6 | 15 |
| AMCW | - | - | 3.1 (0.0018°) | - | 6.3 (0.0036°) | - | 12.6 (0.0072°) | - |

Angle of incidence is defined as the angle between a laser beam and the normal of a surface. The size of the laser spot on the surface increases with the incidence angle. Besides affecting the beam size and the mixed pixels, incidence angle also causes self-occlusion of the cracks. One edge of the crack occludes the interior of the crack. When

the visible depth of the crack from the scanner position is close to the noise in the data caused by mixed pixels and measurement noise, the crack disappears in the data. Therefore, it is not possible to distinguish whether a crack is visible or not because of the self-occlusion of the crack due to high incidence angle or mixed pixel effects. For the experiments we limited the incidence angle to 60° , which allows observation of all of the cracks. In addition to 0° and 60° , 30° was considered as an intermediate value.

It is not feasible to evaluate all of the combinations of the experiment parameters. The combination of all of the parameter sets yields an exponentially large number of test cases. Instead of testing for all possible combination, a single parameter was tested at a time (Table 2-3). A set of reference values, which would yield the best detection results were determined. Using the reference values, we aimed at obtaining an upper bound of the test parameters. Hence, when the values are changed, the detection rates were expected to go down and the minimum detected crack width was expected to increase. One of the parameters was changed while others were kept fixed at reference values. The same procedure was repeated for all of the parameters. In total four test cases were obtained (Table 2-3). Each case was repeated five times and averaged values are used in the presentation and interpretation of the results.

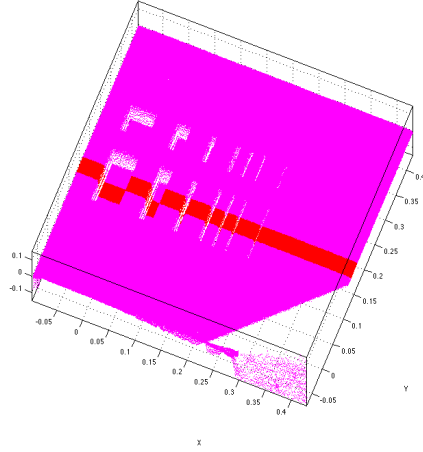
Table 2-3 Experiment parameters were tested one at a time, by changing one by one while keeping the others fixed at the reference values. This way four test cases were obtained. Shaded cells show the fixed parameters in each test case, while unshaded cells show the varied parameter.

| Parameter | Reference Value | Case 1 | Case 2 | Case 3 | Case 4 |
|--------------------|---------------------------------|---|---------------------------------|---------------------------------|---------------------------------|
| Sampling interval | 0.5 mm (PTOF) 0.0018° (AMCW) | 0.5, 1.5, 3.1, 4.3, 5, 6.3, 10, 12.6, 15mm (PTOF) 0.0018°, 0.0036°, 0.0072° (AMCW) | 0.5 mm (PTOF) 0.0018° (AMCW) | 0.5 mm (PTOF) 0.0018° (AMCW) | 0.5 mm (PTOF) 0.0018° (AMCW) |
| Range | 10 m | 10 m | 10, 20, 30, 40 m | 10 m | 10 m |
| Crack orientation | Vertical (90°) | 90° | 90° | 90°, 45°, 0° | 90° |
| Angle of incidence | 0° | 0° | 0° | 0° | 0°, 30°, 60° |

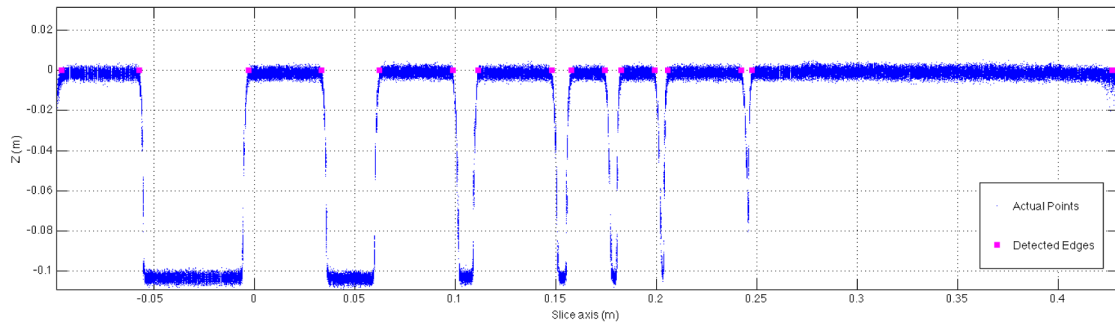
2.3.3. Automated Detection Algorithm

In order to analyze the data objectively, we need a consistent method for detecting cracks. A manual approach is not useful in this case for two reasons. First, manual measurement involves subjective selection of edge points and is not reliable [17]. Second, the manual method cannot produce consistent results, since it is not possible to select the same point across different scans. Therefore, an automated approach is adopted. The automated approach is based on the voting method of Tang et al. (2009) and introduces improvements over the method [17]. The main steps of the adopted approach are:

- 1- Setup a local coordinate system for every scan using the targets placed on the blocks.
- 2- Extract a 3D slice along the block perpendicular to the dimension being measured (Figure 2-2a).
- 3- Identify edges to determine the width of each crack (Figure 2-2b).
- 4- Extract measurements and store result.



(a)



(b)

Figure 2-2 Laser scan points are analyzed on a slice of points extracted across the surface of the blocks (highlighted in red) (a). Every point is classified as being a crack point or a surface point by analyzing the spread of the local neighborhoods (b). The transition between crack points and surface points is marked as an edge.

The crack measurement step has two sub-steps: crack edge detection and width measurement. The edges are detected by sliding a window of fixed size (i.e., number of points) along the slice. For every window (i.e., local neighborhood), the standard deviations of the distance of points within the window from the block surface are computed. A threshold is used to classify the points as being on the block surface or inside the crack. More precisely, if the number of points that are within 2σ distance to the

surface are less than the number of points that are farther than 2σ within a window, then the window position is marked as a crack. The standard deviation (σ) is computed for every scan on an undamaged section of the block with the assumption that noise is uniform over the surface of the block. Every point on the slice was tagged either as belonging to the surface or a crack (Figure 2-2b). The boundaries between the on-surface points and the points belonging to cracks are marked as the crack edges.

The large variation of sampling intervals used in the experiments prevents using a fixed window size for all scans. For a very dense scan (0.5 mm sampling interval), using a small window size results in too many false positives. The reason is that the spread of the points in a small local neighborhood can be large compared to the average noise level across the surface. On the other hand, a large window size can result in cracks being missed. Therefore, the best detection window size should be identified individually for every scan. Essentially, the window size should minimize the false positives and measurement errors and maximize detection of crack edges. Using trial and error over a variety of data sets from the experiments, it was found that 80% of the number of points per unit area gives good results in terms of false positives and crack identification. The window size is calculated for every scan based on the average point density on the surface for every scan. For example, if the point density is 100 points/cm², then a window size of 80 points was used.

Points are classified by comparing the points' neighborhoods to the plane. If the reference plane does not represent the local neighborhood, points can be misclassified. In actual damaged building components, such as walls, surfaces are almost never perfectly planar. In order to cope with this limitation for analyzing data from an actual structural

component, the algorithm was adapted to 3D. Instead of analyzing the points on a slice, the points are analyzed in actual 3D coordinates. For every point in the cloud, points within a radius R from the selected point were used to compute a local plane. RANSAC, a robust procedure, which estimates model parameters using only the inliers [56], was used to estimate a plane from the points within the radius. Therefore, the off-surface points, such as cracks or gaps between bricks, are treated as outliers in RANSAC and excluded from the plane estimation. The closest K points are used to classify the selected point using the local neighborhood as described in the previous paragraphs. A radius of 10 cm and a neighborhood size of 3 points were used to classify the points in 3D.

2.4. Results

The results of the analyses are presented and discussed in this section. Two kinds of results will be presented for each data set: minimum crack width that can be detected for each scanning parameters, and crack depths measured for each crack width. Independent variables are plotted against the minimum crack widths detected using the automated algorithm. The graphs present the minimum crack widths that were detected using the sliding window algorithm. Every data point in the graphs mean that all of the cracks that are equal to or greater than that data point are visible for the corresponding independent variable (i.e., x-axis value). Average crack depths measured for different crack widths will be presented in tabular form.

2.4.1. Effects of Sampling Interval on Minimum Detected Crack Width and Measured Crack Depth

Effects of sampling interval were tested by fixing the range, crack orientation, and incidence angle at reference values and varying the sampling interval. The smallest crack

widths detected by the algorithm using different sampling intervals are presented in Figure 2-3.

Using the PTOF scanner, the smallest crack (1.25 mm) was detected using 0.4 mm and 1.5 mm sampling intervals at 10 meters. The 1.25 mm crack was missed using the 86% of the beam width as the sampling interval. As the sampling interval increases, the smallest detected crack width increases. With the PTOF scanner, at sampling intervals larger than 6 mm, the detected smallest crack widths are different for 5 cm and 10 cm deep cracks. As the sampling interval increases, the differences between the detected smallest crack on the 5 cm deep block and the 10 cm deep block increase.

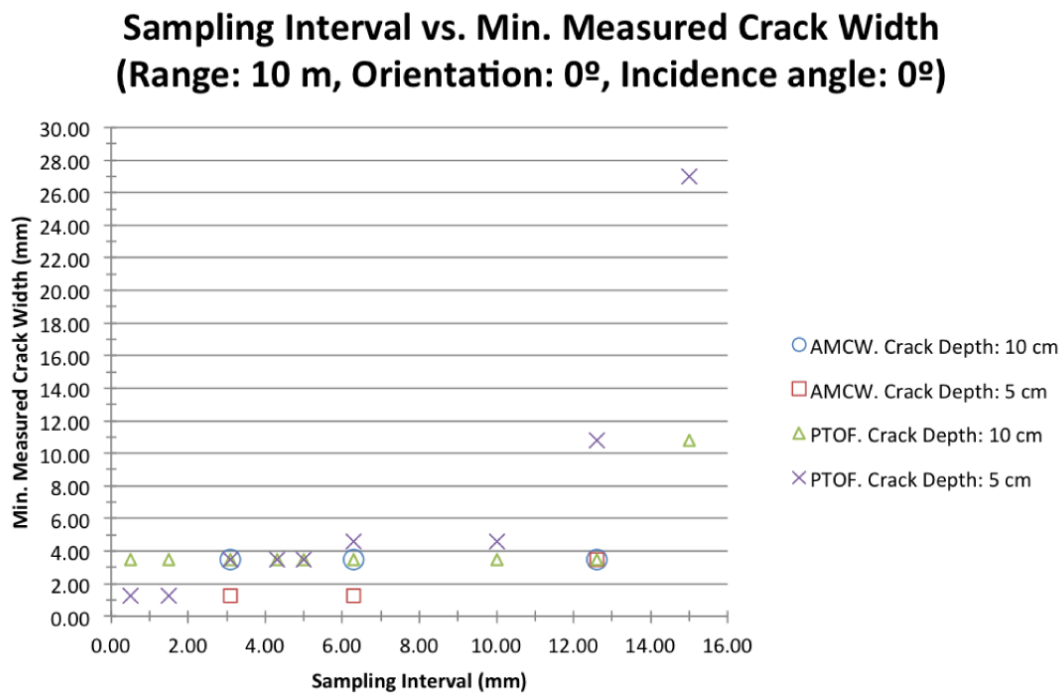
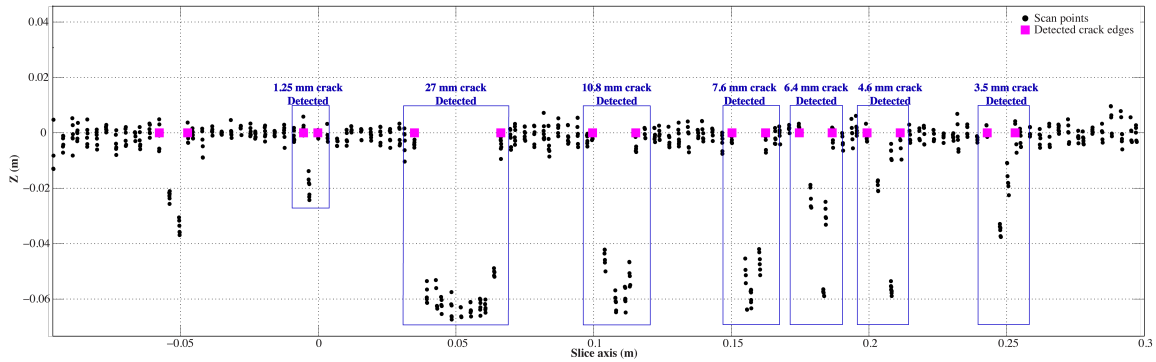


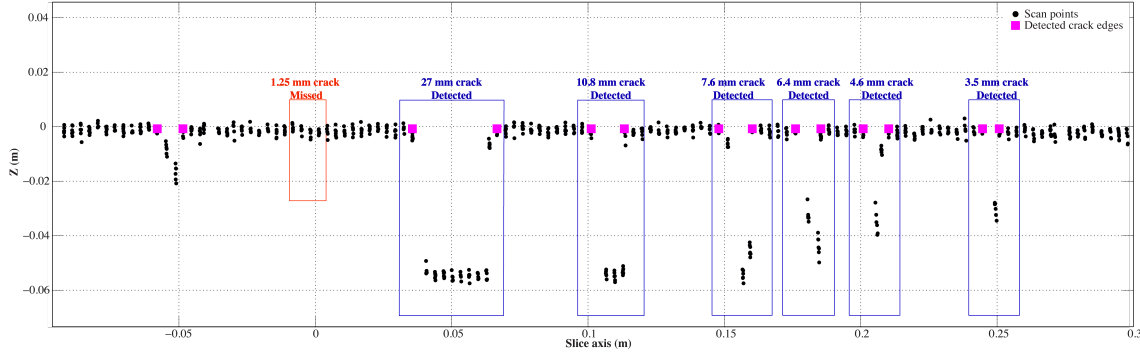
Figure 2-3 Smallest crack widths that were measured for different sampling intervals. 1.25 mm crack is detected using a sampling interval denser than 1.5 mm for the PTOF scanner or 6.3 mm for the AMCW scanner

Although the smallest sampling interval supported by the AMCW scanner (3.4 mm at 10 m range) is larger than the smallest crack width (1.25 mm), it was possible to detect the smallest crack width (Figure 2-4a). Using the same sampling interval, 1.25 mm crack could not be detected with the PTOF scanner (Figure 2-4b). Visual observation confirms that the PTOF scanner returned no points that can be classified as crack points at the same location.

The difference in the results of the two scanners can be explained by their mixed-pixel behaviors. The PTOF scanner records the foreground distance if a proportion of the laser falls on the surface [17]. Since, the laser spot is much larger than the crack width ($\sim 5 \text{ mm} > 1.25 \text{ mm}$), the foreground distance is recorded. On the other hand, the distance recorded by the AMCW scanner can be anywhere depending on the foreground and the background distances. Thus, several points inside the crack are recorded with incorrect depth values ($\sim 2 \text{ cm}$) (Figure 2-4a). Similar difference in behavior of the two scanners is observed at 6.4 mm sampling interval (Figure 2-3).



(a)



(b)

Figure 2-4 Cross section of scan points and detected edges for AMCW and PTOF scanners. AMCW scanner was able to produce points inside the 1.25 mm crack (a), whereas PTOF scanner returned no points that can be classified as crack points at the same location (b). Please note the crack at $x = -0.05$ cm. That particular crack is an extra crack, which is an artifact of the block construction, and is not used.

Measurement results show that the crack measurement results are always larger than the actual values (Table 2-4). This is caused by the edge losses as a result of the mixed pixel effect. The measured crack widths are often two to three times the actual crack widths.

At 10 meters range, the beam width of both scanners is approximately 5 millimeters. Therefore, at sampling intervals greater than 5 millimeters, consecutive laser beams do not overlap and only the sampling interval defines the resolution [18]. The effect of such phenomena can be observed at sampling intervals larger than 5 millimeters. Especially after 6.30 millimeters although the actual crack widths are different (e.g., 3.50 mm and 10.80 mm for 10 cm and 5 cm deep samples respectively using the PTOF scanner with 12.60 mm sampling interval) the measured widths are equal (i.e., 25.70 mm). The measured values are approximately twice the sampling interval, which means that one laser beam hits the interior of the crack and the two points on either side of the crack are detected as crack edges. The only exception is the 27 mm crack on the 5 cm deep sample, which was detected using 15.00 mm sampling interval. Since 27.00 mm is larger than the

twice of the sampling interval minus the laser beam width, there is a possibility that the edge losses due to the finite beam size and sampling increase the measured value. This suggests that for sampling intervals larger than the beam width, cracks that are smaller than twice the sampling interval minus the beam width may not be distinguished. However, further research using a finer sets of beam widths and sampling intervals are required to verify the claim. Also, note that the depths of the cracks do not play a role on the measured widths when large sampling intervals are used, and hence measured values are equal to each other for the two blocks. The reason is that the distance between laser spots rather than the edges formed by surface points and crack points controls the measured width using large sampling intervals.

Table 2-4 Mean and standard deviation of crack width measurements of the smallest detected cracks at 10 meters using varying sampling intervals (all units in mm). The orientation of the cracks is set to vertical and incidence angle of the laser beam is fixed to 0°. The mean and standard deviations are calculated for 5 repeated scans using the same configuration. Note that only three sampling intervals are available for the AMCW scanner.

| Sampling Interval (mm) | PTOF Scanner | | | | | | AMCW Scanner | | | | | |
|------------------------|-------------------|-------|----------|--------------|-------|----------|-------------------|-------|----------|-------------|-------|----------|
| | Fixed range (10m) | | | | | | Fixed range (10m) | | | | | |
| | Block 1 | | | Block 2 | | | Block 1 | | | Block 2 | | |
| | Actual | Mean | σ | Actual | Mean | σ | Actual | Mean | σ | Actual | Mean | σ |
| 0.50 | 3.50 | 5.15 | 0.07 | 1.25 | 3.26 | 0.71 | | | | | | |
| 1.50 | 3.50 | 5.94 | 0.05 | 1.25 | 3.50 | 0.69 | | | | | | |
| 3.10 | 3.50 | 9.37 | 0.04 | 3.50 | 6.00 | 0.12 | 3.50 | 7.79 | 1.48 | 1.25 | 5.47 | 1.44 |
| 4.30 | 3.50 | 8.41 | 0.03 | 3.50 | 8.60 | 0.08 | | | | | | |
| 5.00 | 3.50 | 9.94 | 0.06 | 3.50 | 10.02 | 0.08 | | | | | | |
| 6.30 | 3.50 | 11.51 | 0.03 | 4.60 | 12.59 | 0.12 | 3.50 | 12.13 | 0.14 | 1.25 | 12.01 | 0.04 |
| 10.00 | 3.50 | 20.00 | 0.03 | 4.60 | 19.72 | 0.05 | | | | | | |
| 12.60 | 3.50 | 25.27 | 0.06 | 10.80 | 25.27 | 0.13 | 3.50 | 25.02 | 1.00 | 3.50 | 25.07 | 0.96 |
| 15.00 | 10.80 | 30.43 | 0.07 | 27.00 | 45.48 | 0.26 | | | | | | |

For the measured depths of cracks a prominent trend can be observed, such that the measured depth decreases as the actual crack width gets smaller or the sampling interval gets larger (Table 2-5). Especially for cracks, which are narrower than the laser beam significant depth loss occurs. For the most extreme cases, the captured depth is less than 10% of the actual crack depth. For example, 3.5 mm wide crack on block 2 appears to be

7.6 mm deep on average when scanned with the PTOF scanner using a sampling interval of 5 mm, whereas the actual depth is 108 mm. It can be observed that as the crack width gets smaller the depth loss increases. This is because the percentage of the laser beam hitting the surface increases with the crack getting smaller. As a result the influence of the surface on each returned signal increases. Therefore, the resulting points get closer to the surface, rather than being deep inside the crack.

The second observation is that the depth loss also increases with the sampling interval, when all of the other parameters are kept constant. For example, using 0.5 mm sampling interval with the PTOF scanner, the 3.5 mm crack on Block 1 appears to be 52 mm deep on average, whereas the same crack appears to be 10 mm deep when scanned using 12.6 mm sampling interval. The same trend can also be observed for the AMCW scanner. However, the depth losses are much smaller for the AMCW scanner. For the same 3.5 mm crack on block 1, using a sampling interval of 3.1 mm, the AMCW scanner records an average depth of 82.7mm, whereas the PTOF scanner records a depth of 32.1 mm. This might be explained through different mixed pixel responses of the two scanners and using Tang et al.'s mixed pixel model [17]. Tang et al.'s model shows that edge losses increase with higher sampling intervals, because the recorded location of the edges depend on the sampling interval and the mixed pixel behavior. The AMCW scanner and the PTOF scanner record different edge locations for the same conditions, as also shown in Table 2-4. The AMCW scanner records wider cracks as result of its signal mixing property. It was shown in the previous paragraphs of this section, the capturing of depth for thin cracks, is only possible, when there are mixed pixels. Therefore, the captured

depth of cracks becomes a function of the sampling interval and the mixed pixel property of the scanner.

Table 2-5 Mean depth measurements at fixed range, crack orientation, and angle of incidence. Depth measurements show a decreasing trend with increasing sampling interval or decreasing actual crack width.

| | Sampling interval (in mm) | Crack widths (in mm) | | | | | | | |
|--------------|---------------------------|----------------------|-------|-------|-------|-------|------|------|------|
| | | 52.5 | 27 | 10.8 | 7.6 | 6.4 | 4.6 | 3.5 | 1.25 |
| PTOF Scanner | Block 1 | | | | | | | | |
| | 0.5 | 108.5 | 108.4 | 107.3 | 106.5 | 105.3 | 99.1 | 52.0 | |
| | 1.5 | 107.7 | 107.6 | 106.3 | 105.5 | 104.5 | 96.3 | 48.3 | |
| | 3.1 | 106.1 | 106.7 | 104.4 | 103.7 | 99.9 | 35.4 | 32.1 | |
| | 4.3 | 106.9 | 106.2 | 104.1 | 103.1 | 96.2 | 89.9 | 26.7 | |
| | 5.0 | 105.4 | 106.2 | 105.3 | 104.7 | 104.0 | 93.5 | 30.1 | |
| | 6.3 | 104.7 | 105.3 | 102.3 | 104.4 | 98.1 | 97.6 | 17.9 | |
| | 10.0 | 105.7 | 104.2 | 103.3 | 100.9 | 27.6 | 33.7 | 12.0 | |
| | 12.6 | 104.0 | 103.3 | 103.2 | 39.8 | 29.0 | 19.8 | 10.0 | |
| | 15.0 | 104.4 | 104.1 | 49.2 | | | | | |
| | Block 2 | | | | | | | | |
| | 0.5 | 59.8 | 59.5 | 58.9 | 58.2 | 58.9 | 54.1 | 41.8 | 12.9 |
| | 1.5 | 58.4 | 57.9 | 58.3 | 57.3 | 56.3 | 50.3 | 40.5 | 11.6 |
| | 3.1 | 57.4 | 56.7 | 56.1 | 55.9 | 46.3 | 38.7 | 33.8 | |
| | 4.3 | 58.2 | 57.4 | 56.5 | 57.2 | 56.2 | 24.9 | 8.2 | |
| | 5.0 | 57.2 | 56.5 | 55.9 | 55.2 | 51.6 | 51.8 | 7.6 | |
| | 6.3 | 56.1 | 56.3 | 55.3 | 56.8 | 55.7 | 30.9 | | |
| | 10.0 | 55.8 | 56.0 | 32.5 | 54.2 | 12.3 | 36.1 | | |
| | 12.6 | 54.9 | 55.7 | 52.6 | | | | | |
| | 15.0 | 47.3 | 45.7 | 11.9 | | | | | |
| AMCW Scanner | Block 1 | | | | | | | | |
| | 3.1 | 116.0 | 117.0 | 108.8 | 107.4 | 104.8 | 95.6 | 82.7 | |
| | 6.3 | 115.7 | 113.4 | 108.1 | 101.8 | 42.7 | 84.1 | 91.7 | |
| | 12.6 | 110.6 | 110.5 | 91.5 | 66.1 | 72.9 | 97.8 | | |
| | Block 2 | | | | | | | | |
| | 3.1 | 69.8 | 68.0 | 64.3 | 61.8 | 61.4 | 59.5 | 38.5 | 23.7 |
| | 6.3 | 67.1 | 66.1 | 62.9 | 56.1 | 43.4 | 27.7 | 28.1 | 21.5 |
| | 12.6 | 70.9 | 64.6 | 44.0 | 36.2 | 61.0 | 53.7 | 26.9 | |

2.4.2. Effect of Range on the Minimum Detected Crack Width and Measured Crack Depth

The second set of results present the relationship between the minimum crack widths that were detected by the algorithm for different range values (Table 2-6). The angle of incidence, and crack orientation are fixed at reference values. Sampling intervals for the AMCW scanner can only be set to angular values, which results in different sampling

intervals in millimeters at different ranges. Therefore, two scanners are evaluated separately. A fixed sampling interval of 0.5 millimeters at all ranges is used with the PTOF scanner. The AMCW scanner was set to 0.018° sampling interval which produces 3.1, 6.3, 9, 4, and 12.6 millimeters sampling intervals at 10, 20, 30, and 40 meters respectively.

All of the cracks were detected regardless of the range using the PTOF scanner. Thus, it can be concluded that range is unimportant in terms of detection as long as the sampling intervals are set at the reference values used in these experiments, which produced best results for the PTOF scanners under investigation. On the other hand, using the AMCW scanner, 1.25 mm width crack is detected up to 20 meters. At 30 meters, the smallest detected crack width is 3.5 millimeters. At 40 meters, 4.6 millimeter cracks are detected. The range noise was measured to be between 2.72-9.53 millimeters for the AMCW scanner for the ranges tested, which shows an increasing trend with range. As noise increases and the measured depth of cracks decrease, noisy points and crack points becomes indistinguishable, and hence the algorithm fails in detecting these thin cracks.

The measurements seemingly remain more stable for the PTOF scanner (i.e., within ~5-~7 millimeters for 3.50 millimeter actual crack width) (Table 2-6). However, with the AMCW scanner, the measured values increase as the range increases. The doubling of the measured values can be attributed to the fact that the sampling interval is fixed in terms of angular resolution. Therefore, the distance between the points increases as a function of the range. For example, the sampling interval is approximately 3.1 mm at 10 m, whereas at 20 meters, the sampling interval increases to 6.3 mm. The range noise of the PTOF scanner was measured to be between 1.43-1.54 millimeters at 10m - 40 m

range on the tested surface, which explains the better performance of PTOF scanner at higher ranges compared to the AMCW scanner.

Table 2-6 Mean and standard deviation of crack width measurements of the smallest detected cracks using fixed sampling intervals at varying ranges (all measurement units are in millimeters). The orientations of the cracks are fixed to vertical and incidence angle of the laser beam is 0°.

| Range (m) | PTOF Scanner | | | | | | AMCW Scanner | | | | | |
|-----------|---------------------------------|------|----------|---------|------|----------|--|-------|----------|---------|-------|----------|
| | Fixed sampling interval (0.5mm) | | | | | | Varying sampling interval by range (0.0018°) | | | | | |
| | Block 1 | | | Block 2 | | | Block 1 | | | Block 2 | | |
| | Actual | Mean | σ | Actual | Mean | σ | Actual | Mean | σ | Actual | Mean | σ |
| 10.00 | 3.50 | 5.15 | 0.07 | 1.25 | 3.26 | 0.71 | 3.50 | 7.79 | 1.48 | 1.25 | 5.47 | 1.44 |
| 20.00 | 3.50 | 7.32 | 0.39 | 1.25 | 4.00 | 0.38 | 3.50 | 13.88 | 0.12 | 1.25 | 9.72 | 1.51 |
| 30.00 | 3.50 | 5.29 | 0.37 | 1.25 | 5.19 | 0.29 | 3.50 | 29.29 | 4.69 | 3.50 | 24.96 | 5.99 |
| 40.00 | 3.50 | 6.33 | 0.23 | 1.25 | 3.64 | 0.20 | 4.60 | 20.29 | 0.10 | 4.60 | 27.64 | 0.15 |

The measured depth values show a decreasing trend especially for cracks, which are thinner than the beam width. For the PTOF scanner, this can be related to the increasing laser spot size with range, which is a function of the angular speed of the laser beam. As the spot gets larger, more of the laser spots hit the surface returning more response from the surface, rather than the inside of the cracks. Therefore, the measured depth decreases.

Table 2-7 Mean depth measurements at fixed crack orientation, sampling intervals, and angle of incidence. Measured depths have a decreasing trend with range.

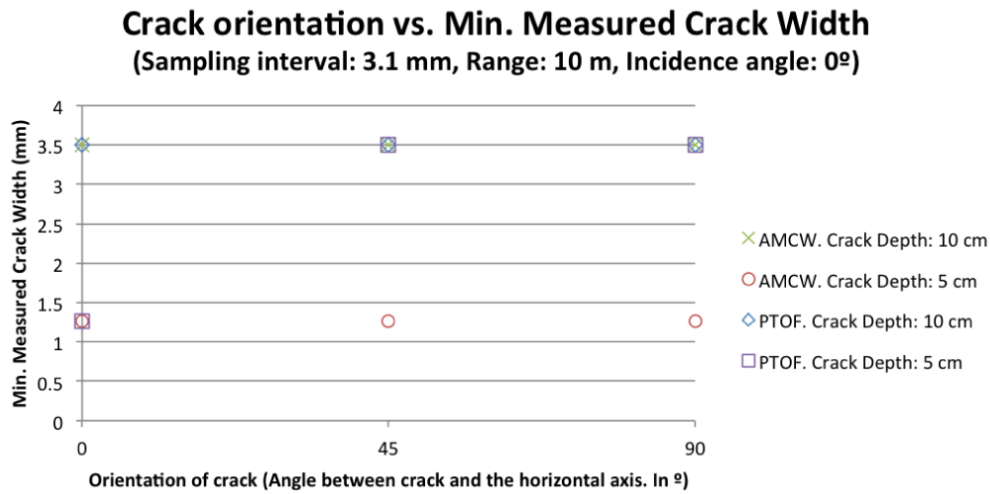
| | Range (in m) | Crack widths (in mm) | | | | | | | |
|--------------|-----------------|----------------------|-------|-------|-------|-------|------|------|------|
| | | 52.5 | 27 | 10.8 | 7.6 | 6.4 | 4.6 | 3.5 | 1.25 |
| PTOF Scanner | Block 1 | | | | | | | | |
| | 10 | 108.5 | 108.4 | 107.3 | 106.5 | 105.3 | 99.1 | 52.0 | |
| | 20 | 107.9 | 108.4 | 107.7 | 107.6 | 83.8 | 96.3 | 26.7 | |
| | 30 | 108.2 | 108.4 | 107.8 | 106.3 | 63.7 | 89.9 | 48.3 | |
| | 40 | 107.9 | 108.0 | 106.6 | 105.3 | 60.8 | 93.5 | 30.1 | |
| | Block 2 | | | | | | | | |
| | 10 | 59.8 | 59.5 | 58.9 | 58.2 | 58.9 | 54.1 | 41.8 | 12.9 |
| | 20 | 59.9 | 59.6 | 59.9 | 59.3 | 58.8 | 57.8 | 49.4 | 16.1 |
| AMCW Scanner | 30 | 59.0 | 58.4 | 58.5 | 57.4 | 54.4 | 44.1 | 36.5 | 38.6 |
| | 40 | 59.7 | 58.7 | 58.8 | 56.7 | 52.9 | 41.6 | 27.0 | 9.4 |
| | Block 1 | | | | | | | | |
| | 10 | 116.0 | 117.0 | 108.8 | 107.4 | 104.8 | 95.6 | 82.7 | |
| | 20 | 125.8 | 121.4 | 109.6 | 93.4 | 86.9 | 65.3 | 74.3 | |
| | 30 | 121.6 | 120.0 | 99.4 | 69.0 | 51.6 | 46.5 | 34.9 | |
| | 40 | 116.2 | 109.9 | 62.0 | 65.0 | 46.0 | 45.2 | 27.9 | |
| | Block 2 | | | | | | | | |
| | 10 | 69.8 | 68.0 | 64.3 | 61.8 | 61.4 | 59.5 | 38.5 | 23.7 |
| | 20 | 75.4 | 74.5 | 60.2 | 59.8 | 46.8 | 48.1 | 24.8 | 20.1 |
| | 30 | 72.3 | 69.3 | 54.9 | 45.9 | 37.1 | 27.7 | 21.3 | 16.3 |
| | 40 | 76.2 | 59.3 | 42.4 | 35.1 | 42.9 | 32.9 | | |

2.4.3. Effect of Crack Orientation on the Smallest Detected Crack Width

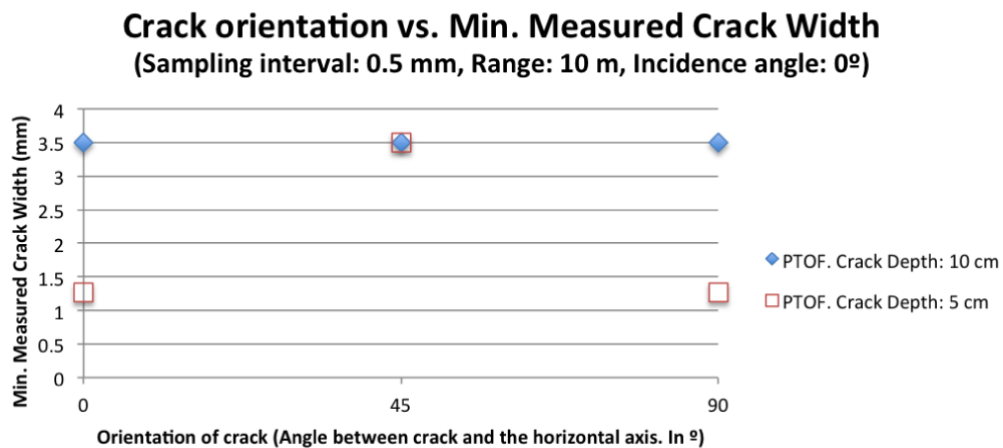
The third set of results presents the minimum crack width detected for varying crack orientations. Specifically, vertical, 45° diagonal, and horizontal cracks were scanned. The sampling interval was set separately for the two scanners. The AMCW scanner was set to 3.1 mm sampling interval. The PTOF scanner was set to 0.5 mm and also to 3.1 mm sampling intervals for comparison with the AMCW scanner.

The results show that using the AMCW scanner the 1.25 mm width crack can be detected at any orientation with 3.1 mm sampling interval (Figure 2-5). Using the same sampling

interval and the PTOF scanner, the 1.25 mm width crack is only detected when the crack is horizontal, and at 45° and 90° the smallest crack that is detected is 3.5 mm wide. Using 0.5 mm sampling interval, 1.25 mm crack can be detected at 0° and 90° orientation with the PTOF scanner. The PTOF scanner is not able to detect the 1.25 mm crack at 45° crack orientation using any of the scanner configurations tested in this study. These results suggest that the anisotropic behaviors of the two scanners are also different.



(a)



(b)

Figure 2-5 Smallest crack widths that were detected at different crack orientations. The AMCW scanner is able to consistently detect the smallest crack of 1.25 mm regardless of the crack orientation (a). On the other hand, the PTOF scanner is able to detect the 1.25 mm crack only at 0° and 90° orientations using 0.5 mm sampling interval, and at 0° using 3.1 mm sampling interval.

Measurement results show that with the PTOF scanner, errors are smaller using a denser scan (0.5 mm) compared to a relatively coarse scan (3.1 mm) (Table 2-8). Additionally, using the same scanner and 0.5 mm sampling interval, mean measurement values are similar for the same crack at different orientations (i.e., between 5.15 and 5.71 mm for

the 3.5 mm crack). On the other hand, when 3.1 mm sampling interval is used, the measurement values for the same crack range between 5.91 and 9.37 mm.

Using the AMCW scanner, the crack width measurements are distributed over a wider range compared to the PTOF scanner using the same sampling interval (i.e., 3.1 mm). For the 3.5 mm wide crack on block 1, the measured crack width is 7.79 mm when the crack is vertical (i.e., 90°), whereas the same crack is measured to be 15.68 mm when it is horizontally oriented (i.e., 0°). The vertical scanning speed of the AMCW scanner is much faster than its horizontal speed (1500 rounds per minute vertically vs. 1 round per 202 seconds horizontally at high resolution) results in tall and narrow beam spot on the surface (Tang et al., 2009). Therefore, the edge losses on the horizontal crack, which is measured vertically, is larger than the vertical crack, which is measured horizontally.

Table 2-8 Mean and standard deviation of crack width measurements of the smallest detected cracks using fixed sampling intervals at varying crack orientations (all measurement units are in millimeters). The range is fixed to 10 m and incidence angle of the laser beam is 0°. Crack orientation is defined as the angle between the crack and the horizontal axis. With the PTOF scanner two sampling intervals were used: 0.5 mm and 3.1 mm at 10 meters range. With the AMCW scanner only 3.1 mm sampling interval was tested.

| Crack orientation (°) | PTOF Scanner | | | | | | AMCW Scanner | | | | | |
|-----------------------------|----------------------------------|------|----------|---------|------|----------|----------------------------------|-------|----------|---------|------|----------|
| | Fixed sampling interval (3.1 mm) | | | | | | Fixed sampling interval (3.1 mm) | | | | | |
| | Block 1 | | | Block 2 | | | Block 1 | | | Block 2 | | |
| | Actual | Mean | σ | Actual | Mean | σ | Actual | Mean | σ | Actual | Mean | σ |
| | 90.00 | 3.50 | 9.37 | 0.04 | 3.50 | 6.00 | 0.12 | 3.50 | 7.79 | 1.48 | 1.25 | 5.47 |
| 45.00 | 3.50 | 6.23 | 0.27 | 3.50 | 5.35 | 0.99 | 3.50 | 9.98 | 0.58 | 1.25 | 3.69 | 1.53 |
| 0.00 | 3.50 | 5.91 | 0.18 | 1.25 | 4.93 | 1.17 | 3.50 | 15.68 | 3.15 | 1.25 | 5.60 | 1.34 |
| | Fixed sampling interval (0.5 mm) | | | | | | | | | | | |
| 90.00 | 3.50 | 5.15 | 0.07 | 1.25 | 3.26 | 0.71 | | | | | | |
| 45.00 | 3.50 | 5.71 | 0.14 | 3.50 | 5.08 | 0.18 | | | | | | |
| 0.00 | 3.50 | 5.52 | 0.23 | 1.25 | 2.76 | 0.18 | | | | | | |

Measured crack depths seem to be less affected by the orientation of the cracks (Table 2-9). Although there is a general trend of recording the depths of cracks shallower than they are as the crack width gets smaller, the depth measurements for the same crack with different orientations do not vary more than a centimeter for almost all of the cases.

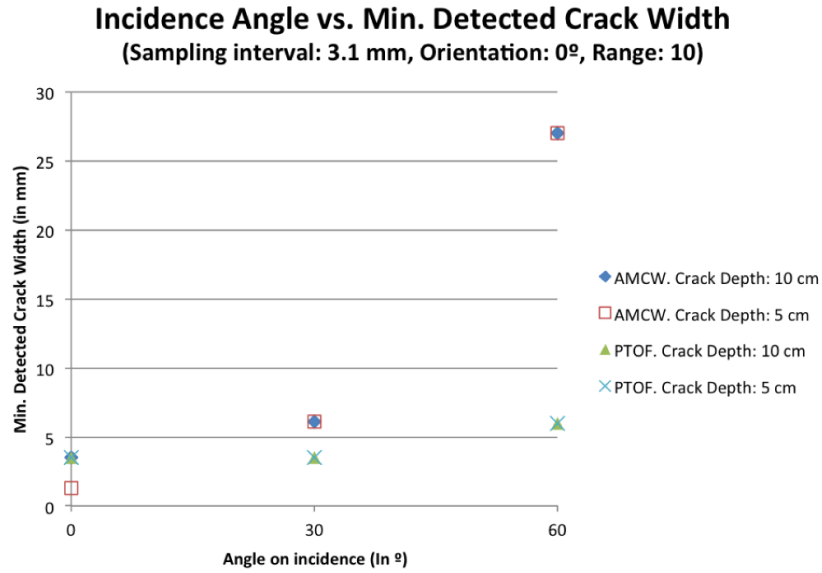
These variations are much less than what we observed for other parameters, such as range. For the horizontally oriented 6.4 mm crack on block 1, the PTOF scanner recorded a depth of 55.5 mm when a sampling rate of 0.5 mm was used. Using the same scanner and the sampling interval, the same crack was measured to be about 105 mm deep for when it was vertical or diagonal. We have not been able to explain the large variation for this case as none of the depth measurements of the other cracks on the same block have such large differences.

Table 2-9 Mean depth measurements at fixed range, sampling interval, and angle of incidence. Crack orientation has a less of an effect on crack depth measurement compared to range and sampling interval.

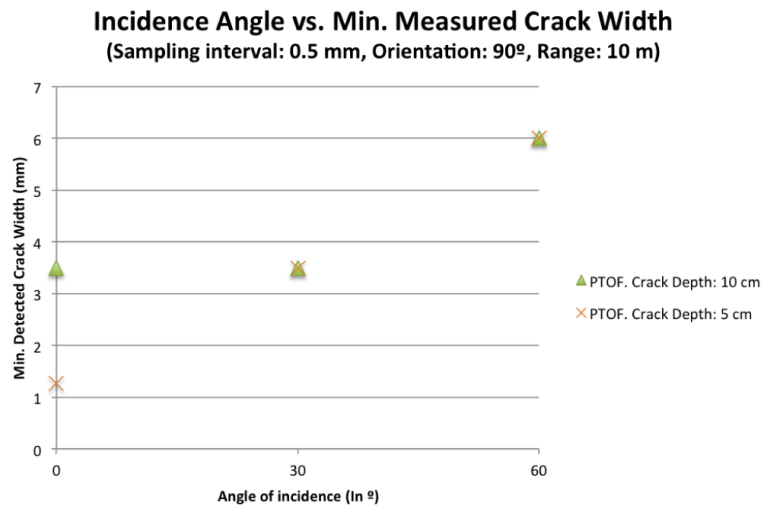
| | | Crack widths (in mm) | | | | | | | |
|-------------------|--------------------------------------|----------------------|-------|-------|-------|-------|-------|------|------|
| Crack Orientation | | 52.5 | 27 | 10.8 | 7.6 | 6.4 | 4.6 | 3.5 | 1.25 |
| PTOF Scanner | Sampling Interval : 0.5 mm | Block 1 | | | | | | | |
| | | Vertical | 108.5 | 108.4 | 107.3 | 106.5 | 105.3 | 99.1 | 52.0 |
| | | Diagonal | 107.0 | 107.1 | 106.3 | 106.0 | 104.9 | 98.4 | 51.4 |
| | | Horizontal | 107.7 | 107.7 | 106.6 | 105.9 | 55.5 | 99.1 | 51.0 |
| | | Block 2 | | | | | | | |
| | | Vertical | 59.8 | 59.5 | 58.9 | 58.2 | 58.9 | 54.1 | 41.8 |
| | Sampling Interval : 3.1 mm | Diagonal | 58.5 | 58.6 | 58.1 | 57.5 | 53.8 | 39.0 | 37.3 |
| | | Horizontal | 59.0 | 58.9 | 58.4 | 58.3 | 57.3 | 54.5 | 41.5 |
| | | Block 1 | | | | | | | |
| | | Vertical | 106.1 | 106.7 | 104.4 | 103.7 | 99.9 | 35.4 | 32.1 |
| | | Diagonal | 105.6 | 106.3 | 104.1 | 103.0 | 102.4 | 91.5 | 37.2 |
| | | Horizontal | 105.6 | 105.7 | 104.4 | 103.0 | 93.2 | 64.0 | 46.5 |
| AMCW Scanner | Sampling Interval : 3.1 mm (0.0018°) | Block 2 | | | | | | | |
| | | Vertical | 57.4 | 56.7 | 56.1 | 55.9 | 46.3 | 38.7 | 33.8 |
| | | Diagonal | 57.2 | 56.5 | 56.0 | 56.1 | 54.3 | 45.2 | 23.0 |
| | | Horizontal | 57.2 | 56.8 | 55.8 | 55.9 | 54.9 | 51.5 | 28.9 |
| | | Block 1 | | | | | | | |
| | | Vertical | 116.0 | 117.0 | 108.8 | 107.4 | 104.8 | 95.6 | 82.7 |
| | Sampling Interval : 3.1 mm (0.0018°) | Diagonal | 116.7 | 116.0 | 109.9 | 111.9 | 93.7 | 83.4 | 76.9 |
| | | Horizontal | 118.5 | 116.0 | 114.3 | 104.7 | 75.6 | 83.0 | 65.3 |
| | | Block 2 | | | | | | | |
| | | Vertical | 69.8 | 68.0 | 64.3 | 61.8 | 61.4 | 59.5 | 38.5 |
| | | Diagonal | 69.8 | 67.1 | 63.3 | 62.9 | 57.7 | 48.7 | 31.2 |
| | | Horizontal | 70.2 | 68.2 | 70.4 | 61.9 | 53.7 | 46.4 | 32.4 |

2.4.4. Effect of Incidence Angle on the Smallest Detected Crack Width

The last set of analyses involves evaluating laser scanners for detecting cracks at different angles of incidences (Figure 2-6). The angle of incidence is defined as the angle between the laser beam and normal of the surface being scanned. Incidence angle is set to 0°, 30°, and 60°.



(a)



(b)

Figure 2-6 Smallest detected crack width as a function of the incidence angle of the laser beam with the surface.

The results show that the performances of the two scanners in detecting cracks diminish as the angle of incidence increases. The PTOF scanner, however, is able to detect smaller cracks at high incidence angles (i.e., 60°). Using 3.1 mm sampling interval, at 60° the PTOF scanner is able to detect 6 mm cracks. At 0° and 30° incidence angles, the PTOF

scanner is able to detect 3.5 mm cracks. On the other hand, the AMCW scanner is able to detect 6 mm cracks at 30° and 27 mm cracks at 60° incidence angle.

The projection of cracks on the scanner frame is proportional to the cosine of the incidence angle. Therefore, for an incidence angle other than 0°, the scanner is effectively imaging cracks that look smaller than their actual values. Additionally, as discussed in the previous sections, the depth of the crack is an important parameter for a successful detection. For a thin crack, the full depth of the crack may not be visible from the scanner position. If the full depth is not visible, then the depth of the crack is inversely proportional to the sine of the incidence angle and the actual crack width. For example, the 1.25 mm crack's full depth is not visible from 60°. The distance between the edge that is closer to the scanner and opposite crack wall defines the depth of the crack. The 1.25 mm crack seems like 0.63 mm wide and 1.4 mm deep at 60° incidence angle. These two effects cause a poor detection of thin cracks at large incidence angles.

We observed that for incident scans, depth is mainly controlled by the self-occlusion of the inside of the crack by the crack edges rather than the mixed pixels. For example, at 30° incidence angle for a 10 mm wide crack, the visible depth is $10 \text{ mm} / \sin(30^\circ) = 20 \text{ mm}$ plus the variation due to noise. It was observed that for none of the cases except the 0° incidence angle cases, the full depth of the cracks are visible. Therefore, crack depths are not evaluated for varying incidence angles.

Table 2-10 Mean and standard deviation of crack width measurements of the smallest detected cracks using fixed sampling intervals at varying beam incidence angles (all measurement units are in millimeters). The range is fixed to 10 m and the cracks are vertically aligned. Incidence angle is defined as the angle between the laser beam hitting the surface and the normal of the surface. With the PTOF scanner two sampling intervals were used: 0.5 mm and 3.1 mm at 10 meters range. With the AMCW scanner only 3.1 mm sampling interval was tested.

| Incidence angle (°) | PTOF Scanner | | | | | | AMCW Scanner | | | | | |
|----------------------------------|----------------------------------|------|----------|-----------|------|----------|----------------------------------|-------|----------|-----------|-------|----------|
| | Fixed sampling interval (3.1 mm) | | | | | | Fixed sampling interval (3.1 mm) | | | | | |
| | 10 cm deep | | | 5 cm deep | | | 10 cm deep | | | 5 cm deep | | |
| | Actual | Mean | σ | Actual | Mean | σ | Actual | Mean | σ | Actual | Mean | σ |
| 0.00 | 3.50 | 9.37 | 0.04 | 3.50 | 6.00 | 0.12 | 3.50 | 7.79 | 1.48 | 1.25 | 5.47 | 1.44 |
| 30.00 | 3.50 | 6.57 | 0.52 | 3.50 | 7.56 | 1.74 | 6.10 | 10.64 | 1.15 | 6.10 | 8.92 | 0.76 |
| 60.00 | 6.00 | 8.80 | 2.41 | 6.00 | 8.85 | 2.47 | 27.00 | 29.74 | 3.92 | 27.00 | 26.42 | 2.90 |
| Fixed sampling interval (0.5 mm) | | | | | | | | | | | | |
| 0.00 | 3.50 | 5.15 | 0.07 | 1.25 | 3.26 | 0.71 | | | | | | |
| 30.00 | 3.50 | 5.77 | 0.75 | 3.50 | 6.98 | 1.58 | | | | | | |
| 60.00 | 6.00 | 9.23 | 0.63 | 6.00 | 6.79 | 0.66 | | | | | | |

2.5. Evaluation of the results on a real case

There are three main differences between the test blocks and actually damaged construction material. First, the test blocks have smoother and flatter surfaces than a regular concrete or brick surface. Second, the crack edges are sharp ($\sim 90^\circ$) and smooth. A crack on a brick or concrete generally has a much rougher edge. Third, the two opposite edges of the cracks are coplanar. Especially on brick walls, pieces of broken bricks can be dislocated out of the wall plane, which gives the cracks a different characteristic.

The results obtained from the artificial cracks are compared to the results obtained from a real damaged wall. The tested structure is a half-scale three-story, three-bay planar reinforced concrete frame with aerated concrete block infills in the middle bay. The frame was loaded at the story levels with hydraulic jacks to failure.

The wall was scanned using a pulsed time of flight scanner from three different locations. The first set of scans was taken from 3.8 meters using 0.5, 1.5, and 5.0 millimeter sampling intervals. The second set was taken from 9.6 meters range using the 0.5, 1.0, 5.0, 15.0 millimeters sampling intervals. The first two scans have 0° incidence angle with the

center of the wall. The third set of scans was taken from 6.7 meters range with an angle of incidence of 60° using 1.0 mm sampling interval. Although, we tried to locate the scanner as close as possible to the ranges used in the first part of the experiments, the scanner locations were limited by the physical conditions of the experimental setting and were decided based on the occlusions of other equipment in the environment.

The cracks on the actual wall were measured using a digital caliper, which constitutes the ground truth. The crack widths range from less than a millimeter upto several millimeters (Figure 2-7). Crack widths are grouped into vertical, horizontal, or diagonal. The smallest cracks that were recognized using the algorithm are wider than the values that were found for the hydrostone blocks for similar configurations.

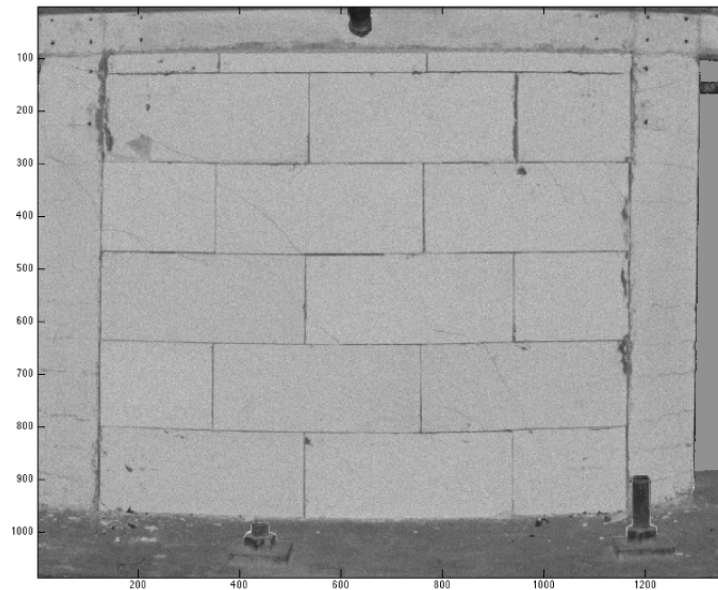


Figure 2-7 The infill wall has several cracks ranging from less than a millimeter upto several centimeters. Figure presents the intensity image of the scan with 0.5 mm sampling interval at 3.8 m range. The wall is located at the mid bay on the first story of a three-story three-bay reinforced concrete frame. The frame was loaded to failure using a real earthquake record.

Table 2-11 Minimum crack sizes that were recognized on the real wall are larger than the results obtained for the hydrostone blocks.

| Sampling Interval (mm) | Range: 3.8 m, Incidence angle: 0° | | | Range = 9.53 m, Incidence angle: 0° | | | | Range = 6.7 m, Incidence angle: 60° | |
|------------------------------------|--------------------------------------|------|------|--|------|------|----|--|--|
| | 0.5 | 1.5 | 5 | 0.5 | 1 | 5 | 15 | 1 | |
| Smallest detected horizontal crack | 2.40 | 4.27 | 4.27 | 2.40 | 3.90 | 4.27 | - | 4.27 | |
| Smallest detected vertical crack | 2.33 | 3.00 | 3.00 | 2.33 | 2.33 | 3.00 | - | 3.00 | |
| Smallest detected diagonal crack | 1.84 | 3.36 | 3.36 | 1.84 | 2.33 | 3.36 | - | - | |

A close investigation of the cracks reveals that the cracks are not deeper than a couple of millimeters. On the other hand, the cracks on the hydrostone blocks are 5 and 10 centimeters. Since, cracks are too thin, it was not possible to measure the actual depth of the cracks. Based on the visual investigation of the wall, it was confirmed that cracks appeared to be only about 1 cm deep. In reality, the cracks extended through the wall, however the cracks partially closed after the lateral load was removed. The shallow nature of the cracks prevents forming of point measurements inside cracks. The first-response type of behavior of the pulsed time-of-flight scanner further limits the capability of the scanner in imaging thin and shallow cracks. The response obtained from the wall surface dominates the response obtained from the inside of the crack. The same phenomenon was also observed for thin and shallow cracks on the hydrostone blocks.

On this actual wall, we observed that a large crack width does not guarantee detection. For example, there are two cracks on the wall that are 2.4 mm wide. The cracks have almost identical orientations. They are on the same masonry unit. Although, they have the same conditions, one of them was never detected in any of the scans. The reason was assessed to be the visible depth of the crack being too shallow. Upon closer investigation,

we saw that the noise around the shallower crack is the same as the noise values on flat regions, which suggests that the scanner did not record any difference for the shallower crack. We can argue that using a different algorithm may not solve the problem since the data distribution on the surface is relatively uniform. In the previous sections, we showed that some cracks that could not be detected by our PTOF scanner were detected using the AMCW scanner, which is known to produce more mixed pixels. We could also argue that we may be able to detect some of the mentioned shallow cracks on the wall using an AMCW scanner, as the potential is demonstrated in Section 4.1. However, the noisy character of the AMCW scanner coupled with the surface irregularities of the real wall might produce very noisy data on flat regions too, which would make the detection a difficult problem.

2.6. False Detection

We observed two additional potential problems from an application perspective. The first problem is related to distinguishing between gaps formed by partial filling of spaces between bricks with mortar and actual cracks, and detecting when the bricks have separated versus undamaged mortar. The second problem is related to continuously detecting cracks along their paths.

For fully automated damage detection, the algorithms used should be able to distinguish between mortar and actual cracks. Since, we used a simple point classification method, the mortars and surface irregularities resulted in false positives on the real wall. This problem can potentially be addressed by making use of the fact that brick layouts follow certain patterns. By analyzing the patterns in the data at larger scales, points classified as being off-surface could be further classified as being an actual feature of the wall or

being cracks. Similar approaches have been suggested for classifying distress types and crack patterns in pavement images [57, 58]. However, further research is needed. Another problem is related to classifying opening of bed and head joints of masonry units, which is actually cracking of the wall in a different form. Under lateral loads, opening of joints may also be accompanied by degradation of mortar between the bricks. In the data we obtained from the real case, we observed that when joints opened they also resulted in a greater depth. This could have happened as a result of the grinding of two bricks on mortar under cyclic earthquake loads, resulting in loss of material and hence deeper crevices between bricks or due to the fact that the bricks have separated. The change in depth along mortar joints could be used to distinguish between cracks between bricks and undamaged mortar. However, at lower damage levels, such distinguishing features may not be evident.

It necessary to include a discussion on detection of cracks along their paths without losing continuity since continuously detecting cracks is important for damage assessment. It was reported in previous research on crack detection from 2D images that due to shortcomings of algorithms, deficiency in the quality of images, or camera hardware limitations continuity of cracks might be lost as discussed in Section 2.2. Therefore, for determining potential advantages and disadvantages of laser scanners over images in terms of continuous detection is important from research as well as application perspective. Additionally, results on the hydrostone blocks and the real wall indicate that orientation, depth, and width of cracks determine whether cracks will be detectable in the scans. In reality, we know that cracks can change direction along their paths. It is also safe to assume that visible depth of cracks may change too.

The classified data was first inspected visually. If we define continuity as uninterrupted spanning of crack points from one end to the other end of the crack, then we can say that all of the cracks on the hydrostone blocks were continuously detected. On the other hand, we observed local thinning of cracks by misclassification of points near edges. Noting that all of the cracks in the data were measured to be 2-3 times wider than their actual values, it is difficult to conclude whether this is actual thinning or accidental recording of these pixels close to the block surface.

Similarly, the classified data obtained from the real wall case was inspected. In this data set, it was observed obvious interruptions along cracks and also mortar joints between bricks even for the widest openings. Both straight and curved cracks were interrupted. This may be due to change in depth or width along the crack paths.

2.7. Conclusions

The results show that almost all of the cracks that are of value to the damage assessment of reinforced concrete buildings can be detected using a laser scanner. However, successful detection depends on selection of the scanning parameters and laser scanner technology being used. The differences in the performance of the two scanners are caused by the differences in the mixed pixel behavior of the scanners. While the signal mixing behavior of the AMCW scanner helps in recording of points inside cracks and hence facilitates a better detection of the cracks, the first response measurement model of the PTOF scanner prohibited detection of crack points. On the other hand, the first-response behavior of the PTOF scanner can help for a better imaging of surfaces for detection of deformations, because the scans would contain less outliers for surface fitting. The depth of the cracks did not impact detection of cracks with the AMCW scanner using the three

pre-defined sampling interval settings. The effect of depth on the PTOF scanner increased as the sampling interval increased.

Cracks were always measured to be larger than the actual values due to edge losses. Measured crack widths ranged from two times the actual crack width up to two times the sampling interval. For a thin crack and a large sampling interval, the crack is measured to be approximately two times the sampling interval. Although the experimental results do not provide a complete validation, we can argue that this is possible if a single point is returned inside the crack and two points are returned on the two sides of the crack on the surface. If as a result of the mixed pixel effect, one (or both) of the surface points are classified as a crack point, then the measured width increases.

Crack detection results for the actually damaged wall are less favorable than the results obtained for the hydrostone blocks. The smallest crack sizes detected on the wall are larger than the smallest crack widths detected on the hydrostone blocks. The difference is thought to be due to the shallow depth of the cracks on the wall. Although, it was not possible to measure the ground truth depth values, most of the cracks on the wall were identified to be less than a centimeter. Since the crack depth impacts the mixed pixel behaviors of scanners, thin cracks cannot be detected when they are also shallow.

The results of this study can be used in several ways. The graphs can be used to assess the minimum crack widths that can be detected from a laser scan data given the scanner technology and scanner parameters. Additionally, these results can be mapped to actual damage behavior. For example, for a known damage mode (e.g., ductile flexure) as described in [1], we can identify which of the damage severities (e.g., moderate) can be

identified using a particular scan. The results obtained from the hydrostone can be used as the upper bound of the damage detection performance of laser scanners.

The results and discussions in this study point to several future research directions. First, we observed that the current models of effective laser scanner resolution are not adequate in quantifying the performance of laser scanner for damage detection. As a future research direction, modeling of the resolution of laser scanner accuracy can be studied. The model will also include estimating width and depth measurement errors, given the laser scanner and crack properties. If such a model can be developed, then the errors can potentially be compensated to make up for the errors, and more accurate measurements can be obtained.

This study used a perfectly controlled environment for comparison of various crack detection methods for damage assessment. The results of this study are readily applicable to concrete and other materials with similar surface characteristics (e.g., reflectivity, surface roughness, etc.). However, detection of cracks is also important for other applications and materials, such as steel. Applicability of the results for these material types should be investigated in the future.

Additionally, other image data could be fused with the scan data and several 3D and 2D image sources could be used in conjunction for more accurate detection. By building on the results of the described experiments, it would be possible to compare technologies and develop effective approaches for fusion of different data sources.

Chapter 3 Information Requirements for Earthquake Damage Assessment of Reinforced Concrete Walls

3.1. Introduction

Damage modes and severities need to be determined through visual assessment and strength analysis [1]. Building Information Models (BIM) can potentially support representing the damaged conditions of the buildings and building information that is important for damage assessment, such as the configuration of structural components, reinforcement details, and finite element models [11, 13, 19-22]. Hence, BIMs can be used to support the engineering analyses for the damage assessment tasks, such as those for strength analysis [13, 19]. However, current BIMs are not developed to represent damaged conditions of buildings [11, 12, 23]. Therefore, representing the damage information in BIMs need to be investigated further.

Representation of a phenomena requires abstraction of information, which depicts the common structure of all of the features required for damage assessment [59]. The abstraction should also support all of the details of individual damage modes. Through this way, the abstraction process can support all of the damage modes for reinforced concrete walls. This requires bottom-up discovery of the hierarchical structure of information requirements. Therefore, we need a structured way of studying the damage assessment guidelines, sort them into hierarchies of damage information, and determine the abstraction of damage information. Using the results of such an information requirement identification study, it would be possible to support various tasks associated with damage assessment.

This chapter studies the information items regarding all of the damage parameters, such as cracking, spalling, crushing, reinforcement bar damage, and residual displacements. The identified information requirements will be used for developing a BIM schema for representing damage conditions and for automatically assessing the damage modes and severities of reinforced concrete (RC) walls.

3.2. Damage Assessment Procedures Based on FEMA 306

Following earthquakes, a three-step procedure is applied [1, 60, 61]. First, within few days after an earthquake, experts perform rapid assessment to classify whether the buildings in the impacted area are safe, unsafe, or require restrictions in their usage [60]. Safe buildings can be used without any restrictions. Unsafe buildings should not be entered under any circumstance. Some restrictions on the usage of a building can be time limits or by the location. For example, an inspector might restrict the access to certain parts of a building, which contain potential hazards. Engineers generally have less than 30 minutes to perform a rapid assessment per building [60]. Second, a detailed assessment is performed on those buildings that were tagged for restricted usage [61]. Detailed assessment is similar to the rapid assessment in execution and function, but it is more thorough. Finally, within the weeks after an earthquake, engineering analyses are performed on safe and restricted buildings, in order to quantify possible effects of damage on the structural properties of structural components and to design retrofitting measures [1]. In all of these stages, collection of the damage data and analysis of the visual damage information using engineering knowledge are key factors for accurate assessment of the damage levels [1].

The engineering analysis, which is the last step described above, has more complex requirements than rapid and detailed assessments. The goal of an engineering analysis is to determine the remaining strength, stiffness, and displacement capacity of structural components [1]. In order to determine the remaining capacities of damaged components, the source of the current damage and its nonlinear mechanism must be determined. This is not a straightforward task since the loads on the components and the relative stiffness of connected components influence the damage mode and severity.

The engineering analysis procedure of FEMA 306 has a five step process for the identification of the damage modes and severities using the visual damage information and capacity calculations [1]. The first step involves assembling information about the earthquake and a specific building, which involves identifying the components making up the lateral and vertical load bearing system of the building. The second step involves identifying types of components by determining the governing inelastic behavior of each element. FEMA 306 defines five types of components: stronger pier, weaker spandrel, stronger spandrel, weaker pier, and pier-spandrel panel zone. This step requires calculations for comparing the relative strengths and stiffness of components. The third step involves documenting the damage. The fourth step involves the classification of the observed component damage by determining the damage modes and damage severities using strength calculations and visual observations. Damage patterns observed on the components are used to determine the damage severity for the determined damage mode of a component. The fifth and last step involves the verification of the results of the analysis by comparing the results of the visual assessment and the strength calculations for the components.

The main goals of the information assembly step (the first step in the above process) are: (1) Gathering information about the damaging earthquake and generating a capacity curve for the building by conducting structural analysis, and (2) Collecting information about the structural design of a building and the configuration of the load bearing system. The information about the damaging ground motion is generally made available shortly after the earthquake. The procedures for analyzing structural models to generate capacity curves and estimating maximum global displacements are standardized according to accepted practices [62].

Gathering building information entails reviewing construction and structural drawings, previous structural computations, construction records, and previous inspection reports. Such information is useful for identifying structural components by performing strength calculations, and for determining the scope of the field inspections and testing programs. For example, if the locations and sizes of reinforcing bars are known accurately, expensive and intrusive tests may not be necessary [1]. Inaccuracy of the information gathered in this step might reflect to the overall results as discrepancies between calculations and visual observations. Additionally, in the evaluation stage, expected strengths can be penalized up to 25% depending on the confidence on the accuracy and completeness of information, which would increase the retrofitting costs [62].

The engineers are expected to identify the types of components (e.g., weaker spandrel, stronger pier, etc.) by anticipating the inelastic lateral mechanism for each element. An element entails a vertical or horizontal portion of a building, which resists lateral and vertical loads. An element is an assembly of components, such as wall piers, beams, columns, slabs, etc. For example, a structural wall with openings can be made up of

components, such as piers and beams. The components in such a configuration will also include the piers on a different axis, which make up the flanged sections. The identification of these components is central to the overall process and requires calculation of strengths of the components and a thought process by the engineer to anticipate the lateral the behavior of the components using the visual damage patterns.

Intrusive and non-intrusive tests are performed to document the damage, material strengths, and relative ages of cracks. Visual observation is the most important non-intrusive test to document the earthquake damage. Some of the special techniques include selective removal of material, material sampling, sounding, petrography, spectral analysis, and penetrating radar. Tests, which require specialized equipment and experienced personnel to perform, are generally expensive. Such expensive tests can be reduced by having access to accurate and complete information on existing structural conditions of the building.

For each component of the structural system, the engineer classifies the damage according to behavior mode and severity. The engineer also categorizes the severity of damage for each type of damage encountered within any component. FEMA 306 guideline classifies damage for reinforced concrete walls into common, less common or uncommon modes [1]. The research described in this paper focuses only on the common modes. Only unreinforced masonry is considered for infilled frames, since reinforced infills are not very common in reinforced concrete construction [1]. The damage modes that are considered in this study are as following (the letters in parenthesis indicate the codes of the damage modes):

- 1- Ductile Flexure (A): Moment strength governs the strength of the component.

- 2- Flexure/Diagonal tension (B): Initially, the moment strength governs. High-ductility shear strength is less than the moment strength. Low-ductility shear strength is higher than the moment strength.
- 3- Flexure/Diagonal compression (C): Initially, the moment strength governs. High ductility web crushing strength is less than the moment strength.
- 4- Flexure/Sliding shear (D): Initially, the moment strength governs. Sliding shear strength is less than the moment strength.
- 5- Flexure/Boundary compression (E): Moment strength is higher than all other modes even after possible degradation.
- 6- Pre-emptive diagonal tension (H): Low-ductility shear strength is less than the moment strength.
- 7- Global or individual pier foundation rocking (M & N): The lateral force, which would impose rocking should be less than all other strengths.

The results of the strength analysis and visual assessment should corroborate. If the results of the two analyses do not corroborate, the potential error sources need to be checked and the analysis repeated. FEMA 306 lists several potential error sources. The distribution of the lateral forces, which was used in the structural analysis, may be different from the actual. The strength of the components may differ from the actual. The intensity of the damaging ground motion may differ from that assumed in the structural analysis.

There can be several problems in the engineering analyses. The design and construction documents can become outdated as a result of retrofitting or remodeling of the building.

The calculation of strength of components and structural analysis are performed by interpreting the information on the construction drawings and design documents, which might be obsolete. The current FEMA 306 process requires manual re-entry of information into computer programs, which is error-prone and redundant. Manual documentation of damage can lack important details about the observations, the inspection may not be as thorough as required by the assessment guidelines, and the results may be subjective and incorrect.

3.3. Background Research

3.3.1. Methods for Identification of Information Requirements

Developing a schema for representing the damaged conditions of buildings and support the visual assessment tasks, requires the information requirements of such a schema. Methods for identifying information requirements for developing representations and reasoning mechanisms can be grouped into two: Exhaustive listing and Structured methods.

3.3.2. Exhaustive listing

If the problem being studied is relatively small, the information requirements can be identified by studying the process, which the representation will support, and listing all the entities or concepts, which are involved in the solution of the problem [13, 22, 63, 64]. In this approach, studying standards, mathematical equations, which are involved in the process, documents and research studies, are common. Mathematical models and computational methods can also derive the information identification. For example, for

finite element procedures, the finite element model and the solution method determine the structure and the content of the representation method [65-67].

Methods based on listing requirements are not well structured. The information requirements for designing the information model or decision system are not collected, studied, and evaluated in a formal way. A drawback is that the relative importance or hierarchy of information items cannot be studied objectively. For well-defined problems, such as a mathematical computation, or small-scale problems, unstructured methods may be easy to apply and yield direct results rapidly. However, a limitation of this approach is that as the number of entities increases and the problem becomes more complex the organization and classification of information becomes more difficult [68].

3.3.3. Affinity Diagramming Method

Affinity diagramming is used for discovering common themes and issues among individual examples of a work practice [69]. Affinity diagrams are built by induction to create a representation of a work practice starting from its details and moving towards general concepts by grouping details and generating new insights about overarching patterns of data. Since the structure of an affinity diagram is built from detail, differences between individual examples can be accommodated.

A common process to build an affinity diagram starts with gathering statements or requirements by studying the target work practice (e.g., user interviews) and follows as grouping these statements by their affinities (i.e., statements which say similar things) and building a hierarchical structure by creating super-groups that have affinities in several levels (generally 3 or 4 groups) [69].

Considering the complexity of the damage assessment tasks, using a structured approach, such as affinity diagramming approach is appropriate. The affinity diagram can be built for the visual damage assessment process by first exhaustively listing all of the statements describing the damage modes and treating each damage mode as examples of the same work practice. The affinities between statements in the descriptions of the damage modes can be discovered through an induction process: the statements are grouped in multiple levels to reveal new insights about the patterns of features, which engineers look for during the damage assessment process. In the study described in this chapter, we have decided to incorporate affinity diagram approach to identify the information requirements for developing a schema for damage assessment of structural walls, in order to be able to study the information requirements in a structured way.

3.4. Approach

The affinity diagram was built in two steps: First, statements that make up the damage descriptions in the FEMA 306 guidelines were extracted. Each statement was recorded on note cards. Second, affinities were identified between these statements by induction. The interpretation of the statements and potential affinities are determined by considering the domain knowledge. The note cards were grouped, regrouped, and organized to reveal patterns in the information in multiple levels.

In the first step, information was collected about the visual damage assessment practice. In total, 278 statements were extracted. In some occasions, further interpretation of the statements was required to deduce the meaning of the statements. For example, some of the individual statements are meaningful only in the context of a given damage mode. The statement “Reinforcement has fractured” in the ductile flexural (A) damage mode

refers to the fracturing of the flexural reinforcement, not just any reinforcement [70]. This can be deduced from the fact that this type of behavior can occur if a component has sufficient reinforcement to prevent shear failure and flexural reinforcement is not heavy [70]. Hence, moment demand exceeds the shear demand. Such statements were modified to depict the exact meaning. Each statement was written on a note card along with its damage mode, an identification number for the statement, and the damage severity, at which the statement is observed.

The statements constitute the first level of the affinity diagram. The second step included building up a structure from particular to general, starting from the first level. The process is as follows. First, a note containing a single statement is put on the board. Other statements are browsed to see which statements have an affinity with the first statement. Two notes are said to have an affinity if they say similar things [69]. Two statements are identified as having an affinity if they help differentiating between different damage modes. Notes having an affinity are put together.

The goal of the affinity diagram is to build a hierarchy of statements in such a way that the grouping in the hierarchy will help in differentiating between different damage modes. In order to illustrate the process of grouping, consider the following statements about cracking (Table 3-1). It can be seen that the statements are about different types of cracks (i.e., flexural, shear, or any type of crack regardless of type), there are width comparisons, and some of the widths are recurring (e.g., 0.8 mm, 1.6 mm, etc.). One way of grouping these statements is by highlighting the crack type as the overarching pattern of the statements and group by recurring crack widths:

- Level 2 – Type of cracks, which are narrower than 3.2 mm

- Level 1 - Flexural crack width < 3.2 mm
- Level 1 - Shear crack width < 3.2 mm

This type of grouping ignores the fact that crack widths are only meaningful if the type of the crack is known (e.g., flexural, shear), which is one of the primary indicator of the damage mode. For a certain damage mode, we expect to see cracks of a certain type to be wider than the others [1]. For example, wide flexural cracking and much narrower shear cracks or no shear cracks at all may be an indication of ductile flexural behavior. On the other hand, X shaped cracking extending along the diagonals of a wall with little or no flexural cracking may indicate a brittle shear type of behavior. In other words, crack width is secondary to the type of crack.

A more useful way of grouping the same statements is by highlighting the crack width as the overarching pattern and grouping by crack type:

- Level 2 – Width of flexural cracks
 - Level 1 - Flexural cracks < 3.2 mm
 - Level 1 - Flexural cracks < 4.8 mm

This grouping recognizes that the crack type should be known before setting a limit on the crack width, for determining the damage mode. Thus, the crack width is put at a lower level than the crack type. When the affinity diagram is built this way we can obtain the patterns in the statements, which help differentiating between different damage modes, while keeping the details at the lower levels, which help determining the damage severities for the damage modes.

Table 3-1 A selected subset of statements about crack types and widths. The statements contain crack types and crack widths.

| # | Statement |
|----|---|
| 1 | Flexural crack width < 3.2 mm |
| 2 | Flexural crack width < 6.4 mm |
| 3 | Flexural crack width < 6.4 mm |
| 4 | Flexural crack width < 4.8 mm |
| 5 | Shear crack width > 4.8 mm & < 9.6 mm |
| 6 | Shear crack width < 3.2 mm |
| 7 | Shear crack width < 1.6 mm |
| 8 | No shear cracks |
| 9 | Shear crack width > 1.6 mm |
| 10 | Shear crack width < 3.2 mm |
| 11 | No shear crack width exceeds 3.2 mm |
| 12 | Shear crack width > 3.2 mm & < 9.6 mm |
| 13 | Shear crack width < 3.2 mm |
| 14 | No shear crack width exceeds 3.2 mm |
| 15 | Shear crack width may exceed 1/8 but cannot exceed 9.6 mm |
| 16 | Shear crack width < 3.2 mm |
| 17 | Crack width < 9.6 mm |
| 18 | Crack width < 3.2 mm |
| 19 | Crack width < 1.6 mm |
| 20 | Crack width < 1.6 mm |
| 21 | Crack width does not exceed 9.6 mm |
| 22 | All crack widths < 6.4 mm |
| 23 | Crack widths does not exceed 9.6 mm |
| 24 | No crack width exceeds 4.8 mm |

There are other statements, which talk about cracking (Table 3-2). These statements seem like they may fit into the hierarchy, which was identified in the previous paragraph. However, considering the meaning of the statements and how these statements are used to distinguish between different behavior modes, one realizes that there are stronger affinities among the statements in Table 3-2. The first three statements are used to distinguishing the initiation of core-crushing. Statements 4-6 are used to locate damage for core crushing. The location of crushing helps differentiate between a shear dominated mode or boundary crushing mode. The remaining statements are important for distinguishing between flexure and pre-emptive shear type of behavior. Similar to the

previous example, all of the statements in Table 3-2 were studied to understand the precedence of the information for identifying damage modes.

Table 3-2 Other statements extracted from the guideline about cracking.

| # | Statement |
|----|--|
| 1 | No significant spalling or vertical cracking |
| 2 | No significant spalling or vertical cracking |
| 3 | No vertical cracking or spalling |
| 4 | Spalling or vertical cracking at toe regions in plastic hinge zone |
| 5 | Spalling or vertical cracking at toe regions in plastic hinge zone |
| 6 | Vertical cracks at the extreme fibers of the plastic hinge zone |
| 7 | One or more wide shear cracks begin to form |
| 8 | Wide shear cracks concentrated in a single crack |
| 9 | Wide flexural cracking and spalling should be concentrated in the plastic zone |
| 10 | Minor flexural cracking may extend beyond the plastic hinge zone |
| 11 | Flexural cracks beyond plastic hinge zone don't exceed 1/8" |
| 12 | Flexural cracking and spalling concentrated at the hinge zone |
| 13 | Flexural cracking may extend beyond p. hinge zone |

The grouping was repeated at the third and fourth levels to build a hierarchy. The statements for reinforced concrete walls, unreinforced masonry walls, and infilled frames were considered separately. Therefore, the study resulted in three affinity diagrams. The next section will present the final diagrams and discuss the findings.

3.5. Results and Discussion

All 278 statements were used to create a structure for the identification of damage modes (Tables 3-3, 3-4, and 3-5). Reinforced concrete and masonry have different mechanisms for failure and, hence, different damage modes. Therefore, the statements for reinforced concrete, masonry, and additional modes for infilled frames were considered separately. Due to the small number of statements for the additional modes of infilled frames (22 statements), they are only considered in three levels versus four levels in reinforced concrete and masonry (Table 3-5).

Complementing patterns and differences between reinforced concrete and masonry information requirements are identified. The emerging pattern is that cracking is the main damage indicator. Out of 278 statements, 156 statements are about cracking. This corresponds to 56% of the total count. The remaining statements are distributed among the other damage indicators (spalling, crushing, buckling and fracture of reinforcement, and residual displacement). Out of the 5 Level 3 groups of reinforced concrete, three groups are about cracking and crack properties (Table 3-3). The other two groups are about location and quantity of other damage indicators. For masonry components four out of seven and for infilled frames two of five level 3 groups are about cracking (Table 3-4 and Table 3-5). Similar to reinforced concrete, damage location emerges as an important feature for damage mode identification. Additionally, separation of masonry from infills and partial or total walking type of damage are defined for masonry.

The damage indicators of both masonry infilled frames and reinforced concrete components have largely the same overarching patterns of information requirements at Level 3. The only difference is the movement mode of infills, which constitutes about 7% of the statements on masonry damage, and 4% of the overall statements.

Table 3-3 The affinity diagram for reinforced concrete components. Level 1 contains the individual statements extracted from the FEMA 306 guideline and is hidden for brevity. Cracking and crack properties emerge as the most important feature in the diagram, followed by the location and quantity of the other damage indicators.

| Concrete | | | Statement Count | Percent |
|---------------------------------------|------------------------|--|-----------------|----------------|
| Level 4 | Level 3 | Level 2 | 83 (Total) | |
| Crack properties | | | 47 | 57% of total |
| | Crack point property | | 25 | 53% of Level 4 |
| | | Flexural crack size | 5 | |
| | | Shear crack size | 12 | |
| | | Any/all crack size | 8 | |
| | Crack path property | | 10 | 21% of Level 4 |
| | | Continuity of flexural cracks along component | 4 | |
| | | Degradation of concrete along cracks | 2 | |
| | | Amount lateral offset along sliding plane | 4 | |
| | Crack pattern property | | 12 | 26% of Level 4 |
| | | Type of concentrated single crack | 7 | |
| | | Concentration of flexural cracks in the plastic hinge zone | 5 | |
| Properties of other damage indicators | | | 36 | 43% of total |
| | Damage location | | 15 | 42% of Level 4 |
| | | Spalling or crushing location and amount | 7 | |
| | | Location of buckled rebars | 3 | |
| | | Spalling or vertical cracking location | 5 | |
| | Damage quantity | | 21 | 58% of Level 4 |
| | | Spalling or vertical cracking | 6 | |
| | | Residual displacement amount | 7 | |
| | | Buckled or fractured bars | 8 | |

Table 3-4 Cracking is the main damage indicator in masonry, similar to reinforced concrete. The affinity diagram shows other features in addition to size and type of cracks, such as opening of head joints and sliding of bed joints.

| Masonry | | | Statement | |
|---|---------|---------|-------------|----------------|
| | | | Count | Percent |
| Level 4 | Level 3 | Level 2 | 173 (Total) | |
| Crack properties | | | 96 | 56% of total |
| Crack point property | | | 23 | 24% of Level 4 |
| Size of cracks | | | 5 | |
| Size of opening of head joints | | | 5 | |
| Sliding/opening of bed joints | | | 13 | |
| Crack path property | | | 44 | 46% of Level 4 |
| Spalling and unit damage along cracks | | | 9 | |
| Cracks go through units | | | 9 | |
| Sliding off supporting bricks along crack | | | 3 | |
| Amount of offset along cracks | | | 13 | |
| Crack pattern property | | | 25 | 26% of Level 4 |
| Continuity of horizontal cracks | | | 2 | |
| Continuity of diagonal cracks | | | 2 | |
| Patterns of cracks | | | 10 | |
| Location of concentrated cracks | | | 3 | |
| Type of concentrated cracks | | | 2 | |
| Type and number of cracks in a region | | | 4 | |
| Amount of cracked courses in units | | | 6 | |
| Properties of other damage indicators | | | 77 | 44% of total |
| Damage location | | | 60 | 78% of Level 4 |
| Location of brick crushing | | | 12 | |
| Location of mortar crushing | | | 3 | |
| Location of cracking of bed joints and spalling | | | 13 | |
| Location of cracks with various orientations | | | 20 | |
| Location of regional crushing | | | 5 | |
| Location of falling masonry | | | 3 | |
| Location of spalling of face shells | | | 2 | |
| Mortar separation around perimeter | | | 2 | |
| Crushing of mortar and bricks around perimeter | | | 3 | |
| Location of movement of face shells | | | 2 | |
| Movement modes of components | | | 12 | 15% of Level 4 |
| Type and existence of total walking of piers | | | 4 | |
| Existence of total movement of spandrels | | | 5 | |
| Existence of partial out-of-plane movement of walls | | | 1 | |
| Existence of partial rotation of component | | | 2 | |

Table 3-5 Affinity diagram for additional modes of infilled frames. Due to the low number of statements, only three levels were considered.

| Infilled Frames | | Statement Count | Percentage |
|---------------------------------------|-------------------------------|-----------------|--------------|
| Level 3 | Level 2 | 22 (Total) | |
| Crack properties | | 13 | 59% of total |
| | Crack location | 7 | |
| | Size and extent of X-cracking | 6 | |
| Properties of other damage indicators | | 9 | 41% of total |
| | Spalling extent and location | 6 | |
| | Fractured rebar location | 1 | |
| | Crushing location | 2 | |

The main observations from the affinity diagram agree with the experimental studies on behavior of structural systems. Generally, damage initiates as cracking [71, 72]. Other damage indicators add onto cracking as damage progresses [73]. Often existence of other damage indicators marks the transition of the damage severity to an upper level (e.g., moderate to heavy) or the failure of component. Therefore, it can be said that cracking is always present regardless of other damage indicators.

The type and character of cracks depends on damage behavior of the component [70]. For example, in a ductile flexural behavior, we primarily expect to see cracks in transverse direction to the component axis (i.e., flexural cracks). A vertical crack along the edge of a concrete column may indicate lap-splice splitting. The same cannot be said for all of the other damage indicators. For example, residual displacement alone may not be enough to gain insights into the cause of the damage behavior. Therefore, cracks can be attributed as having special importance in damage detection. The patterns in the affinity diagram agree with these insights.

The affinity diagrams show that there are several important properties of cracks both for concrete and masonry components. First and foremost properties are the type and width. Crack type depends on the alignment of crack with the axis of component and loading direction. Possible crack types are flexural, shear, and vertical cracks. Width is generally not constant along cracks. Therefore, crack width is considered as a point property of cracks. Maximum crack width is measured and recorded for each crack [1]. Similarly, for masonry components, opening of head joints, and sliding of bed joints are considered as point properties. The affinity diagramming study also discovered patterns along the crack paths, such as degradation and sliding along cracks, and continuity of cracking.

Patterns of cracks and properties of crack patterns can be observed as a composite property of cracks (Table 3-4 and Table 3-5). Concentration and number of cracks, location, type, and amount of cracked courses in units are the main properties of crack patterns. Especially, in masonry, the features, which define the patterns are much richer compared to concrete. This can be attributed to the construction of masonry components using two different materials (i.e., masonry units, and mortar), which have different material properties. The relative strength of units and mortar, for instance, determines whether the units will crack along the crack paths creating smoother crack patterns similar to concrete, or whether the cracks will be stair-shaped with intact units.

3.6. Validation

The affinity diagramming study identified the hierarchy of information items, which visually characterize the damage modes for reinforced concrete and masonry structural walls. However, the affinity diagrams do not provide insights into the usefulness or value of the information items. In order to validate the information identification study, a

sensitivity analysis was performed on the identified damage parameters to assess the value of information of each parameter. The analysis utilized an implementation of the seven common damage modes for reinforced concrete as a rule based system in Java programming language, according to FEMA 306.

The validation focused on reinforced concrete components (piers and spandrels). Inside each Level 2 group for reinforced concrete walls, there are eighteen information items that could be used to distinguish the damage modes and severities (Table 3-3). The combinations of these information items and the values they take determine the damage mode and the severity of a component. A rule-based system was implemented, which takes the eighteen parameters as an input and outputs the damage severities for all possible damage modes. The rule-based system follows the damage descriptions for reinforced concrete walls in the Chapter 5 of the FEMA 306. Every damage mode is implemented according to the descriptions in the guideline. The damage modes and damage severities are considered independently. Hence, given eighteen parameters, which describe the damage condition of a component, the rule engine returns an answer for each damage severity of each damage mode.

Some improvements were considered, when implementing the rule-based system. The damage descriptions in the FEMA 306 result in false positives, if they are implemented as they are given. For example, at insignificant severity of the ductile flexural damage mode, shear and flexural crack width limits are given along with the fact that there should be “no significant residual displacement”. When ductile flexure damage mode (A) is implemented by defining only these three cases, every case that contains these three conditions (shear crack width is smaller than the limit; flexural crack width is smaller

than the limit; and no residual displacement), the rule set returns true, even if the case has other damage indicators that do not belong to ductile flexure (e.g., concentrated shear crack).

Table 3-6 The damage modes and severities for every damage mode was implemented according to the descriptions in FEMA 306. Table shows the rules as given in FEMA 306 and the corresponding damage parameters for the Insignificant severity of the ductile flexure mode (A). In order to avoid false positives, damage parameters, which do not belong to the insignificant A damage, have been set accordingly.

| Insignificant A (FEMA 306) | Corresponding implementation | Additional rules for Insignificant A |
|--|------------------------------|--|
| No shear width exceeds 4.8 mm | maxFlex <= 4.8 mm | isBoundaryRebarDamage = false |
| No shear crack exceed 3.2 mm | maxShear <= 3.2 mm | isRebar = false |
| No significant spalling or vertical cracking | maxVert = 0 | displacementSignificance < 2 |
| | isSpalled = FALSE | isShearConcentrated = false isFlexuralConcentrated = false isBoundaryCrushed = false |

In order to avoid false positives, the damage modes were implemented in a way that considers the exclusion of the damage indicators that do not belong to the damage modes (Table 3-6). For example, for the ductile flexural damage mode (A), all of the damage severities exclude concentrated shear cracks, since such shear cracking cannot exist for a ductile flexural mode.

The accuracy of the rule-based system was verified using an actual damaged building. The eighteen damage parameters for each of the forty-two wall components composed of reinforced concrete piers and spandrels were generated semi-automatically from hand-sketches. Twelve of the forty two components were coupling beams and failed in pre-emptive shear with severities ranging from Insignificant to Heavy [25]. The rest of the

thirty components have insignificant damage as a result of overturning. Per the analogy explained in FEMA 307, the prototype used the ductile flexural mode's description to assess the severity of the overturning behavior visually. The prototype implementation correctly identified the damage modes and severities of all of the forty-two components correctly, which verified the accuracy of the implementation.

Table 3-7 Eighteen parameters have been identified based on the affinity diagrams and the damage descriptions, that help determine the damage mode and severity.

| Affinity Diagram Group | Description | Parameter name | Range of error |
|-------------------------------|--|--------------------------|--|
| Crack point property | | | |
| | Maximum flexural crack width | maxFlex | -2.0 - +2.0 mm with 0.5 mm increments |
| | Maximum vertical crack width | maxShear | -2.0 - +2.0 mm with 0.5 mm increments |
| | Maximum flexural crack width | maxVert | -2.0 - +2.0 mm with 0.5 mm increments |
| Crack path property | | | |
| | Existence of a sliding crack and the severity of offset on the sliding plane | slidingSignificance | 0: no sliding crack 1: slight offset along the sliding crack 2: significant offset along the sliding crack |
| Crack pattern property | | | |
| | Existence of a concentrated shear crack | isShearConcentrated | T/F |
| | Existence of a concentrated flexural crack | isFlexuralConcentrated | T/F |
| Damage Location | | | |
| | Maximum shear crack width in the toe region | maxShearInToe | -2.0 - +2.0 mm with 0.5 mm increments |
| | Maximum shear crack width in the web region | maxShearInWeb | -2.0 - +2.0 mm with 0.5 mm increments |
| | Existence of vertical cracks in the toe | isToeVerticallyCracked | T/F |
| | Existence of spalling in the toe region | isToeSpalled | T/F |
| | Existence of spalling in the web region | isWebSpalled | T/F |
| | Severity of spalling in the web region | spallingWebSeverity | 0: no spalling in web 1: slight spalling in web 2: significant spalling in web |
| | Severity of the spalling in the toe region | spallingToeSeverity | 0: no spalling in toe 1: slight spalling in toe 2: significant spalling in toe |
| | Existence of rebar damage in the boundary region | isBoundaryRebarDamaged | T/F |
| | Existence of boundary crushing | isBoundaryCrushed | T/F |
| Damage Quantity | | | |
| | Existence of spalling | isSpalled | T/F |
| | Existence of rebar damage | isRebarDamaged | T/F |
| | Severity of residual displacement | displacementSignificance | 0: no residual displacement 1: slight residual displacement 2: significant residual displacement |

The identified information items for reinforced concrete were validated by analyzing the sensitivity of damage assessment to changes in the damage parameter values. The sensitivity analysis measured the value of information as the ratio of error in the damage assessment to error in the value of each parameter. Base configurations for insignificant, slight, moderate, heavy, and extreme cases were generated for every damage mode based on FEMA 306 (Table 3-9). The ranges of values of the damage parameters were determined based on the values in FEMA 306. The maximum crack sizes for the baseline configurations were selected arbitrarily within FEMA's range of values.

Table 3-8 The assessment results for the base configuration of insignificant ductile flexural damage (RC1A). The base configuration is checked against all damage modes and severities. It can be seen that the base configuration also conforms insignificant D and E type of damage.

| Damage Mode/Severity | Assessment | Damage Mode/Severity | Assessment |
|---|------------|--|------------|
| A (Ductile flexural) & M/N (Pier/wall rocking) | | D (Flexure/Sliding shear) | |
| Insignificant | True | Insignificant | True |
| Slight | False | Slight | False |
| Moderate | False | Moderate | NotUsed |
| Heavy | NotUsed | Heavy | False |
| Extreme | False | Extreme | False |
| B (Flexure/Diagonal tension) | | E (Flexure/Boundary-zone compression) | |
| Insignificant | False | Insignificant | True |
| Slight | NotUsed | Slight | False |
| Moderate | False | Moderate | False |
| Heavy | False | Heavy | False |
| Extreme | False | Extreme | False |
| C (Flexure/Diagonal compression) | | H (Preemptive shear) | |
| Insignificant | False | Insignificant | False |
| Slight | NotUsed | Slight | NotUsed |
| Moderate | False | Moderate | False |
| Heavy | False | Heavy | False |
| Extreme | False | Extreme | False |

In total, twenty-five base configurations were created. In each run, a known amount of error was introduced to one of the eighteen parameters. For crack widths, the error is measured in millimeter from the baseline value. For binary values (e.g., isSpalled), introducing an error converts True to False and vice versa. For the severity type of

parameters (e.g., displacementSignificance, spallingWebSeverity), the error is represented with an integer value with in the -2, +2 range. When changing the value of a parameter, other affected parameters are also changed. For example, setting the “existence of spalling in the toe region” to TRUE, also sets the “existence of spalling” to TRUE. The opposite is not true, since spalling can occur at other regions other than the toe region. The eighteen parameters are varied one at a time for every baseline configuration. The variations were fed into the verified rule-based system. The value of the information items were calculated for every baseline configuration and averaged over all damage modes.

Table 3-9 Base configurations used in the simulations for ductile flexure (A).

| Damage parameter | A (Ductile Flexural) | | | |
|--------------------------|----------------------|--------|----------|---------|
| | Insignificant | Slight | Moderate | Extreme |
| maxShear | 3.0 | 3.0 | 4.0 | 4.0 |
| maxFlex | 4.0 | 6.0 | 6.0 | 8.0 |
| maxVert | 0.0 | 0.0 | 1.0 | 2.0 |
| slidingSignificance | 0.0 | 0.0 | 0.0 | 0.0 |
| isShearConcentrated | FALSE | FALSE | FALSE | FALSE |
| isFlexuralConcentrated | FALSE | FALSE | FALSE | TRUE |
| maxShearinToe | 0.0 | 0.0 | 0.0 | 0.0 |
| maxShearinWeb | 0.0 | 3.0 | 4.0 | 4.0 |
| isToeVerticallyCracked | FALSE | FALSE | TRUE | TRUE |
| isToeSpalled | FALSE | FALSE | TRUE | TRUE |
| isWebSpalled | FALSE | FALSE | FALSE | TRUE |
| spallingWebSeverity | 0.0 | 0.0 | 0.0 | 1.0 |
| spallingToeSeverity | 0.0 | 0.0 | 1.0 | 2.0 |
| isBoundaryRebarDamaged | FALSE | FALSE | FALSE | TRUE |
| isBoundaryCrushed | FALSE | FALSE | FALSE | FALSE |
| isSpalled | FALSE | FALSE | TRUE | TRUE |
| isRebarDamaged | FALSE | FALSE | FALSE | TRUE |
| displacementSignificance | 0.0 | 0.0 | 1.0 | 2.0 |

For every configuration, a results vector was computed, which indicates the change in the results from the base configuration (Table 3-10). The vector quantifies the error in the damage severity assessment for the error in parameter values. For example, in an insignificant ductile flexure damage, where the actual flexural crack width is 4.0 mm and

there is an error of -1.0 mm, then, all other parameters kept constant, it may indicate a moderate pre-emptive shear behavior and no change in the other damage modes (Table 3-10).

The sensitivity of the damage assessment to the change in the value of a parameter is calculated as the error in the parameter value divided by the magnitude of the severity change. The change in damage severity was quantified in a 0 to 5 scale, where 0 represents no change in the given mode and 5 represents a jump from none to extreme severity or from extreme to none. In the example in Table 3-10, the severity for H (pre-emptive shear) changed from no-damage to moderate, jumping over insignificant and slight severities, which corresponds to a change in severity of magnitude 3.

Table 3-10 For every variation in the configuration, the change in the results are recorded in a results vector. Zero indicates no change in severity from the base configuration as a result of the variation.

| Damage Mode | maxFlex | | Result |
|-------------|---------------|-------------------|---------------------------|
| | Base Conf. | Test Case (error) | |
| | 4.0 mm | -1.0 mm | |
| A | Insignificant | Insignificant | 0 |
| B | No Damage | No Damage | 0 |
| C | No Damage | No Damage | 0 |
| D | Insignificant | Insignificant | 0 |
| E | Insignificant | Insignificant | 0 |
| H | No Damage | Moderate | $\frac{ -1 }{ 3 } = 0.33$ |

The values in all 25 variations are then averaged and aggregated into a single table (Table 3-11). Each column in the table represents a damage mode, such that the sensitivity of the damage assessment to perturbations in the values of each parameter can be observed for each mode individually. The rows in the table correspond to the errors in the parameter values. Thus, each cell represents the sensitivity of the severity assessment for a damage mode for given amount of error in the parameter value (e.g., maximum shear crack size).

Zero means that the assessment is insensitive to errors. Larger values represent higher impact to the assessment.

The results show that some of the parameters had minimal or no effect on the classification of the damage severity. Maximum vertical crack width (maxVert) has no effect on the classification of damage. Maximum width of the shear cracks in the toe region had minimal effect if the width of the cracks is underestimated by 2 millimeters. Maximum width of the shear cracks in the web regions also had small effect. However, maxShearInToe and maxShearInWeb contribute to determining the damage severities. On the other hand, since maxVert does not impact the damage classification, it can be eliminated.

The damage modes have varying sensitivities for the damage parameters. For example, flexure/diagonal tension (B) mode is much more sensitive to errors in the maximum width of shear cracks compared to pre-emptive shear (H) mode. Flexure/diagonal tension develops shear cracks more steadily compared to the pre-emptive mode. Shear cracks can open up to about 0.8 mm for insignificant severity and up to 1.6 and 3.2 mm for moderate and heavy severities, correspondingly. On the other hand, the pre-emptive shear mode develops a concentrated shear crack suddenly, as the heavy damage severity is reached. Thus, higher sensitivity of the H mode to isShearConcentrated can be observed Table 3-11.

Table 3-11 Sensitivity of the damage modes to errors in the damage parameters. Higher the number, higher the sensitivity of the damage mode to misclassification of the damage parameter. The analysis shows that maximum vertical crack width has no effect on the classification of the damage and severity. The other parameters have varying degree of impact on the classification.

| Parameter | Size of Error | Average Change in Severity Assessment | | | | | |
|--------------------------|---------------|---------------------------------------|------|------|------|------|------|
| | | A | B | C | D | E | H |
| maxShear | -2.0 | 0.00 | 0.48 | 0.06 | 0.00 | 0.00 | 0.04 |
| | -1.5 | 0.00 | 0.64 | 0.08 | 0.00 | 0.00 | 0.05 |
| | -1.0 | 0.00 | 0.24 | 0.00 | 0.00 | 0.00 | 0.08 |
| | -0.5 | 0.00 | 0.00 | 0.00 | 0.00 | 0.00 | 0.00 |
| | 0.5 | 0.24 | 1.36 | 0.64 | 0.24 | 0.24 | 0.16 |
| | +1.0 | 0.36 | 0.72 | 0.36 | 0.36 | 0.36 | 0.08 |
| | +1.5 | 0.24 | 0.48 | 0.24 | 0.24 | 0.24 | 0.05 |
| | +2.0 | 0.22 | 0.46 | 0.20 | 0.22 | 0.22 | 0.12 |
| maxFlex | -2.0 | 0.30 | 0.30 | 0.00 | 0.06 | 0.30 | 0.30 |
| | -1.5 | 0.48 | 0.40 | 0.00 | 0.08 | 0.48 | 0.40 |
| | -1.0 | 0.12 | 0.00 | 0.00 | 0.00 | 0.12 | 0.60 |
| | -0.5 | 0.24 | 0.00 | 0.00 | 0.00 | 0.24 | 0.00 |
| | 0.5 | 1.44 | 1.20 | 0.48 | 0.48 | 1.44 | 0.32 |
| | +1.0 | 0.92 | 1.04 | 0.32 | 0.44 | 0.92 | 0.16 |
| | +1.5 | 0.61 | 0.69 | 0.21 | 0.29 | 0.61 | 0.11 |
| | +2.0 | 0.50 | 0.56 | 0.20 | 0.26 | 0.50 | 0.08 |
| maxVert | -2.0 - +2.0 | 0.00 | 0.00 | 0.00 | 0.00 | 0.00 | 0.00 |
| isSpalled | 1 | 0.52 | 0.16 | 0.16 | 0.68 | 0.52 | 0.12 |
| isToeVerticallyCracked | 1 | 0.40 | 0.16 | 0.16 | 0.52 | 0.40 | 0.12 |
| spallingWebSeverity | -2 | 0.00 | 0.26 | 0.22 | 0.08 | 0.00 | 0.00 |
| | -1 | 0.00 | 0.52 | 0.44 | 0.16 | 0.00 | 0.00 |
| | 1 | 0.52 | 0.68 | 0.32 | 0.52 | 0.52 | 0.12 |
| | 2 | 0.26 | 0.34 | 1.20 | 0.26 | 0.26 | 0.06 |
| spallingToeSeverity | -2 | 0.04 | 0.00 | 0.00 | 0.08 | 0.04 | 0.00 |
| | -1 | 0.08 | 0.00 | 0.00 | 0.16 | 0.08 | 0.00 |
| | 1 | 0.76 | 0.16 | 0.16 | 0.52 | 0.76 | 0.12 |
| | 2 | 0.38 | 0.08 | 0.08 | 0.26 | 0.38 | 0.06 |
| slidingSignificance | -2 | 0.00 | 0.00 | 0.10 | 0.10 | 0.00 | 0.00 |
| | -1 | 0.00 | 0.00 | 0.00 | 0.20 | 0.00 | 0.00 |
| | 1 | 1.40 | 1.28 | 0.60 | 1.88 | 1.56 | 0.68 |
| | 2 | 0.70 | 0.64 | 0.30 | 1.56 | 0.78 | 0.34 |
| isToeSpalled | 1 | 0.64 | 0.16 | 0.16 | 0.56 | 0.64 | 0.12 |
| isBoundaryRebarDamaged | 1 | 1.40 | 1.48 | 0.60 | 0.52 | 1.56 | 0.88 |
| isBoundaryCrushed | 1 | 1.40 | 1.28 | 0.60 | 0.72 | 1.56 | 0.68 |
| isRebarDamaged | 1 | 1.40 | 1.04 | 0.80 | 0.68 | 1.56 | 0.44 |
| displacementSignificance | -2 | 0.20 | 0.00 | 0.00 | 0.00 | 0.20 | 0.00 |
| | -1 | 0.40 | 0.00 | 0.00 | 0.00 | 0.40 | 0.00 |
| | 1 | 0.48 | 0.40 | 0.16 | 0.00 | 0.64 | 0.16 |
| | 2 | 0.50 | 0.54 | 0.16 | 0.26 | 0.58 | 0.24 |
| maxShearinToe | -2 | 0.00 | 0.00 | 0.00 | 0.08 | 0.00 | 0.00 |
| | -1.5 - +2.0 | 0.00 | 0.00 | 0.00 | 0.00 | 0.00 | 0.00 |
| maxShearinWeb | -2.0 | 0.00 | 0.18 | 0.00 | 0.00 | 0.00 | 0.00 |
| | -1.5 | 0.00 | 0.24 | 0.00 | 0.00 | 0.00 | 0.00 |
| | -1.0 - +2.0 | 0.00 | 0.00 | 0.00 | 0.00 | 0.00 | 0.00 |
| isWebSpalled | 1 | 0.52 | 0.68 | 1.28 | 0.52 | 0.52 | 0.12 |
| isShearConcentrated | 1 | 1.40 | 1.48 | 0.60 | 0.72 | 1.56 | 2.96 |
| isFlexuralConcentrated | 1 | 1.40 | 1.28 | 0.60 | 0.68 | 1.40 | 0.68 |

The validation study showed that the damage state of a reinforced concrete wall can be represented using seventeen damage parameters. The damage parameters include the widths of shear and flexural cracks, locations and/or severities of spalling and crushing, rebar damage and residual displacements.

By averaging the results of the sensitivity analysis for each parameter across all damage modes we can obtain the mean effect of each parameter on the damage assessment (Table 3-12). The mean values clearly show the relative importance of the parameters. Considering the time constraints in the field for data collection, the results can potentially be used to drive the data collection towards on more impacting parameters to make efficient use of resources.

Table 3-12 By averaging the change of damage age assessment across all of the damage modes, the mean effect of each damage parameter on the assessment can be obtained

| Parameter | Average change across all damage modes |
|--------------------------|---|
| maxShear | 0.20 |
| maxFlex | 0.38 |
| maxVert | 0.00 |
| isSpalled | 0.36 |
| isToeVerticallyCracked | 0.29 |
| spallingWebSeverity | 0.28 |
| spallingToeSeverity | 0.18 |
| slidingSignificance | 0.51 |
| isToeSpalled | 0.38 |
| isBoundaryRebarDamaged | 1.07 |
| isBoundaryCrushed | 1.04 |
| isRebarDamaged | 0.99 |
| displacementSignificance | 0.22 |
| maxShearInToe | 0.01 |
| maxShearInWeb | 0.02 |
| isWebSpalled | 0.61 |
| isShearConcentrated | 1.45 |
| isFlexuralConcentrated | 1.01 |

3.7. Conclusions

This chapter identified the information requirements for determining the damage modes and severities of earthquake damaged reinforced concrete walls and coupling beams. The research approach uses the affinity-diagramming method for identifying an abstraction and hierarchy of the information items, which are required for developing a representation. The study is validated by performing a sensitivity analysis on the damage modes and severities. The following conclusions can be drawn from the study:

For both reinforced concrete and masonry walls, cracking is the most important information item for determining the damage mode and severity. Crack width, type, and location are important parameters associated with cracks. For other damage indicators, such as spalling, crushing, and rebar damage, the important parameters are location and severity. Location of damage is defined based on the region on the components (e.g., hinge, web, and toe).

The information items can be grouped under five broader categories, three of which belong to crack properties and the other two describe properties of the other damage indicators, such as spalling, crushing, residual displacement, and rebar damage. The same hierarchy also applies to masonry wall components. Thus, it can be said that although the appearance and the specific parameters for defining damage modes and severities for masonry is different from reinforced concrete, similar patterns of information can be expected.

For reinforced concrete wall components (piers and spandrels), the damaged condition can be represented using 17 parameters. These parameters include, the maximum widths of shear and flexural cracks, existence and/or severity of spalling, crushing, and rebar

damage, severities of residual displacements, sliding on a lateral plane, and concentration of shear and flexural cracks.

The damage modes of reinforced concrete wall components have varying degrees of sensitivity to errors in the 17 damage parameters. The assessment is least sensitive to the width of shear cracks on the web region. Most effective parameters are the concentration of cracks, particularly shear cracks, and damages in the boundary region, such as rebar damage and crushing.

The hierarchies and the damage parameters, which were identified in this study, elucidate two aspects of the visual damage assessment problem. First, the results of the study describe the information content of a potential information model. The objects and the relationship between the objects, which form the information model, can be derived using the affinity diagrams. Second, the types and details of the queries needed to extract the necessary information for performing the damage assessment tasks can be developed using the findings of the study.

Two future research directions are developing a BIM based representation of damage for structural walls and integrating the visual damage assessment with strength analysis by building on the damaged representation.

Chapter 4 Representation of Earthquake Damage for Reinforced Concrete Buildings using Building Information Models

4.1. Introduction

The main goal of the research described in this chapter is to develop a schema to represent the damaged conditions of reinforced concrete walls in order to support the visual assessment tasks for engineering analysis. The information requirements of damaged condition representation were described in Chapter 3. It was found that the damage information on reinforced concrete components can be grouped under five broad categories, three of which are about cracking. The other two groups are about the locations and quantities of the other damage indicators, such as spalling, crushing, rebar damage, and residual displacement. The information requirements for performing the visual assessment tasks will be discussed in more detail in Section 2.

In this chapter, building on the findings of the information requirement identification study, a BIM-based schema is developed for reinforced concrete walls. The information requirements in Chapter 3 were analyzed to design a schema. While the schema was developed with a specific focus on reinforced concrete components, to validate its generality, we have evaluated how well it also supports masonry type of wall components. It is found that the schema can support 54% of the information requirements of the masonry damage. The limitations are mainly due to the damage indicators, which are strictly specific to masonry, such as opening of joints or crushing of mortar between the

masonry units, and falling off of masonry. On the other hand, the schema has the necessary structure to support the queries related to these missing damage indicators, such as the location of damage.

4.2. Information Requirements of Visual Damage Assessment

The information requirements of the visual damage assessment for supporting the engineering analysis, was identified in Chapter 3 using an affinity diagramming approach. The result of the study is the hierarchy of information items, which can be used to describe damage (Table 4-1). Briefly, in order to construct the diagram, statements were extracted from the FEMA 306 guideline, which describe damage for common damage modes and all damage severities. These statements were grouped into four levels. The first level contains the statements.

An emerging pattern in the diagram is that cracking is the most important damage indicator. More than half of the Level 2 statements are about cracking. Widths of various types of cracks (i.e., shear, flexure) are grouped under the point properties of cracks, as the width of the cracks are generally measured at several locations on the cracks. Features, which can be attributed to an entire crack are grouped under the crack path property. These include the degradation of concrete along cracks, lateral offset along a crack (i.e., sliding plane), and continuity of a crack along the cross-section of a component. Cracking properties, which are defined according to the properties of a collection of cracks are grouped under the pattern properties of cracks.

For the other damage indicators, such as spalling and crushing of concrete, rebar damage and residual displacement, the emerging patterns are the damage location and damage quantity. Damage location is defined as a region on the component, such as the hinge

region or web region. The damage severities are either a binary value (i.e., whether there is damage or not), or defined in terms of the severity. The engineer assesses the severity of the damage.

Table 4-1 The affinity diagram for reinforced concrete wall components. Statements were extracted from the FEMA 306 guideline and grouped into four levels in increasing generality. Level 1 contains the individual statements and is hidden for brevity. In the diagram, cracking and crack properties emerge as the most important feature in the diagram, followed by the location and quantity of the other damage indicators.

Reinforced Concrete Walls

| Level 4 | Level 3 | Level 2 |
|--|---------|---------|
| Crack properties | | |
| Crack point property | | |
| Flexural crack size | | |
| Shear crack size | | |
| Any/all crack size | | |
| Crack path property | | |
| Continuity of flexural cracks along component | | |
| Degradation of concrete along cracks | | |
| Amount lateral offset along sliding plane | | |
| Crack pattern property | | |
| Type of concentrated single crack | | |
| Concentration of flexural cracks in the plastic hinge zone | | |
| Properties of other damage indicators | | |
| Damage location | | |
| Spalling or crushing location and amount | | |
| Location of buckled rebars | | |
| Spalling or vertical cracking location | | |
| Damage quantity | | |
| Spalling or vertical cracking | | |
| Residual displacement amount | | |
| Buckled or fractured bars | | |

4.3. Background research

The purpose of this research is to develop a schema to represent information about damage occurred in a building after a major event, such as an earthquake. This is a first step towards a vision to automate the entire damage assessment procedure, including the

strength analyses. This chapter specifically focuses on developing an information model to support the engineering analysis. Given this focus, we have considered, built on and extended previous research studies on automation of damage detection and assessment, and reviewed their respective representation methods for damage parameters.

4.3.1. Representation of Damaged Conditions

Previous studies on the automated damage assessment can be classified based on two consecutive steps associated with the process. As the first step, several studies have attempted to automate the detection of damage parameters using computer vision techniques from 2D or 3D images [7, 27, 28, 31, 32, 34-36, 38, 39, 46, 74]. The main purpose of such studies is to accurately detect damage parameters, such as cracking, spalling, crushing and rebar damage from images. The results of the automated detection are then incorporated into a decision making tool to derive conclusions about the condition of a building [38, 39, 75], which constitutes the second step of the process.

The specifics of the data models for representing damage parameters depend on the decision mechanisms or the purpose of the automation. Most of the studies in the prior work have targeted automating the rapid assessment of structures, within which the main purpose is to classify the building as safe, unsafe, or to allow restricted usage by focusing on the most critical hazards in minimal time and using minimal resources (i.e., time, equipment, personnel). Cracking and spalling are the damage parameters used in these studies. Crack length, width, and orientation are used as the main crack parameters [38, 75]. In the existing image-based damage assessment research, the end results of the damage detection step are damage maps which are images with pixels labeled as damage and non-damage (e.g., [38]).

Using the damage maps, it is possible to extract dimensions of cracks and spalled regions [38]. German et al. (2013) took it a step further by proposing a fragility analysis to assess the vulnerability of the damaged frames, composed of columns and beams, using the results of the image based crack and spalling detection [75]. In the mentioned study, certain damage events, such as longitudinal or diagonal cracking, spalling, and buckling are related to damage indices for columns, such as drifts, based on experimental observations [75]. The damage indices are used, along with the building type and column arrangement, to query fragility curves in order to estimate the probability of experiencing a certain level of damage in an aftershock given the main shock damage. The mentioned study uses a database to link the damage parameters, such as spalling and cracking, to columns, and demonstrates that if the damage indicators can be detected accurately, the damage information can be used along with structural analysis for structural systems.

4.3.2. Building Information Modeling for Damaged Condition Representation

Engineering analysis process involves finding the governing damage modes for components using visual damage indicators and cross-verifying the findings by strength calculations [1, 25]. Within such procedures, it is necessary to perform strength calculations using the reinforcement configuration, material strengths and structural analysis results [1].

From a computational perspective, it is necessary to identify the connected components to determine the extent of the structural sub-assembly, determine the reinforcing bars that contribute to the strength of the components, and use this information, along with internal forces, to calculate the strengths of components. Building Information Models (BIM) can represent such design information and potentially support topological and spatial queries

to find connected components and contained reinforcement bars [13, 19-21, 76]. Design computations can be performed on BIMs, including strength calculations [13]. Earlier studies also showed that structural analysis models can be incorporated within BIMs [20]. Generation of as-is Building Information Model, which represents existing conditions of buildings and using as-is BIMs to support various engineering decisions are becoming common practices [10, 23, 77]. However, current BIMs build on design centric modeling approaches [78]. Geometries are often assumed to be perfect and representing imperfections, such as deformed shapes and damage, is not directly possible [11, 12, 63]. Therefore, it is necessary to formalize representation methods to support the decisions related to the damage assessment. This chapter describes a BIM based damage representation schema using the damage assessment guidelines, and specifically FEMA 306 [1].

4.4. Development of the Schema for Representing Damage Information

In order to develop a representation schema for the damaged conditions, a four-step procedure is followed. First, the unique concepts, which need to be represented are identified. Second, a set of potential entities were identified from the determined requirements. This step is mainly performed on the information items gathered in the first step. Third, the corresponding potential objects are abstracted using object-oriented modeling methods. In other words, the necessary attributes for the objects are determined, objects are decomposed or aggregated together, and relationships and cardinality of the relationships are determined. Finally, design patterns are applied for completing the schema [79].

Crack information is represented using three entities (Figure 4-1). The CrackStation entity represents a point location on a crack. The station attribute represents the location of the crack width measurement. The CrackPath entity represents a crack segment as detected by the computer vision methods or as documented by the inspector in the field. A CrackPath entity is defined by a set of CrackStations and the type of the crack (i.e., flexural, shear, vertical). Crack type is determined by the orientation of the crack.

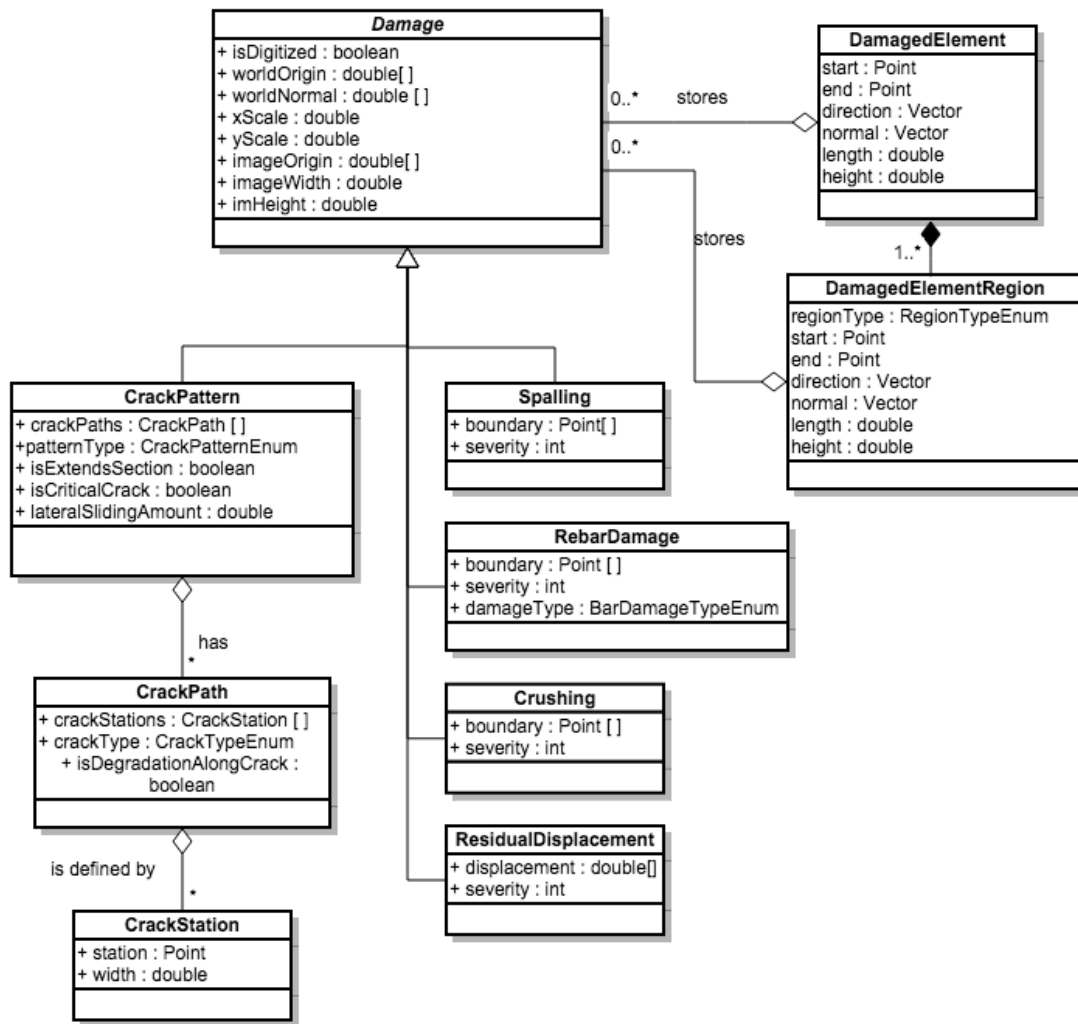


Figure 4-1 The final schema is developed by integrating the requirements of each damage parameter.

CrackPattern entity, which is a collection of CrackPaths, is at the top-most level of the crack representation. Introducing such a container entity has three purposes. First, cracks are sometimes only visible in pieces. Second, if vision sensors are used, cracks cannot always be detected as a single continuous piece [74]. Due to the limitations of the imaging device, algorithms used in the detection, or lighting conditions, discontinuities can occur [27, 32, 38]. Additionally, there may be occlusions that cover the cracks partially [25]. Finally, CrackPattern entity supports representing and analyzing

collections of cracks for the concentration of the cracking damage and sliding shear types of damage as required by the damage parameters.

In order to represent and analyze sliding cracks and concentration of cracks, the schema needs the capability to represent crack patterns composed of several cracks. Sliding cracks are composed of at least two cracks. As a result of the gravity loads some portion of the crack may close up, however sliding cracks are thought of as a single damage. Within the CrackPattern entity, several attributes represent the condition of the crack. IsExtendsSection attribute determines whether a crack is extending from one side of the wall section to the other. If the CrackPattern has a critical sliding section, then IsCriticalSection attribute is set to true. If there is spalling or degradation along the cracks in the CrackPattern, then IsDegradationAlongCrack is set to true. If it is a critical sliding crack, lateralSlidingAmount defines the amount of sliding observed at the critical plane.

Concentration of the crack is defined as having two or a few cracks on the component that are larger than the others. For example, in the heavy to severe cases of ductile flexural damage, it is expected to have at least one flexural crack that is larger than the other flexural cracks and all of the shear cracks in the plastic hinge region, where the bending actions concentrate [1]. FEMA 306 does not specify crack width limits for crack concentration and leaves the decision as to what is considered a concentrated crack to the engineer.

The other damage indicators are Spalling, Crushing, RebarDamage, and ResidualDisplacement. Spalling and Crushing have defining boundaries. The severity of the spalling and crushing are represented by an integer value. Possible values of the severity are 0 (e.g., no spalling), 1 (insignificant), and 2 (significant). Using integers as

opposed to using enumerations allow comparing the severity of damage. There are no established quantification for the severity of spalling and crushing [1]. The decision is mainly left to the engineer. However, researchers suggested using the area of spalling as a measure of the severity [75]. The boundary attribute enables calculating the area of spalling.

The `DamagedElement` represents the entire analysis surface of a component (Figure 4-2). If the flanges are considered as a part of a building component, then the `DamagedElement` also spans the flanges at the center of the wall. The visual damage assessment only requires a 2D representation. Therefore, the `DamagedElement` entity is a 2D entity located at the center axis of the wall. `DamagedElementRegion` entities are located on the same plane as the containing `DamagedElement`.

The `DamagedElementRegion` entity represents regions on the components (Figure 4-1). Plastic hinge regions are generally thought of as extending from one side of the component to the other. For a constant cross-section component, this gives a rectangular region. Similarly, boundary and web regions are rectangular. Thus, the regions are modeled as being rectangular in shape. The types of the regions are enumerated as `PlasticHinge`, `Web`, `Boundary`, and `Toe`.

In summary, in order to represent damage on reinforced concrete walls, it is proposed that the component geometry be simplified to a planar representation and regions on the components be represented as planes attached to the simplified geometry. The `DamagedElement` entity can be linked to the existing BIM standards by associating the `DamagedElement` to the structural components. In the case of IFC, it is proposed that the `DamageElement` be linked to `IfcBuildingElement`, which represents the superclass of all

building elements, including walls. The representation of the damage is, thus, related to the building components through the DamageElement entity.

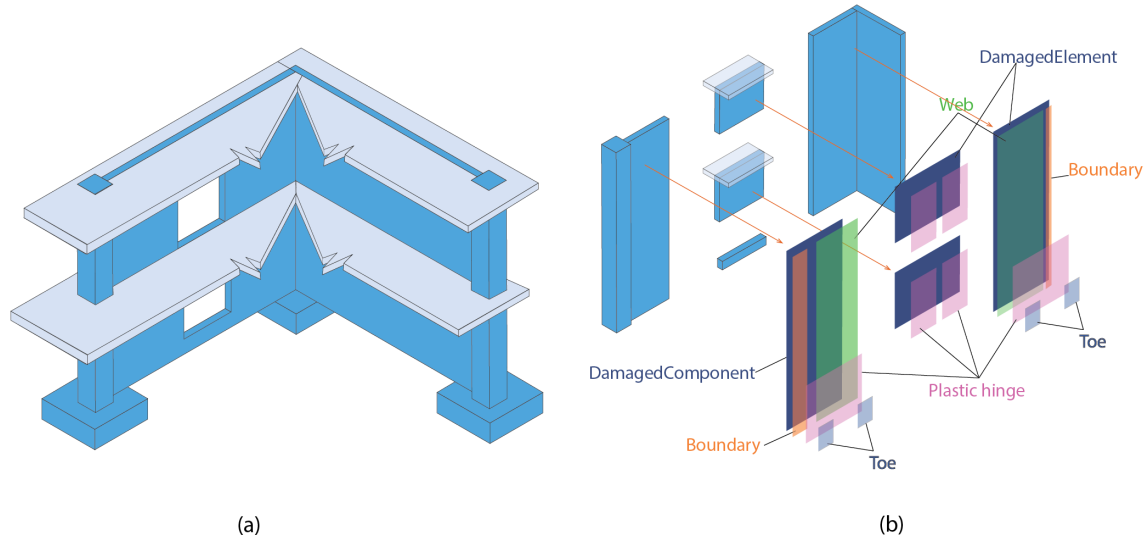


Figure 4-2 The assembly of components, which resists the earthquake forces can contain a variety of structural components, such as piers, slabs, columns, beams (a). For the damage assessment, the component assemblies are divided into segments based on their type of contribution into the non-linear mechanism (e.g., coupled pier mechanism). The DamagedElement entity represents these segments with a 2D slice across the main wall axis (b). The DamagedElementRegion entity is placed on the same plane with the DamagedElement and represents the regions on the components.

4.5. Validation

The developed representation schema for reinforced concrete walls was validated from two perspectives: 1. Coverage of the damage parameter space on a case study, 2. Generality to support the representation of damage on masonry walls.

4.5.1. Coverage of the parameter space for a damaged RC building

The representation capability of the schema for reinforced concrete walls, a model of a damaged building was built using the schema and the model was ran through an implementation of the damage modes, which are described in FEMA 306.

The building is a two-story reinforced concrete structure, which was built in the 1950s [25]. Shear walls resist the lateral forces in both directions. Some of the walls have openings for doors. The building was damaged during an earthquake and professionally evaluated. The damage modes of the twelve coupling beams are pre-emptive shear with severities ranging from Insignificant to Heavy [25]. The rest of components (e.g., wall piers) have insignificant damage as a result of overturning, which is similar to ductile flexure in appearance [25]. In total, 42 piers and spandrels were analyzed in the system.

4.5.1.1. Rule-based System for Visual Assessment

In order to validate the schema for generality, a rule-based system, which is an implementation of the damage modes in FEMA 306 was used. The rule-based system is developed based on the findings of the affinity diagramming study, described in Chapter 3, and the FEMA 306 guideline. In the system, the visual damage state of a component is represented using 17 damage parameters (Table 4-2). The system takes the values of the 17 parameters as the input and outputs the potential damage modes and severities for building components.

Table 4-2 Seventeen parameters have been identified based on the affinity diagrams and the damage descriptions, that help determine the damage mode and severity.

| Affinity Diagram Group | Description | Parameter name |
|-------------------------------|--|--------------------------|
| Crack point property | | |
| | Maximum flexural crack width | maxFlex |
| | Maximum shear crack width | maxShear |
| Crack path property | | |
| | Existence of a sliding crack and the severity of offset on the sliding plane | slidingSignificance |
| Crack pattern property | | |
| | Existence of a concentrated shear crack | isShearConcentrated |
| | Existence of a concentrated flexural crack | isFlexuralConcentrated |
| Damage Location | | |
| | Maximum shear crack width in the toe region | maxShearInToe |
| | Maximum shear crack width in the web region | maxShearInWeb |
| | Existence of vertical cracks in the toe | isToeVerticallyCracked |
| | Existence of spalling in the toe region | isToeSpalled |
| | Existence of spalling in the web region | isWebSpalled |
| | Severity of spalling in the web region | spallingWebSeverity |
| | Severity of the spalling in the toe region | spallingToeSeverity |
| | Existence of rebar damage in the boundary region | isBoundaryRebarDamaged |
| | Existence of boundary crushing | isBoundaryCrushed |
| Damage Quantity | | |
| | Existence of spalling | isSpalled |
| | Existence of rebar damage | isRebarDamaged |
| | Severity of residual displacement | displacementSignificance |

The implementation of the rules followed the damage descriptions in FEMA 306. All seven common damage modes and applicable severities for these seven modes were implemented. The implemented damage modes are: ductile flexure, pre-emptive shear, flexure/diagonal tension, flexure/web compression, flexure/sliding shear, global rocking, individual pier rocking. More details and an evaluation of the rule-based system is described in Chapter 3.

4.5.1.2. The Results

For the validation, the damage parameters of the components in the case study building were input into the system manually. The cracks and other damages were traced using a Matlab script from hand-sketches. The known dimensions of the reinforced concrete components were used to represent the elements. The registration of the damages with the damaged elements and regions were achieved by spatially intersecting the damage coordinates with the element and region boundaries.

The schema made representing complex cracks possible through the CrackPattern, CrackPath, and CrackStation entities. The building had many examples of partially occluded cracks (Figure 4-3a). Additionally, parts of the crack can close up under loads or may be invisible due to small width. In such cases, parts of a single crack can be aggregated into a single pattern by listing the CrackPaths in a CrackPattern object (Figure 3a).

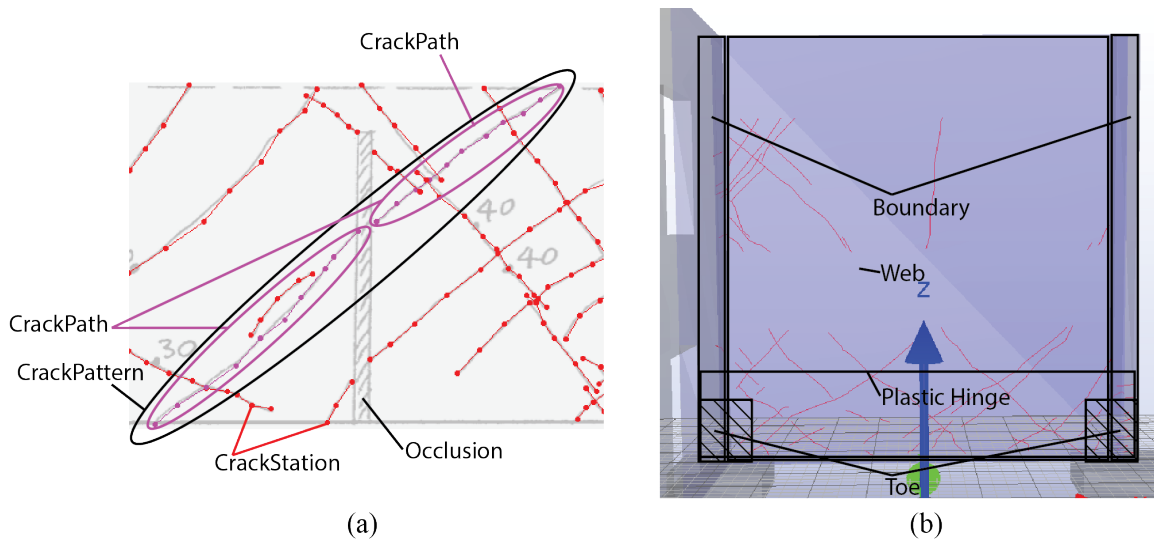


Figure 4-3 The CrackPattern and CrackPath entities enable representing complex cracking on the components (a). Continuity of cracks across occlusions or cracks, which should be evaluated together (e.g., X-shaped cracks) were represented using the CrackPattern entity. For the visual assessment, the regions, which contain the damages were represented using the DamageElementRegion entity (b).

The DamagedElementRegion and the Damage entity enabled locating and querying the properties, such as the severity and the types of damage on the component (Figure 4-3b). Many cracks also extended multiple regions, such as hinge and web. Using the DamagedElementRegion entity together with CrackPattern allowed querying the schema for the accurate locations of cracks.

The rule-based system identified the damage modes and severities of all of the coupling beams and the wall piers. The accuracy of the results indicates that the schema represented the damage successfully for the given building, which contains various severities of pre-emptive shear and overturning type of behavior, which is similar to ductile flexure in appearance [25].

4.5.2. Generality

The validation of generality was performed on the affinity diagram, which was developed for representing damage on masonry components previously in Chapter 3. The generality

of the schema was quantified in terms of how much of the masonry damage parameters can be supported by the schema (Table 4-3).

Table 4-3 The affinity diagram for masonry components show similar patterns at Level 3 and Level 4. In addition to the Level 3 groups in reinforced concrete, masonry requires representing the movement modes. The table also shows the number of statements extracted from the FEMA 306 guideline for masonry damage.

| Masonry | | | Statement Count | Supported | Needs Extension |
|---------------------------------------|--------|---|-----------------|-----------------|-----------------|
| Level4 | Level3 | Level2 | | | |
| Crack properties | | | | | |
| Crack point property | | | | | |
| | | Size of cracks | 5 | x | |
| | | Size of opening of head joints | 5 | | x |
| | | Sliding/opening of bed joints | 13 | | x |
| Crack path property | | | | | |
| | | Spalling and unit damage along cracks | 9 | x | |
| | | Cracks go through units | 9 | | x |
| | | Sliding off supporting bricks along crack | 3 | | x |
| | | Amount of offset along cracks | 13 | x | |
| Crack pattern property | | | | | |
| | | Continuity of horizontal cracks | 2 | x | |
| | | Continuity of diagonal cracks | 2 | x | |
| | | Patterns of cracks | 10 | x | |
| | | Location of concentrated cracks | 3 | x | |
| | | Type of concentrated cracks | 2 | x | |
| | | Type and number of cracks in a region | 4 | x | |
| | | Amount of cracked courses in units | 6 | | x |
| Properties of other damage indicators | | | | | |
| Damage location | | | | | |
| | | Location of brick crushing | 12 | | x |
| | | Location of mortar crushing | 3 | | x |
| | | Location of cracking of bed joints and spalling | 13 | x | |
| | | Location of cracks with various orientations | 20 | x | |
| | | Location of regional crushing | 5 | x | |
| | | Location of falling masonry | 3 | | x |
| | | Location of spalling of face shells | 2 | | x |
| | | Mortar separation around perimeter | 2 | | x |
| | | Crushing of mortar and bricks around perimeter | 3 | | x |
| | | Location of movement of face shells | 2 | | x |
| Movement modes of components | | | | | |
| | | Type and existence of total walking of piers | 4 | | x |
| | | Existence of total movement of spandrels | 5 | | x |
| | | Existence of partial out-of-plane movement of walls | 1 | | x |
| | | Existence of partial rotation of component | 2 | | x |
| Total | | | 163 | 88 (54%) | 75 (64%) |

- *Crack point properties:* In addition to the widths of different types of cracks, masonry damage include opening of head and bed joints of masonry units. Width of cracking on masonry can be represented in the same manner as in reinforced concrete. However, in order to represent the opening of head and bed joints, the schema that is developed for reinforced concrete should be extended.
- *Crack path properties:* Spalling or unit damage along crack paths and offset along cracks can be represented using the reinforced concrete schema using the `isDegradationAlongCrack` and `lateralSlidingAmount` attributes. However, masonry damage also requires representing cracks, which go through masonry units and sliding of an upper portion of a wall off the lower portion. These cannot be represented without extending the schema developed for reinforced concrete.
- *Crack pattern properties:* All of the information requirements of crack pattern properties can be satisfied using the reinforced concrete damage schema. However, additional processing is required to extract the amount of cracked courses in masonry units.
- *Damage location:* The reinforced concrete damage schema is mainly limited in representing the information items in this group. The damage indicators, which are specific to masonry, such as brick crushing, masonry crushing, falling of masonry or face shells, and mortar separation, imposes the limitations. However, the schema is capable of representing the location of damage regardless of the type of damage. Therefore, if the schema is extended to represent these types of

damage indicators, the representation of the information items in this group can be supported.

- *Movement modes of components*: The schema is limited in representing all of the information items in this group, since total or partial movement is not expected on reinforced concrete components.

In summary, the schema is capable of representing 12 of the 28 Level 3 group information items, which are required for masonry damage. These Level 3 groups contain 54% of the total statements, which describe damage on masonry. In order to represent the remaining 66% of the information items, which are specific to masonry damage, the schema should be extended.

4.6. Conclusions

This chapter described a schema for the representation of the earthquake damage on reinforced concrete walls. The research approach built on the findings of a previous information requirements identification study on common damage modes and severities of reinforced concrete. The schema is validated from two perspectives. First, the representation capability of the schema was evaluated by performing a case study on a damaged RC building to assess its coverage with respect to reinforced concrete buildings. Second, the generality of the schema was evaluated for representing damages occur on other types of components, such as masonry components.

The schema is capable of representing the damage to reinforced concrete components, such as cracking, spalling, crushing, rebar damage, and displacement. In the development

of the schema, limitations in determining the continuity of cracks, such as due to occlusions are also considered.

The validation showed that the schema is capable of representing all of the damage information, which is required for all severities of pre-emptive shear and lower severities of the other damage modes. The validation also showed that the schema can be used to represent masonry damage, if new entities for the damage indicators, which are specific to masonry are defined. Representation of many cracking properties and location of the other damage indicators is readily available. In total, 54% of the Level 3 groups inside the affinity diagram for masonry components are supported by the schema.

Chapter 5 Building Information Modeling Based Earthquake Damage Assessment for Reinforced Concrete Walls

5.1. Introduction

This chapter describes a Building Information Modeling (BIM) based approach developed for automating the engineering analyses by integrating the visual assessment and strength analysis. In the developed approach, a BIM, which is assumed to contain structural analysis models, building geometry and configuration, material properties, and reinforcement details, is supplemented with damage records, as required by FEMA 306. The developed approach utilizes such a BIM to perform the engineering analysis for reinforced concrete walls. The transformation mechanisms for extracting the required information from BIM for performing strength analysis and visual assessment are studied in this chapter. These mechanisms include identification of piers and spandrels, determination of cross-sectional properties of connected components, identifying the effective reinforcement amounts and internal forces. Building on the information requirements for visual assessment and the damage representation schema (Chapter 3 and Chapter 4), this chapter elaborates on the strength analysis aspect and combines the visual assessment results and the strength analysis to determine the damage mode and severities of reinforced concrete wall components.

In order to validate the approach, a case study was performed on a previously damaged and professionally assessed structure [1]. The building contains a variety of reinforced concrete walls, such as solid walls and walls with openings. The BIM of the building,

which represents the geometry, reinforcement details, structural analysis results and the digitized hand sketches of the damages of the structural walls, was constructed during the study. A prototype was implemented, which can perform the visual assessment and strength analysis. A total of 42 components including piers and spandrels were assessed and the results obtained using the prototype were compared to the professional assessment.

5.2. FEMA 306, Damage Assessment Procedures

This study focuses on FEMA 306 guideline for the “Evaluation of Earthquake Damaged Concrete and Masonry Wall Buildings”. We have picked this guideline to focus on for three reasons. First, it is the standard document, which the engineers have to follow when assessing the performance of damaged buildings [2]. Second, the guideline builds on a thorough investigation of existing body of research and presents a procedure that can be used for a wide variety of damage modes and component types [2]. Finally, it is being adopted by countries, such as US and New Zealand, thus reaching wider application [3].

The FEMA 306 guideline classifies the results of a wide array of experimental and analytical studies into seven common damage modes and seven other less common modes for reinforced concrete walls [2]. These common damage modes are ductile flexure, flexure/diagonal tension, flexure/diagonal compression, flexure/sliding shear, flexure/boundary compression, pre-emptive tension, and rocking or piers [2].

The damage mode, which requires the smallest lateral force to form is defined as the governing damage mode of a component [2]. For example, initially, the flexural strength of a wall can be lower than the shear strength, thus allowing a flexurally dominated mechanism to form [2]. However, as a result of the degradation of the shear strength at

high displacement demands (i.e., deformations), the shear strength can drop below the flexural strength and dominate the behavior. The combined modes (e.g., flexure/diagonal tension) represent the evolving behavior. Damage severity is the measure of the degradation of the stiffness, strength, and displacement capacity as a result of the earthquake.

Determining the mode and severity correctly is critical in damage assessment. Visual observations of the damage and strength calculations are used together and they allow the engineers to cross-verify their analysis process (e.g., assumptions about component interactions, parameters used in the calculations, etc.) (Figure 5-1).

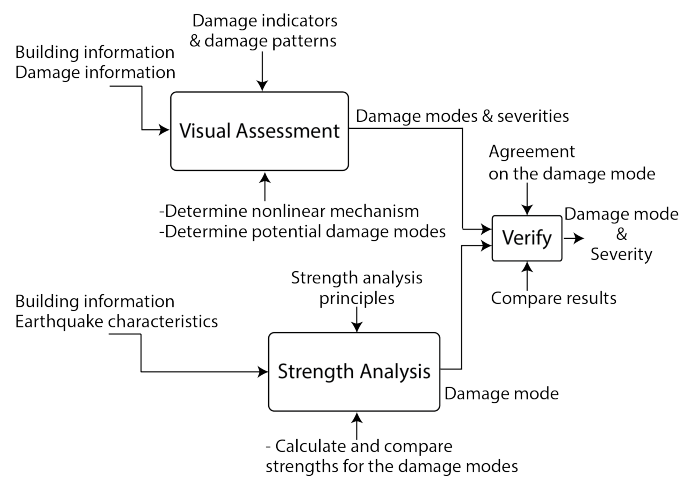


Figure 5-1 FEMA 306 process for determining the damage modes and severities of wall components.

The actual damage behavior of components can differ from theory, which can be determined by strength calculations, due to several reasons, such as differences in material strengths between design and actual, and interactions between building components and loading conditions. The visual observations allow the engineer to determine the actual damage mode of the components by assessing how the damage indicators are formed (e.g., cracking, spalling, crushing, rebar damage, and residual

displacements). However, the visual assessment is not adequate alone to determine the damage mode and severity. A strength analysis is required in addition to the visual assessment. FEMA 306 presents a very detailed analysis of the visual damage indicators for different damage modes.

The strength analysis allows the engineer to determine the theoretical behavior of the wall components. In the strength analysis, the lateral strengths, which would induce different damage modes in terms of minimum shear force, are calculated using strength analysis principles. For example, the shear force, which is required to reach the moment strength can be calculated by first computing the moment strength using strain compatibility equations and dividing the moment strength to the shear span of the component. In order to determine the governing damage mode, the strengths for all possible modes are sorted and the modes, which cannot be reached, are eliminated. Among the remaining damage modes, the mode with the smallest strength governs the behavior.

5.3. Information Requirements of Strength Analysis

The strengths for the damage modes are computed using the material strengths, component geometry, such as the section size and aspect ratio, reinforcement amount and location, and forces on the components, which are obtained from a structural analysis (Figure 5-1) [2, 4, 5]. In the damage assessment procedure, building elements and structural components are distinguished (Figure 5-2). A *component* entails a vertical or a horizontal portion of a building, which resists lateral and vertical loads. An *element* is the assembly of components, such as wall piers, beams, columns and slabs, which resist

forces. For example, a structural wall element with openings is made up of pier and spandrel components.

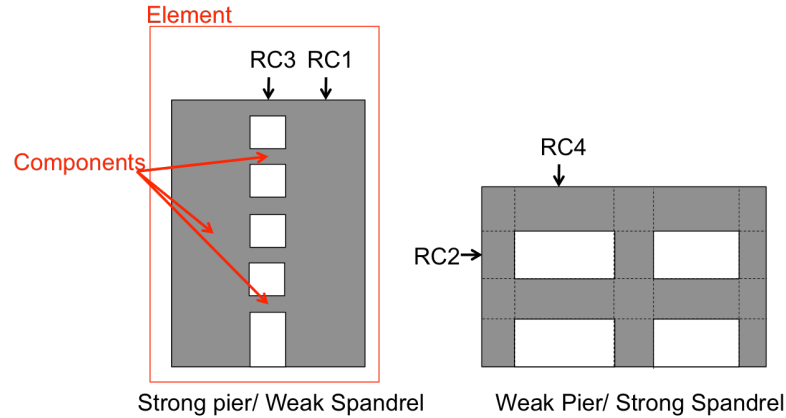


Figure 5-2 In the damage assessment context, an element entails an assembly of components, which resist lateral forces together. A component entails individual piers and spandrels, which make up an element. (RC1: Strong pier, RC2: Weak pier, RC3: weak spandrel, RC4: strong spandrel) [2]

Design codes require proportioning and detailing of components such that the energy is dissipated at the horizontal elements (i.e., beams), while vertical elements (i.e., walls and columns) continue carrying loads [4]. The guideline and seismic evaluation standards call this type of behavior strong pier-weak spandrel (or beam) and code these components as RC1 and RC3, respectively (Figure 2) [2, 5]. Other configurations, such as stronger spandrel-weaker pier (coded as RC2-RC4), can also form in practice. Thus, as a first step of the damage assessment procedure, the behavior classification of each component (whether RC1-RC3 or RC2-RC4) must be determined. This study considered only RC1-RC3 type of behavior as a starting point.

The computation of strengths for the damage modes requires identifying flanged sections, which are formed by connected components, such as the L shaped walls. Calculation of the moment strength involves iterations to find the location of the neutral axis, which satisfies strain compatibility. Thus, actual locations and sizes of longitudinal bars are

needed. The capacities are calculated at critical sections, such as damage regions [2]. For piers, potential damage regions are at the bottom and at each floor level.

| Mode | Material | Component property | Reinforcement | Additional |
|------------------|--|----------------------------|------------------|---|
| M_e | f_{ce}, f_{ye} | $b_w, d, *$ | $A_s, **$ | P, M, V |
| V_n | f_{ce}, f_{ye} | A_{cv}, b_w, h_w, l_w, c | ρ_n, ρ_g | $a_c, \lambda, \alpha, \beta, k_{rc},$ M, V, N_u |
| V_{wc} | f_{ce} | b_w, l_w, A_g | | N_u |
| $V_{sliding}$ | f_{ce}, f_{ye} | l_n, h, b_w, d | A_{vf} | μ |
| Symbols: | | | | |
| M_e | Expected moment strength | | h | Section height. |
| V_n | Nominal shear strength | | α | Coefficient for wall aspect ratio |
| V_{wc} | Web-crushing shear strength | | β | Coefficient for longitudinal reinforcement |
| $V_{sliding}$ | Sliding shear strength | | k_{rc} | Coefficient for ductility demand |
| f_{ce}, f_{ye} | Expected concrete and steel strengths | | μ | Coefficient offriction |
| b_w, d | Section dimensions | | a_c | Coefficient for wall aspect ratio |
| $*$ | Flange dimensions, if flanged | | $**$ | Locations of rebars |
| A_s | Steel area | | P, M, V | Forces on the section |
| A_{cv} | Net area of concrete bounded by the web and the section length | | l_w | Wall length |
| A_g | Gross cross-sectional area | | N_u | Factored axial load |
| l_n | Beam clear span | | | |
| A_{vf} | Area of shear friction reinforcement | | | |

Figure 5-3 In order to determine the damage modes of components, the moment, shear, web crushing, and sliding shear strengths of the components should be calculated. The table shows a breakdown of the capacity equations [2, 4, 5]. The calculations require a large set of information including expected material strengths, component geometries, reinforcement sizes and locations, and forces on the sections.

The damage mode is determined for every component individually. In order to determine the damage modes, strengths for potential damage modes are calculated at the damage regions. In order to compute the component strengths for different damage modes, material properties, component geometry (such as section size, aspect ratio etc.), reinforcement details, and internal forces of the components for different load cases are required. Figure 5-3 summarizes the required parameters or coefficients to compute strengths for different damage modes utilizing the equations given in FEMA 306[5] and ACI 318-11 [34]. The moment strength is calculated using strain compatibility.

Based on these discussions, an engineering analysis requires: 1. Methods of representing all of the necessary information for the strength analysis and the visual assessment, and 2.

Methods for reasoning and transforming the information in order to be able to evaluate several scenarios pertaining to different structural configurations and damaged conditions.

5.4. Background Research

The previous research studies have been investigated from two perspectives. First representation approaches to structural information and damage indicators will be reviewed. Second, transformation methods from information models will be covered.

5.4.1. Representation of Structural Information

5.4.1.1. Structural Analysis Models

Structural analysis oriented methods generally build on mathematical models of behavior of structural systems, such as finite element principles [6]. The geometry and the topology of structures are represented either explicitly or implicitly in finite element representations [6-9]. The material properties of concrete and steel, and damage behavior of the components are captured and represented implicitly in the stiffness matrices and damage models in the form of force-displacement curves [6]. External forces and the response of the system are stored at nodes of the model [9]. Values at intermediate points on the elements are obtained by interpolation of the nodal values.

The results of the finite element analyses can be represented and stored in a variety of formats and media, including dedicated databases, plain text files, or as will be discussed in the next section, in Building Information Models. Regardless of the storage method, the node-element mesh representation is common in all finite element procedures [8].

Structural analysis models are appropriate for storing and querying the forces on nodes or elements, but they are not well-suited for all of the damage assessment tasks. If a

structural component is modeled with a single element, obtaining its internal forces may be a straight forward task. When a wall is modeled with several finite elements, however, getting wall forces require integration of element forces at a specific section which requires additional computations and definitions then typical structural analysis approach. Moreover, structural analysis models may not represent the actual geometry accurately. It is common to grossly simplify the geometry of the structure while maintaining the structural behavior accuracy. Therefore, structural analysis models alone cannot satisfy the needs for representing the geometry and the damaged conditions.

5.4.1.2. Building Information Modeling

Semantically-rich Building Information Models are developed to support architectural design, engineering of the structural, mechanical, and electrical systems, construction activities, and facility operations and management [10]. Extensions have been proposed to the current BIM standards to provide the information necessary to support structural design [11, 12].

Several models exist for representing building information [13-15]. However, existing models are either not developed for reinforced concrete or cannot represent all of the building information, which is required for damage assessment including the damage information. This study used Industry Foundation Classes (IFC) for the representation of the component geometry and reinforcement details, which is an industry standard for building information exchange [13]. IFC is capable of representing building geometry, reinforcement information, structural analysis models, and basic material information as required for the strength analysis.

5.4.2. Transformation Mechanisms

Using models for a purpose other than their original intent requires querying and transforming the model content [16]. In the damage assessment context, the BIM should be transformed into appropriate representations for performing strength calculations and visual assessment. Formalisms have been suggested for the transformation mechanisms of design information into the other stages of projects, such as construction [16]. These transformations include aggregation of components, elaboration of components, introduction of temporary structures, and mapping of relationships between components as the product model changes [16] .

Current BIM standards, support representing relationships, such as spatial hierarchies and links between structural analysis models and building components [13]. However, these spatial relationships are not always implemented in the current BIM generation programs [17]. Therefore, we need to develop transformation mechanisms to determine the relationships between components. Recursive Boolean operations can be used to determine the connections and to divide connected elements into individual entities [18]. Additionally, Boolean operations can be used to for a variety of purposes including computing cross-sections across 3D geometries and finding the containment of elements.

5.5. Approach

The proposed approach for determining the damage modes and severities of structural walls integrates the visual assessment and strength analysis using a Building Information Model as the information source. The proposed approach takes the design BIM and the damage records as input (Figure 5-4). The BIM is assumed to contain the accurate as-is geometry of the building, actual reinforcement details, material properties, and the

internal forces on the components. The damage records may contain the crack paths and widths, spalling, crushing, and rebar damage locations and residual displacements. The information contained in the BIM is used to extract the damage parameters, which are used to perform visual assessment tasks, and to extract the strength parameters, which are used to calculate the strengths of the components for various actions, as outlined in the previous sections.

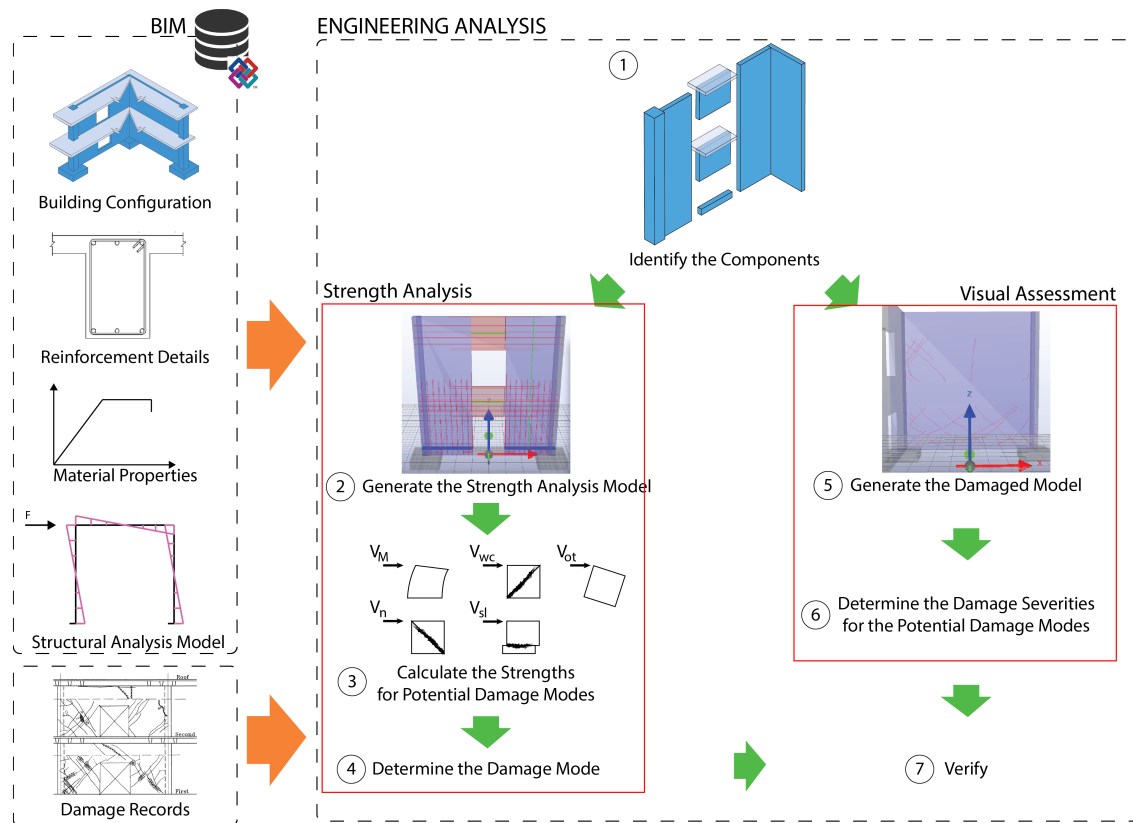


Figure 5-4 The proposed approach takes a BIM and damage records as input. Two analyses, a strength analysis and a visual assessment are performed to determine the damage modes and severities of components.

The identification of the components (i.e., piers and spandrels) is required for both analyses (Figure 5-4). The identification step involves determining the connected components, dividing the components into piers and spandrels, and computing the cross-section properties.

There are often no rules or clear guidelines as to how components should be modeled in a BIM (Figure 5-5). Therefore, the components can be modeled in a number of ways. Walls and columns may or may not be divided at floor levels. A flanged section or a wall with boundary elements can be modeled individually or the entire section can be a single model entity. Determining the cross-section properties requires correctly identifying the connected components and computing the new cross-section formed by the union of the composing elements. There can also be openings on the walls, which may result in a coupled wall mechanism structurally. The coupled wall mechanism consists of piers and spandrels. In order to be able to process the structural behavior of the piers and the spandrels, the wall should be divided into its constituent building components.

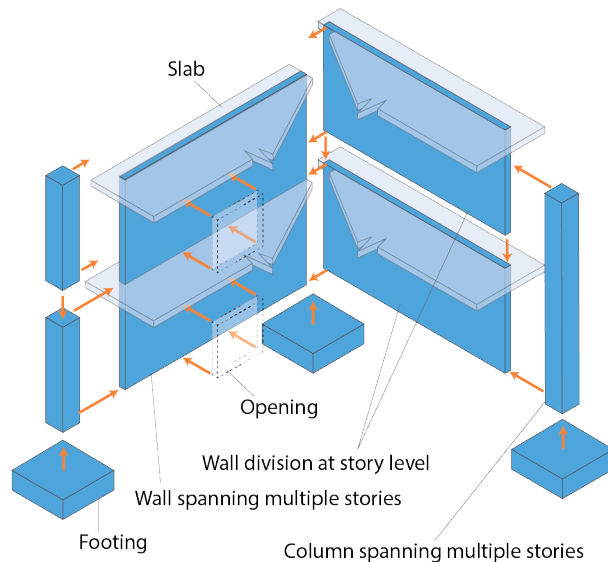


Figure 5-5 A structural wall system can be modeled in a number of ways in a BIM. Components may or may not be divided at floor levels and can contain openings. For a strength analysis of the wall sections, the wall elements should be divided into pier and spandrel components.

Two integrated models are generated using the BIM input and the identified components in the previous stage: strength analysis mode and the damaged model. Strength analysis model stores the structural analysis results for each of the building components (Figure 5-

4, Steps 2 and 5). Additionally, the critical sections, where the strengths are calculated as well as the reinforcing bars at these sections are stored. Critical sections are typically defined at locations where damage is expected. Typical critical sections for piers extending multiple floors are at floor levels and at the base of the pier. The damaged model represents the damage parameters, such as cracking, rebar buckling/fracture, residual displacement and spalling/crushing.

Similar to the FEMA provisions, the main output of the strength analysis step is the governing damage modes for each wall pier and spandrel. The damage mode is determined by the strength analysis where the design forces on each structural component is compared to the strengths for different types of potential damage modes (Figure 5-4, Step 3). The visual damage assessment considers all of the seven common damage modes as equally applicable and determines the damage severity of each mode according to the definitions and limits given in FEMA 306 (Figure 5-4, Step 6). The verification entails comparing the results of the strength analysis and the visual assessment and determining whether the two analyses agree on the results (Figure 5-4, Step 7).

The damage assessment tasks require the generation of the damage schema and the computation of the parameters, which will be required for the strength analysis and the visual assessment. The following sections will discuss the formalization of the steps of the approach. Since the representation of the components along with damage and other structural information, the representation will be discussed first.

5.6. Representation of the Components for Damage Assessment

In order to support the strength analysis and the visual assessment aspects of the damage assessment, two separate representations are integrated. In order to represent the visual

damage assessment parameters, a damage schema is used. The strength calculations are supported through a design and detailing schema, which is capable of performing code-based calculations for checking reinforcement amounts and moment and shear capacities [12].

The strength analysis model contains a `CriticalSection` entity for representing the locations where strengths are calculated on damage regions (Figure 5-6). The `CriticalSection` holds references to the longitudinal bars and the transverse bars passing at that location. In the strength analysis model, a wall pier is represented as a single component from the bottom to the top of the building. `CriticalSections` are generated at the locations, where damage is expected, such as at the bottom of the pier and at floor levels.

The strength analysis model represents one or more critical sections on every component (Figure 5-6). The critical sections are the calculation points, which are needed for the engineering analysis. The critical sections are defined at locations where damage is expected, such as the floor levels of piers. For every critical section a set of shear or moment strengths corresponding to different damages are calculated given the reinforcement at the section, critical section geometry, and forces on the section (Figure 5-3). The internal forces are extracted from the structural analysis model inside the design BIM at the `CriticalSection` locations by interpolating the nodal forces. The `CriticalSection` represents the cross-section geometry. The forces at the `CriticalSection` location are extracted from the structural analysis model, which is embedded inside the IFC model.

The `LongitudinalPattern` and `TransversePattern` entities represent the parameters for the reinforcement bars passing at the `CriticalSection` location inside an element.

LongitudinalPatterns represent the size and the location of the reinforcing bars from a reference location on the section, such as the top of the section. The areas of the longitudinal bars are also stored. The TransversePattern represents the size, spacing, and the angle of the shear bars (Figure 5-6). LongitudinalBar and TransverseBar classes are derived from the Rebar super-class, which stores the reference to the original IfcReinforcingBar class. The geometry of the longitudinal and transverse bars are represented using an extruded solid composed of a circular cross-section profile and a polygon representing the bar shape.

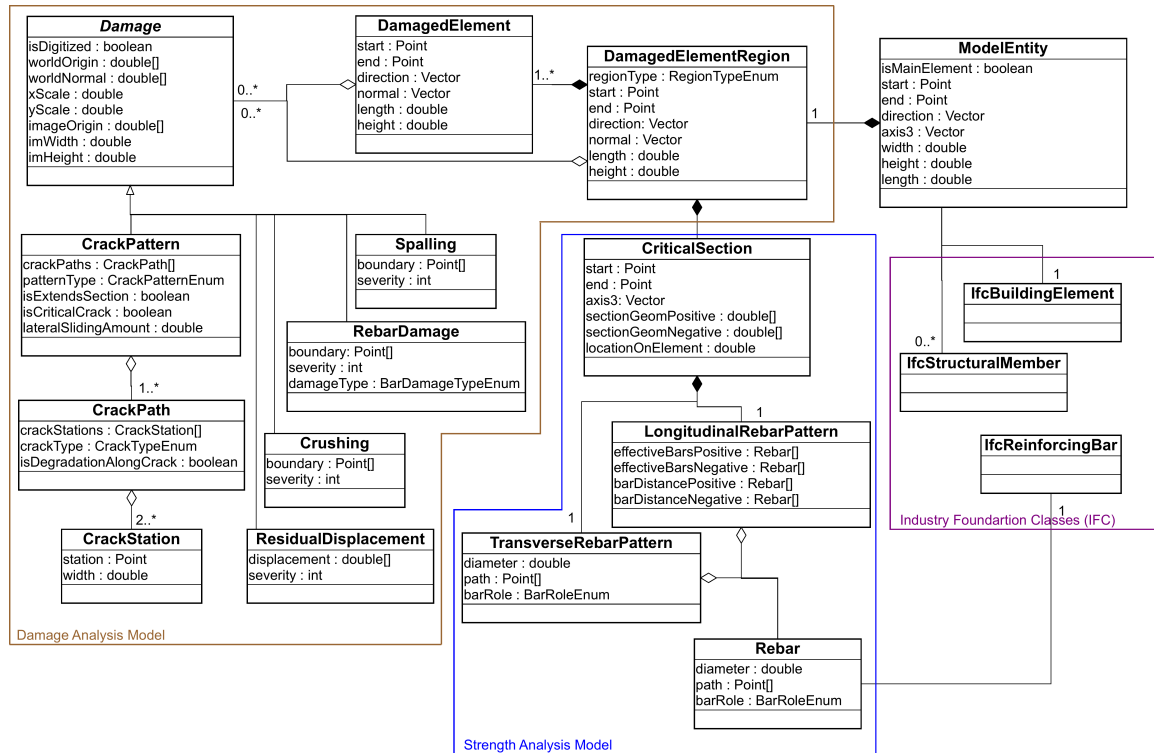


Figure 5-6 The engineering analysis is supported through the integration of two models. A damaged model represents the damaged conditions of the components. A strength analysis model supports the calculation of strengths for damage modes. A model entity, which replaces the IfcBuildingElement entity for the easiness of computations in the prototype implementation, integrates the two models for building elements.

The damaged model includes a set of entities for representing cracking, spalling, crushing, rebar damage, and residual displacement (Figure 5-6). The damaged elements are

represented using a 2D planar representation, which is located on the center axis of each component and extends the entire component. Regions, such as the plastic hinge region, toe/heel regions, and boundary and web regions are represented on the damaged elements. Different types of damage, such as cracking, rebar damage, crushing, spalling and residual displacement, are abstracted into corresponding classes in the proposed schema. The cracks are represented using a series of entities. The CrackStation represents a point on a crack along with the width of the crack at that point. The CrackPath stores a list of CrackStations and represents a single continuous crack. The CrackPattern represents a collection of CrackPaths, which need to be processed together. For example, the crack may partially close or occlusions may exist on the walls, which prohibit continuous detection. Additionally, certain crack patterns, such as X-shaped cracks are important for damage assessment. Using the pattern, path, and station entities complex cracks can be represented easily.

The DamagedElement and DamagedElementRegion entities provide a 2D representation of the piers and spandrels. These two entities are used as containers for damage information. The DamagedElement represents the entire component area and is represented along the center axis of the component. The DamagedElementRegion represents various regions on the components, such as plastic hinge, boundary, web, and toe. Utilizing containers for the damage allow querying the locations of different damage types.

The two models are integrated through the building components. As a proof of concept and to make the computations involving 3D geometries easier, a ModelEntity object was introduced to replace the IfcBuildingElement in the internal representation. The

IfcBuildingElement is the superset of building elements, such as walls, columns, beams, slabs, and foundations. The ModelEntity represents the geometries similar to the parameterized representations of IFCs [13]. The start and end points represent the main axis of the 3D body, which is analogous to the Axis representation in IFC [13]. Axis3 defines the extrusion direction. Later on in the process, the axis representation allows determining the combined geometry of the multiple components, such as flanged sections, using vector operations. Similar to the IfcBuildingElement, ModelEntity is linked to IfcStructuralElements, which is used for representing structural analysis results. This link should be identified in the model transformation.

5.6.1. Identification of Piers and Spandrels

The goal of this step is to identify and generate the structural components. These components can be piers with or without flanged sections or spandrels connecting the piers. Two steps of determining the components are division of building elements if they have openings, and finding the connections between the components. In the proposed approach, the first step divides the building elements into piers and spandrels (Figure 5-2). A pier is a vertical component, which primarily carries the gravity loads and the lateral loads. The spandrels are horizontal components, which transfer the forces between the piers. As the piers and spandrels are determined, the effective flange widths, if required, for each pier and spandrel are computed and connection between different components is established.

The division step creates one or more ModelEntity for every element in the BIM. Each resulting ModelEntities represent either a spandrel or a pier. If the element has openings, at least three ModelEntities are generated: A pier to the left of the openings, a pier to the

right of the openings, and beams above and below the openings (Figure 5-7 and Figure 5-8).

The geometries of the piers and the beams are calculated by vector operations using the axes and extruded geometry of the openings and the building element. The cross-sections of piers are computed directly using the extrusion profile (e.g., base profile). If the pier is flanged, the union of the profiles is computed to obtain the total cross-section of the flanged section. The extrusion height determines the pier height. The heights of the spandrels can be obtained by computing the height between two openings or the openings and the upper and lower edges of the wall.

```
//Divide elements
For every IfcBuildingElement -> Element
  If Element has no openings
    Create the ModelEntity for Element -> MEw
  else
    Create the left pier ModelEntity -> MElp
    Create the right pier ModelEntity -> MErp
    Create the beam ModelEntities -> [MEb_0, MEb1_ ... MEb_n]
    Create the relationships between the piers and the beams
  endif
end for
//Find connected components
For each ModelEntity -> Entity_i
  For each ModelEntity ≠ Entity_i -> Entity_j
    If Entity_i ∩ Entity_j
      Link Entity_i and Entity_j
    endif
  end for
end for
```

Figure 5-7 The transformation for generating the components for damage assessment first divides the building elements, if they have openings and creates the ModelEntities for each piece. Then, the relationships are established between the connected components in order to form the flanged sections and maintain the connection relationship between the divided components.

The computations for obtaining pier and spandrel geometries can be performed in a straightforward fashion using geometric operations in the 3D space. The prototype implementation considered the common geometric representations for the IfcBuildingElement [13]. Therefore, the subtypes of the IfcBuildingElement can be processed using the same method.

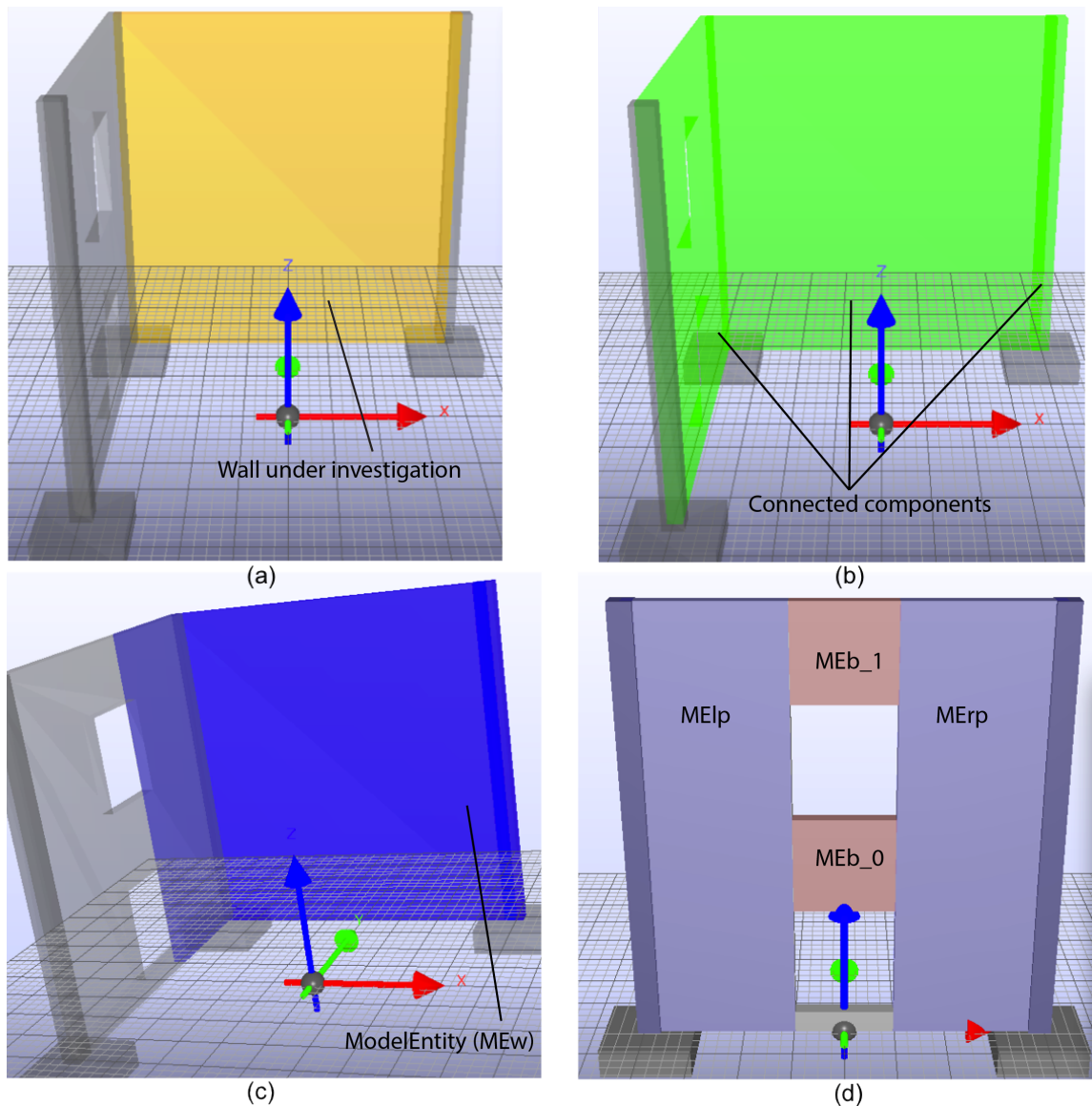


Figure 5-8 The first steps of the assessment procedure are the division of elements into components and determining the connected components. For the wall under consideration (yellow) (a), the connected walls and boundary elements are determined (MEw, highlighted in blue) (c). If a wall has openings, it is divided into piers (MElp, MErp) and spandrels (MEb_0, MEb_1) (c and d).

Connected components are found by a double loop over all of the ModelEntities, which are created in the previous step (Figure 5-8). First, a ModelEntity is taken from the list of entities in the building. For every ModelEntity, which is not equal to the main ModelEntity, intersection is checked by a Boolean operation. If the two entities intersect,

they are linked together to form the parts of a flanged section using the connectsTo attribute of the ModelEntity.

5.6.2. Generation of the Strength Analysis Model

The goals of this step are determining the critical sections for every component, determining the geometries of the flanged sections, finding the effective reinforcements inside the sections and calculating the component strengths at the sections. The objects created in this step are directly used for calculating the capacities of the ModelEntities. The piers can have CriticalSections at the bottom of the piers, at story levels and at any location, where damage is expected. The algorithm can calculate the CriticalSections at any location on the component.

```
//Find CriticalSection geometry using vector operations
Calculate effective flange widths for the compression and tension sides
Calculate flange width and thicknesses, web length and width
Calculate offsets of flanges with respect to the web axis
Calculate the corners of the flanges and the web

//Determine rebars
For each IfcReinforcingBar in the IFC model -> Bar
    If Bar ∩ CriticalSection
        Store Bar in CriticalSection
    end if
end for

//Determine the forces at section
For each IfcStructuralCurveMember -> Member
    if Member ∩ CriticalSection
        Link Member to CriticalSection
    end if
end for
```

Figure 5-9 A critical section represents a cross-section through a component and spans the web and flanges of the component. The reinforcing bars and the structural analysis model elements at the section are calculated by finding the intersection of the section and the bars and the elements.

The critical section geometry is defined using an array, which contains the top flange width and thickness, web thickness and web height, and bottom flange width and thickness. These parameters are calculated from the ModelEntities, which represent each part of the section (i.e., flanges and web) by vector operations using the axis and the

dimensions of the ModelEntity (Figure 5-9). If the flanges are not aligned with the wall axis, the flange offsets are calculated.

The effective flange widths are calculated according to the suggestions in FEMA 306 (Figure 5-10) [2]. The effective flange width on the compression side is calculated as $(0.3*hw+bw)$, where hw is the wall height, and bw is the wall thickness. On the tension side, the effective flange width is calculated as $(hw+bw)$. Additionally, the corners of the CriticalSection plane are calculated to be used for finding the reinforcing bars crossing the section. Finally, the location of the critical section is assigned.

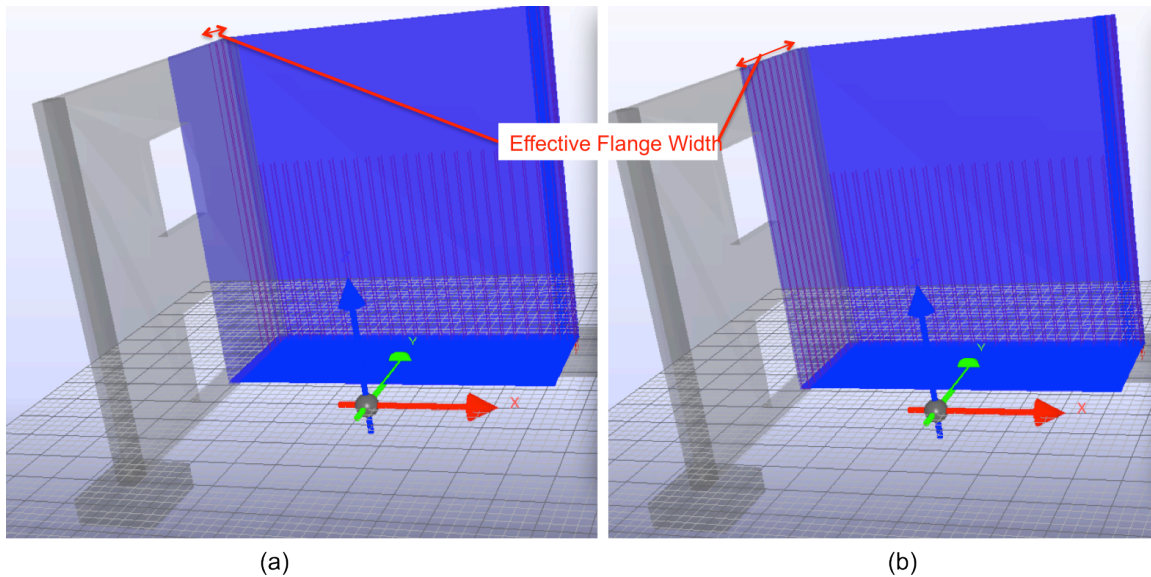


Figure 5-10 Effective flange widths and effective reinforcement within the effective flanges are computed for the compression and tension of the flanges. The effective reinforcing bars for tension (a) and compression (b) are computed separately. The distance of the bars from the center of the main wall determines, whether the bars will be considered for tension or compression. For the wall in the given figure, the critical section is at the bottom of the wall.

The longitudinal reinforcing bars crossing the section are calculated by intersecting the critical section plane and the reinforcing bars in the BIM (Figure 5-10). The intersection is calculated by first parameterizing the critical section plane and the reinforcing bars in 3D space. The intersection is calculated by simultaneously solving the two parametric equations for the critical section and the reinforcing bar.

The transverse bars, which are closest to the critical section, are used to determine the spacing between the bars. Ideally, the bars on each side of the section are selected. The total shear area of the bars are calculated by intersecting the linear segments of the bars with a plane perpendicular to the critical section and counting the number of segments crossing the plane. The angle of the bar is used to calculate the cross-section area. The longitudinal bar pattern and the transverse bar pattern at the CriticalSection are represented using the two pattern entities (Figure 5-6).

5.6.3. Determination of the Damage Mode

Using the strength equations of FEMA 306, the strengths for all damage modes are calculated for every pier and spandrel at the CriticalSections. The CriticalSection entity contains all of the information for calculating the strengths. Specifically, the size of the cross-section, reinforcing bars passing through the section, internal forces for different actions, such as earthquake and gravity are represented.

Table 5-1 The strength against the potential damage modes are calculated using strength equations given in standards.

| Damage Mode (code) | Calculation Approach |
|---|---|
| Ductile flexure (A) | Moment strength is calculated using strain compatibility. The lateral force (V_m), which is required to reach the moment strength, is found by dividing the moment strength by the shear span (M/V). |
| Flexure/Diagonal Tension (B) | Initially, the moment strength (V_m) governs. High-ductility shear strength (V_n^{high}) is less than the moment strength. Low-ductility shear strength (V_n^{low}) is higher than the moment strength. |
| Flexure Diagonal Compression (C) | Initially, the moment strength (V_m) governs. High ductility web crushing strength (V_{wc}) is less than the moment strength. |
| Flexure/Sliding Shear (D) | Initially, the moment strength governs (V_m). Sliding shear strength (V_{sl}) is less than the moment strength. |
| Flexure/Boundary Compression (E) | Moment strength (V_m) is higher than all other modes even after possible degradation. |
| Pre-emptive diagonal tension (H) | Low-ductility shear strength (V_n^{low}) is less than the moment strength. |
| Global or Individual Pier Foundation Rocking (M or N) | The lateral force (V_o), which would impose rocking should be less than all other strengths. |

According to FEMA 306, the determination of the damage modes is based on the shear strengths calculated for each major damage mode (Table 5-1). The proposed approach follows the FEMA 306 provisions. For wall piers, as a first step the strengths are calculated. The modes, which cannot be reached, are eliminated. For example, if the low ductility shear strength (V_n^{low}) is lower than the lateral force required to reach the moment strength (V_m), ductile flexure type damage (A) is not expected. Therefore, ductile flexure is eliminated as a potential damage mode. On the other hand, if the moment strength is lower than the low ductility shear strength (V_n^{low}), shear dominated behavior is not possible. Hence, the diagonal tension damage type (H) is eliminated. Among the

remaining damage modes, the one with the lowest strength is taken as the governing damage mode.

5.6.4. Generate the Damaged Model

Using the geometrical union of the components determined in the previous steps, DamagedElements and DamagedRegions can be determined. These two entities are represented as 2D planes passing through the center of the components. The center section is found by a Boolean intersection operation of a plane passing through the axis of the wall and all the connected components. The axis and the direction of the wall, which are represented in BIM, are used to determine the cutting plane. The result is a rectangular section that spans the flanges, the main component, and all the extensions of the main component that extend beyond the story, which the main component is assigned to (Figure 5-11). The DamagedRegions are instantiated on the DamagedElement using the parameters defined in the standard damage assessment guidelines.

The final step in the transformation is the registration of the damage indicators (cracks, spalling, etc.) with the DamagedElements and DamagedRegions. This step establishes the associations between the damage indicators and the components and the regions. Registration is performed by finding the intersections of the DamagedRegions and the damages.

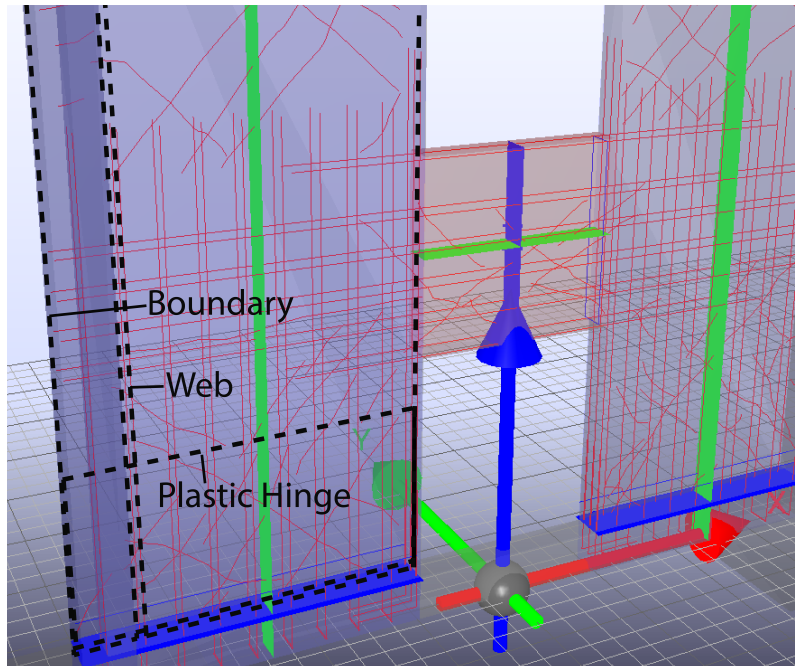


Figure 5-11 In the final state, the assembly of components are divided in to piers (blue) and spandrels (red) (if any), the damaged schema is generated and the damage indicators are superimposed on to the divided components. The figure also shows the reinforcing bars and the critical sections (highlighted in blue) on which the capacity analyses will be performed. The green cross-sections are temporarily used for calculating the shear area of the transverse bars.

5.6.5. Determination of the Damage Severities

The observed damage patterns determine the damage severity of the components. Initially, our approach assumes that all of the damage modes are equally probable independent of the strength calculations. A rule-based engine for determining the severities for all damage modes was implemented and verified. The damage description and damage severity classifications of FEMA 306 Chapter 6 were implemented (Chapter 3). As a result of an information requirements study, seventeen damage parameters were determined (Table 5-2) and utilized to determine the damage severities of components.

Table 5-2 Seventeen damage parameters define the damage state of a component.

| Category | Description | Parameter name |
|-------------------------------|--|--------------------------|
| Crack point property | | |
| | Maximum flexural crack width | maxFlex |
| | Maximum shear crack width | maxShear |
| Crack path property | | |
| | Existence of a sliding crack and the severity of offset on the sliding plane | slidingSignificance |
| Crack pattern property | | |
| | Existence of a concentrated shear crack | isShearConcentrated |
| | Existence of a concentrated flexural crack | isFlexuralConcentrated |
| Damage Location | | |
| | Maximum shear crack width in the toe region | maxShearInToe |
| | Maximum shear crack width in the web region | maxShearInWeb |
| | Existence of vertical cracks in the toe | isToeVerticallyCracked |
| | Existence of spalling in the toe region | isToeSpalled |
| | Existence of spalling in the web region | isWebSpalled |
| | Severity of spalling in the web region | spallingWebSeverity |
| | Severity of the spalling in the toe region | spallingToeSeverity |
| | Existence of rebar damage in the boundary region | isBoundaryRebarDamaged |
| | Existence of boundary crushing | isBoundaryCrushed |
| Damage Quantity | | |
| | Existence of spalling | isSpalled |
| | Existence of rebar damage | isRebarDamaged |
| | Severity of residual displacement | displacementSignificance |

According to the affinity diagramming study, described in Chapter 3, the damage parameters include five main categories (Table 5-2). The first three categories include crack properties. Crack point properties are the maximum widths of flexural, shear, and vertical cracks. The formation of a sliding plane and the severity of the offset on the sliding plane is the path property of a crack. Concentration of flexural and shear cracks are the two relevant pattern properties for reinforced concrete walls. These crack concentration determine whether sliding shear or diagonal tension type of behavior is governing. Locations of the damage indicators, such as spalling, crushing, rebar damage, and vertical and shear cracks constitute the fourth group of damage parameters. The fifth

group of parameters is related to the severity of the damage indicators such as spalling and residual displacement.

The seventeen damage parameters are fed into the rule based system. The output is the damage severity for all of the damage modes. If the parameters do not satisfy the expected damage patterns for a damage mode, False is returned for all of the severities of that damage mode, which eliminates the damage mode from further consideration. For example, for the ductile flexural mode, a sliding crack at the bottom of a pier is not expected. Thus, if there is a sliding plane in the form of a horizontal crack, which spans the entire cross-section of the component, the ductile flexural damage mode is eliminated.

The results of the strength analysis and visual assessment should agree. In other words, the governing damage mode, which is determined using the strength analysis, should not have been eliminated in the visual assessment. If the results of the two analyses do not agree, the inputs should be checked. FEMA 306 lists several potential error sources. The distribution of the lateral forces, which was used in the structural analysis, may be different from the actual. The strength of the components may differ from the actual. The intensity of the damaging ground motion may differ from that assumed in the structural analysis. Resolution of these discrepancies requires attention of an engineer. Our prototype implementation can identify whether the results of the strength analysis and the visual assessment agrees or not. However, resolution of the discrepancies is left to the judgment of a structural engineer.

5.7. Validation Case Study

The approach was validated on a case study. An example building from FEMA 307 composed of reinforced concrete solid walls and walls with openings were evaluated

using the prototype implementation of the approach [1]. The prototype was implemented in Java programming language using OpenIFCTools [19].

The proposed strength analysis and visual assessment schemas were to extend the IFC classes. The IFC model of the building was generated and the model contained the 3D components, reinforcing bars and structural analysis results (Figure 5-12). The damaged representation of the walls was also generated using the prototype. The damage records of the building were digitized and converted into the proposed damaged model schema using the transformation mechanisms explained in previous chapters. During the digitization of the damages the damage parameters such as, concentration of the cracks, which require engineering judgment were also captured and represented in the model.

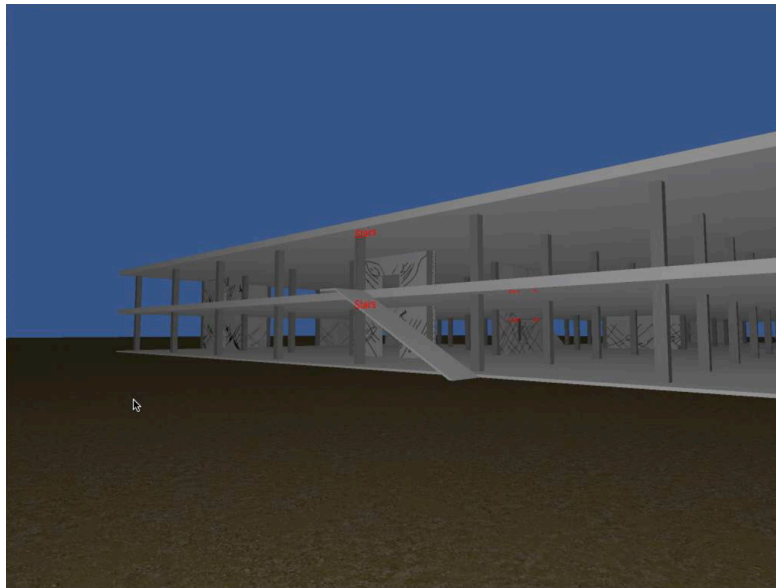


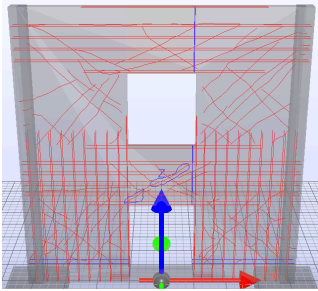
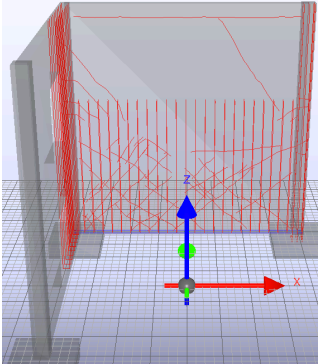
Figure 5-12 A 3D rendering of the building model. The rendered model was used in the user studies (next section). The IFC model of the building contained the building components. The IFC model was extended using the damage and strength analysis schema for the damage assessment.

The example building is a T-shaped reinforced concrete two-story building [1]. The building was designed and constructed in the late 1950s. The floors and the roof are constructed with waffle slabs. Reinforced concrete walls in both directions resist lateral

forces. Several walls have door openings in the middle of the wall. The building has 42 piers and spandrels in total after the division of the wall elements into components. The building was damaged during an earthquake and it was professionally inspected and seismically evaluated at that time. In this case study, we use the documentation that was generated at the time of inspection and evaluation.

The building contained several instances of walls with or without flanges and openings (Table 5-3). The walls with openings were divided into piers and spandrels using the transformation mechanisms outlined in the approach section. The case study only contained regular openings, which have the same width and located on the same vertical grid. Twelve cases had other piers as flanges. The connected components were identified automatically. What portion of the pier is considered as the flange is determined by the effective flange width determined by FEMA 306. The divided and aggregated components were represented inside the schema for the strength analysis and visual assessment tasks.

Table 5-3 The case study contained four basic configurations of buildings, which required different approaches to transformation and representation.

| Case | Transformation | Representation | Instances | Example (Output) |
|------------------------|---|---|-----------|---|
| Walls with openings | Division of component into piers and beams | Represent each pier and spandrel as a ModelEntity | 8 |  |
| | Calculate pier and spandrel section geometries | Represent cross-section geometries in CriticalSection | | |
| Walls without flanges | Division of components and calculation of section geometries, if there are openings | Represent wall as a single or multiple ModelEntities, depending on the existence of opening | 6 |  |
| Walls without openings | Calculate flanged geometry, if flanged | Represent wall as ModelEntity | 10 | |
| Walls with flanges | Find connected components to make flanged sections | Represent each wall and flange as separate ModelEntities | 12 | |
| | Calculate flanged section geometry | Represent cross-section geometry in CriticalSection | | |

Two separate analyses were performed on the identified piers and spandrels: strength analysis and visual assessment of damage. The core component in the strength analysis is the critical section concept, which encapsulates all of the required information for calculating the strengths at any location on the building, as long as the necessary information is in the BIM. The transformation mechanisms enable extracting the necessary information and generating the critical sections. Critical sections were defined at floor levels and at the bases of the piers and on the beams. Effective flange widths were calculated from the aggregation of components. The reinforcing bars within the effective flange widths were calculated using the BIM. Similarly, the geometries of the critical sections (section height, flange and web thicknesses and heights) were determined. Depending on being flanged or not, the critical section shapes were either L-shaped

(flanged) or rectangular (not flanged) with a small boundary elements on the free ends of the wall (Table 5-3).

For all of the critical sections, the strengths for all seven damage modes were calculated automatically. Then, for each component the strengths for different modes were sorted and compared to the forces at the critical sections and potential damage modes were identified by the prototype implementation (Figure 5-13). In a similar manner, visual assessment was performed for all of the components automatically. The results of the visual assessment and the strength analysis were combined to determine the damage mode and the severity of the components. In the example in Figure 5-13, the damage was determined to be insignificant overturning, because the overturning had the lowest strength as determined by the strength analysis, and the damage was insignificant as determined by the visual assessment.

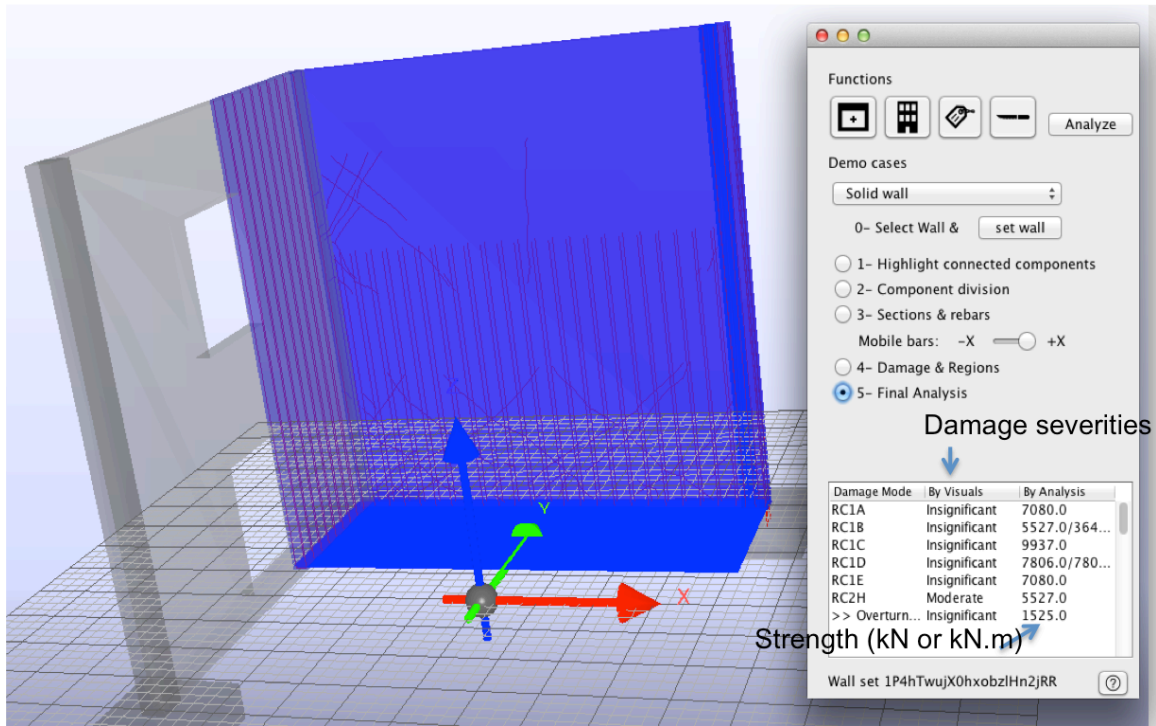


Figure 5-13 A snapshot of the prototype. The window on the right is used for guidance through the steps of the procedure. The building is analyzed one wall at a time. The other walls are hidden from view for easy visualization.

The case study contained various different types of damages including cracks and spalling and degradation of concrete. Although the case study building did not cover all damage parameters and value ranges of existing damage parameters, the reasoning mechanisms and representation mechanisms proposed in this research facilitated the analysis of damages.

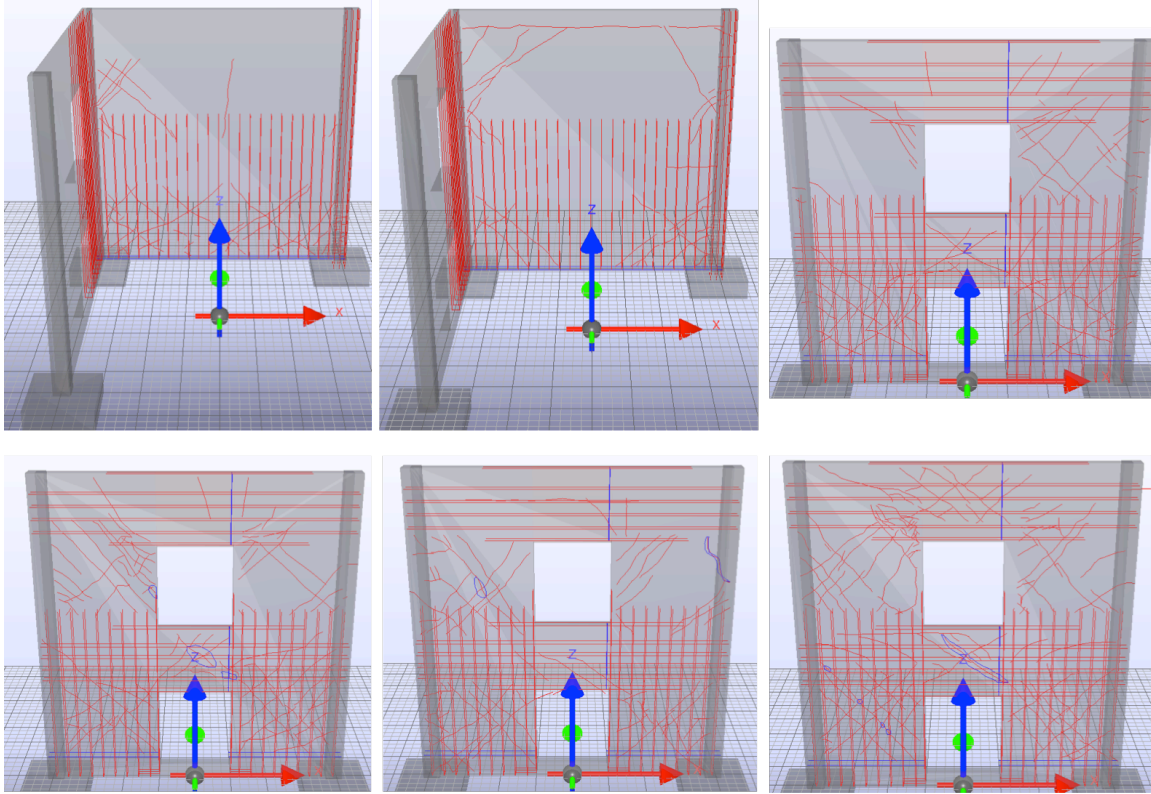


Figure 5-14 In total 18 wall elements, which contain 42 piers and spandrels were assessed visually and by performing strength analyses. Six of the elements containing various crack patterns and spalling are shown. Reinforcing bars, which were used for calculating the strengths are also shown.

The transformation mechanisms enabled extracting the containment relationships between damages and components from raw damage data and component geometry. Similarly, damages could be registered with regions on components (e.g., cracks on web regions). The querying for damage locations is done via the Damage superclass. Hence, if we had crushing or rebar damage, for example, the procedure would have been the same with that of spalling and cracking. The representation of damages enabled finding relationships between damages (e.g., spalling along cracks). Spalling, crushing and rebar damages share the same geometrical representation. Therefore, using the same transformation mechanisms, it is possible to find the relationships between the other damage parameters.

Table 5-4 The representation schema and the reasoning mechanisms facilitated analyzing various forms of complex damages. Damages could be analyzed both individually, as in the case of cracks, and also in relation to another (e.g., spalling along cracks)

| Damage | Piers and Spandrels with Damage | Reasoning | Facilitating Representation |
|---|---------------------------------|--|--|
| Flexural or shear cracking | 42 | Analyze different types of cracking | CrackPath |
| Partially occluded or divided cracks | 8 | Analyze patterns of cracks | CrackPattern |
| Cracks extending multiple regions | 42 | Find relationships between damages and regions | DamageElementRegion & geometric representations of Damage subclasses |
| Degradation of concrete and spalling along cracks | 8 | Find relationships between different damages | Geometric representations of Damage subclasses |
| Spalling at various regions | 8 | Find relationships between damages and regions | DamageElementRegion & geometric representations of Damage subclasses |

The damage modes and severities of all 42 piers and spandrels were assessed using the prototype implementation. The results showed small difference in the calculated strengths for some of the components (5%-10%), however these differences did not affect the damage mode and severity assessments. The differences are potentially due to errors in unit conversions and slight differences in the locations of reinforcement bars and component dimensions. The damage modes and severities identified using the prototype agreed 100% with the results of the professional assessment.

As an additional evaluation, a user study was performed, to compare the assessments of manual and automated methods in terms of the precision and recall of the damage assessment. In the user study, engineers were asked to evaluate a solid wall and the piers and beams of a coupled wall from the same building, which was used in the case study.

Five professionals, who either performed experimental studies on the behavior of reinforced concrete components, or participated in the assessment of damage following past earthquakes, participated in the survey. The participants were given the hand sketches of damages on a solid wall and a wall with two openings. They were asked to

evaluate the solid wall and the two piers and the two beams on the wall with openings separately. The users selected the damage severities for each of the damage modes and whether the damage modes are applicable or not. Users' assessments were compared to the ground truth in terms of precision and recall.

A number of key conclusions were drawn from the user study. First, the users had the tendency to include irrelevant damage modes and miss the correct damage mode in the potential set of damage modes. The tendency was quantified with the 51% precision of the users' evaluations. For the same set of walls, the proposed approach had a similar precision value (46%), which is due to the fact that all of the damage modes were considered as relevant. On the other hand, the users failed to include the correct damage mode in the potential modes for 50% of the cases.

The results, however, should not be taken as definitive but as an indication of the potential of the proposed approach. More studies should be performed with a broader sample of user population using a variety of building configurations.

5.8. Conclusions

This chapter described a BIM based approach for automating the engineering analyses for post-earthquake damage assessment to support visual assessment and strength analysis. The transformations, which are necessary to generate the damaged model and the strength analysis model from a BIM and raw damage information, are developed. The approach was validated on an independently evaluated damaged building. The validation showed that the approach correctly identified the damage modes and severities of 42 piers and beams.

The developed schema used for strength analysis and visual assessment is capable of representing the damage information required for assessing various cases of damage types, such as flexure or shear dominated damage modes and mixed modes. The representation also proved to be flexible for modifying the damage parameters, such as joining or dividing cracks, to test the effects of various cracking patterns on the results of the analysis.

The proposed mechanisms accurately transformed the raw damage information and established the relationships between damages and components and regions. Relationships between different damage types, such as spalling along cracks were also established.

The component representations allowed representing flanged, non-flanged walls with or without openings. The strength analysis model allowed calculating the component strengths at locations suggested by the FEMA 306 guideline. For the strength calculations it was necessary to determine the flanged geometry, effective reinforcing bars in a section under compression and tension, and forces in the section. The model enabled utilizing the information contained in the BIM for determining these properties and calculating the strengths accurately.

Several future directions to extend the research are suggested. On one axis, the proposed research can be extended to include irregular openings and more complex component configurations. The proposed research only considered walls with regular openings. With the modern architecture, however, irregular openings are not uncommon. On the second axis, the research can be extended to include other material types, such as masonry, steel, and mixed constructions.

Chapter 6 Conclusions and Contributions

6.1. Introduction

In this research, in order to support objective and accurate documentation of earthquake damage and engineering analyses of reinforced concrete walled structures, a Building Information Modeling (BIM) based approach was developed for representing the damage information and performing visual damage assessment and strength analysis, and laser scanners were characterized for scanning cracks. The representation capability of the developed BIM based approach was determined by analyzing the coverage of the damage information parameters. The reasoning mechanism for identifying damage modes and severities and the overall approach were validated on a case study, where a damaged building was analyzed using the proposed approach.

The developed approach provides a representation method to represent and reasoning mechanisms to execute the visual assessment and perform strength analyses in order to determine the damage modes and severities of reinforced concrete walls. The approach has three parts: 1) identifying the information requirements for the representation of damage information, 2) extraction of the damage parameters from the visual damage data collected in the field, such as locations and severity of cracks, spalling, rebar damage, crushing, and structural information, such as the locations and sizes of rebars, internal forces, component dimensions, and 3) automated execution of the visual assessment and strength analysis and identification of the damage mode and severity.

In relation to the first part, I have identified the earthquake damage parameters, which need to be represented and developed a representation schema for earthquake damage. The results showed that earthquake damage can be represented using 17 damage parameters, including crack types, locations, and sizes, location and severity of spalling, crushing, rebar damage, and severity of residual displacements. In relation to the second part of this research, I have identified the product model transformations to extract the information contained in the damaged BIM to execute the engineering analyses. During the third part of this research, I have developed several reasoning mechanisms to process the extracted information to automatically perform visual assessment and strength analysis.

The characterization of laser scanners for detecting cracks focused on whether earthquake induced cracks can be captured. A testbed was developed for testing the capabilities of two different laser scanners using various operational parameters, such as scanning distance, angle of incidence, and scan resolution. Width, orientation, and depth are the crack parameters included in the experiments. The results of the experiments provide graphs depicting the relationships between the minimum crack size, which can be detected given the scanner technology, scanning distance, angle of incidence, resolution, and crack orientation. The results show that cracks as small as 1 mm can be detected using laser scanners. The depth of cracks were also found to be an important factor for detecting cracks.

The following sections describe the contributions, practical implications of the research, and future research directions.

6.2. Summary of Contributions

6.2.1. Contribution 1: Characterization of two laser scanners for detecting earthquake induced cracks

Previous studies on laser scanners focused on developing theoretical models or provided experimental data for characterizing the performance of laser scanners for capturing various features, such as thin lines, edges, and surface flatness. However, previous studies have not considered special situations, which apply to detecting cracks. Therefore, previous studies cannot be directly applied to evaluating laser scanners for scanning cracks.

In order to address the gap in research, an experimental testbed for studying the performance of laser scanners was developed by building on the previous experimental and analytical studies and developed. The testbed incorporated important crack parameters for damage assessment, such as width, orientation, and orientation, and prominent laser scanner parameters, such as resolution, angle of incidence, range, and scanner technology. The test range for each parameter was chosen based on the experimental, analytical, as well as, practical application standpoint. The experiments were first executed on artificially created testblocks, which contain various crack sizes and orientations. The results obtained from the artificial blocks were then applied to a real wall case.

The results of the experiments point to the limitations of the measurement model (i.e., Amplitude Modulated Continuous Waveform vs. Pulsed Time-of-Flight), as well as the interplay between the scanner settings and the crack properties. The crack width captured by scanners was always found to be greater than the actual crack width.

6.2.2. Contribution 2: Identification of information requirements for visual assessment earthquake damage on reinforced concrete shear walls

Previous research studies on the automation of damage assessment developed a variety of approaches to the processing of information. However, these studies either considered only a limited set of damage modes and parameters as compared to those, which can occur on reinforced concrete walls. On the other hand, the damage behavior, which can be observed on reinforced concrete walls are not as well separated as it is on other kinds of components, such as frames, and the variety of the damage modes is greater. Therefore, the information items, which characterize earthquake damage on shear walls, need to be studied.

Previous studies on identifying the information requirements for developing representations generally use a listing type of approach, where the items characterizing a problem are listed and studied using the domain knowledge by experts. Such approaches are not appropriate when the number of items is large. Additionally, developing a representation requires building a hierarchy of information to identify the abstractions in the representation schema.

In order to address the limitations listed above, the affinity diagramming approach was applied to build a hierarchy of information for earthquake damage assessment. In total 278 statements were extracted, which describe damage, from the FEMA 306 guideline. The statements were then grouped into 4 levels in a hierarchy. The results show that the damage information on a shear wall can be represented using seventeen parameters (or information items).

The results of the study were validated by analyzing the sensitivity of the damage mode and severity identification to the changes in the values of the seventeen damage parameters. In order to evaluate the value of information, the descriptions of the damage modes and severities in the FEMA 306 were implemented into a rule-based engine, which takes the 18 parameters as the input and outputs the damage modes and severities as the output. Controlled variations of base cases, which are known to conform to the damage modes, were run through the engine. The evaluation engine was verified manually by studying the results one by one and also by comparing the outputs to ground truths. The results showed that except one of the parameters, all 17 parameters were useful in either in determining the damage mode or the damage severity.

6.2.3. Contribution 3: A schema for representing the earthquake damage for supporting the visual assessment

Previous studies on the assessment of damage developed methods for representing crack models for cracking type identification and tagging the damage pixels on images. However, these previous studies fall short in representing earthquake damage parameters and the types of damage indicators, which can be observed on damaged shear walls. Therefore, a schema needs to be developed to represent the earthquake damage.

Building on the object-oriented model development methods, Building Information Modeling practices, and design patterns a schema was developed using the 17 damage parameters. The schema was validated in terms of the coverage of the parameter space, which is formed by the ranges of values, which the all 17 damage parameters take for a real building. The building is an earthquake damaged shear wall building with a total of 42 components of coupling beams, piers, or solid walls. The same evaluation engine,

which was used for validating the value of information was used to determine the coverage. The schema was able to represent all of the information contained in the 42 components.

6.2.4. Contribution 4: An approach for identifying the damage mode and severity of reinforced concrete walls

The requirements the engineering analysis for determining the damage modes and severities of reinforced concrete walls are different than the rapid assessment requirements, which the previous studies primarily researched. Therefore, an approach, which is compatible with the current method of engineering analysis is required.

In this research, an approach was developed for performing the visual assessment and the strength analysis, which are required by the current engineering analysis methods. The approach considers all of the damage modes as equally possible and utilizes the results of the strength analysis to determine the damage and the visual assessment to identify the damage severity corresponding to the damage mode. If the results of the two types of analyses do not agree, the results of the engineering analysis are flagged as containing discrepancies. The approach was validated using a damaged building and the results of the professionally conducted analysis on the building. The approach was verified by comparing the results of the developed automated approach to the results of the professional analysis. The results agreed 100% with the manual analysis. The approach was validated in a user study, where users were asked to identify the damage modes of the selected components. The developed approach provided improved recall rates at the expense of slightly reduced precision, which is a result of treating all of the damage modes equally possible as opposed to pre-eliminating them.

1.8 Future Research Directions

1.8.1 Analytical modeling of the laser scanner errors for detecting cracks

The experiments in this research primarily focused on whether cracks of certain widths, orientations, and depths can be detected or not. Width measurements were also taken from the detected cracks. As the results indicate, the widths of the cracks as measured from the laser scanner data can be 2-3 times of the actual crack widths. The characteristics of the scanner are also important factors. A potential next step for research is developing an analytical model for predicting and correcting errors based on the measurements obtained from the scan data. Prediction of errors given the scanner properties can be beneficial in scan planning. Error correction is potentially beneficial in more accurately estimating the crack widths from the scan data.

6.2.5. Compare and contrast existing crack detection algorithms on 3D point cloud data

The algorithm used in this research was selected for its accuracy for labeling the 3D points into off-surface or on-surface points. However, the algorithm is not capable of distinguishing between different features on the surface. For example, spaces between masonry units and cracks cannot be distinguished readily with the algorithm. There are potential machine learning algorithms, which can perform such distinction. However, further research is needed. A potential research direction is using the experimental testbed to evaluate different algorithms and develop better algorithms for crack detection, which take the laser scanner and surface characteristics into account.

6.2.6. Test more materials for evaluate the applicability of the results of the experiments

The experiments primarily focused on concrete surfaces. However, the results have other potential application areas for detecting damages, such as on asphalt pavement surfaces. The experiments also excluded surface color and texture from the experiments. By performing more experiments on other material types and surface conditions, the applicability and limits for applying the results of the experiments for crack detection on other material types.

6.2.7. Applicability of the damage representation schema to other construction types

Due to the complexity of the damage modes on reinforced concrete walls, I primarily focused on the engineering analysis of structural walls. However, there is a significant reinforced concrete frame building stock, which is vulnerable to earthquake damage. Assessment of damage on reinforced concrete frames can also potentially benefit from the analysis method developed in this research. Additionally, the use case building used for the validations does not contain all types of damage. In the future, the study can be extended as following: 1) different building configurations can be tested, such as framed buildings, structural walls with irregular openings, etc., 2) different building types, such as residential buildings, commercial buildings can be tested, 3) buildings with different kinds of damages can be evaluated.

6.2.8. Research on developing metrics for quantifying the severity of spalling, crushing, and displacement type of damage

Currently, the damage descriptions in the FEMA 306 do not quantify the damage severity of damage indicators, such as spalling objectively. Currently, the decision is left to the engineer. For example, the spalling is classified as insignificant or significant. Accurate metrics (e.g., area and depth of spalling) needs to be developed to accurately evaluate the effects of damage on the structural components. Further research is needed on quantifying these metrics.

Appendix A. Affinity diagrams for the identification of the information requirements for visual damage assessment from the FEMA 306 guideline for earthquake damage assessment

Table 6-1 Reinforced concrete visual damage assessment affinity diagram. Level 1 presents the statements, which were extracted from the Chapter 5 of the FEMA 306 (1999) guideline.

| Reinforced Concrete | | | |
|--|---------|---------|--|
| Level 4 | Level 3 | Level 2 | Level 1 (Statements extracted from FEMA 306) |
| Crack properties | | | |
| Crack point property | | | |
| Flexural crack size | | | |
| Flexural cracks <3/16" | | | |
| Flexural cracks < 1.4" | | | |
| Flexural cracks < 1/4" | | | |
| Flexural cracks < 1/8" | | | |
| Flexural cracks may not be apparent at low levels of ductility | | | |
| Shear crack size | | | |
| Shear cracks > 3/16" & < 3/8" | | | |
| Shear cracks < 1/8" | | | |
| Shear crack width < 1/16" | | | |
| No shear cracks | | | |
| Shear cracks > 1/16" | | | |
| Shear crack width < 1/8" | | | |
| No shear crack exceed 1/8 " | | | |
| Shear crack width > 1/8 & < 3/8" | | | |
| Shear cracks < 1/8" | | | |
| No shear crack exceeds 1/8" | | | |
| Shear cracks may exceed 1/8 but < 3/8" | | | |
| Shear cracks < 1/8" | | | |
| Any/all crack size | | | |
| Cracks < 3/8" | | | |
| Cracks < 1/8" | | | |
| Cracks < 1/4" | | | |
| Cracks < 1/4" | | | |
| Cracks do not exceed 3/8" | | | |

| Reinforced Concrete | | | |
|---------------------------------------|--------------------------------|--|--|
| Level 4 | Level 3 | Level 2 | Level 1 (Statements extracted from FEMA 306) |
| | | | All cracks < ¼” |
| | | | Cracks do not exceed 3/8” |
| | | | No cracks exceed 3/16” |
| | | Crack path property | |
| | | Continuity of flexural cracks along component | |
| | | In the plastic hinge zone, flexural cracks join up across section, which becomes a potential sliding plane | |
| | | Major horizontal flexural crack along the entire wall | |
| | | Development of a major flexural crack along the entire length | |
| | | Flexural cracks join up across one or both ends of section to form a potential sliding plane | |
| | | Degradation of concrete along cracks | |
| | | Degradation of concrete and sliding along the sliding plane begin to occur | |
| | | Some degradation of concrete along the critical crack | |
| | | Amount lateral offset along sliding plane | |
| | | Degradation and sliding along the critical crack | |
| | | Possible small laterall offset along the sliding plane | |
| | | Lateral offset at sliding plane | |
| | | Possible lsmall lateral offset | |
| | | Crack pattern property | |
| | | Type of concentrated single crack | |
| | | Higher shear cracks are concentrated at one or more cracks | |
| | | Shear cracks concentrate at one or more cracks | |
| | | Shear cracks become concentrated at one or more cracks | |
| | | Wide flexural crack concentrated in a single crack | |
| | | Shear cracking concentrated at one or more cracks | |
| | | One or more wide shear cracks begin to form | |
| | | Wide shear cracks concentrated in a single crack | |
| | | Concentration of flexural cracks in the plastic hinge zone | |
| | | Wide flexural cracking and spalling should be concentrated in the plastic zone | |
| | | Minor flexural cracking may extend beyond the plastic hinge zone | |
| | | Flexural cracks beyond plastic hinge zone don’t exceed 1/8” | |
| | | Flexural cracking and spalling concentrated at the hinge zone | |
| | | Flexural cracking ay extend beyond p. hinge zone | |
| Properties of other damage indicators | | | |
| | Location of damage | | |
| | Spalling or crushing location | | |
| | Spalling of web regions begins | | |

Reinforced Concrete

| Level 4 | Level 3 | Level 2 | Level 1 (Statements extracted from FEMA 306) |
|---------|---------|---------|--|
| | | | Heavy spalling and voids in web concrete |
| | | | Limited spalling at web or toe regions |
| | | | Significant spalling of web concrete |
| | | | Limited spalling at web or toe |
| | | | Boundary regions in plastic hinge zone begin to spall and crush |
| | | | No spalling or crushing of concrete within web or center area |
| | | | Location of buckled rebars |
| | | | Buckled boundary longitudinal bar |
| | | | No buckled rebars in the toe region |
| | | | Boundary reinforcement should be exposed and inspected for buckling or cracking. |
| | | | Spalling or vertical cracking location |
| | | | Spalling or vertical cracking at toe regions in plastic hinge zone |
| | | | Spalling or vertical cracking at at toe regions in plastic hinge zone |
| | | | Vertical cracks at the extreme fibers of the plastic hinge zone |
| | | | Vertical cracks and spalling at toe regions |
| | | | Spalling or vertical cracking at toe regions in plastic hinge zone |
| | | | Quantity of other damage indicators |
| | | | Spalling or vertical cracking |
| | | | No significant spalling or vertical cracking |
| | | | No significant spalling or vertical cracking |
| | | | No significant spalling or vertical cracking |
| | | | Possible spalling |
| | | | No vertical cracking or spalling |
| | | | Spalling may occur |
| | | | Residual displacement amount |
| | | | Large residual displacement |
| | | | No significant residual displacement |
| | | | No significant displacement |
| | | | No significant residual displacement |
| | | | No significant residual displacement |
| | | | Significant residual displacement |
| | | | No significant residual displacement |
| | | | Buckled or fractured bars |
| | | | No buckled or fractured rebars |
| | | | No buckled or fractured rebars |
| | | | No buckled or fractured rebars |

Reinforced Concrete

| Level 4 | Level 3 | Level 2 | Level 1 (Statements extracted from FEMA 306) |
|---------|---------|---------|--|
| | | | No buckled or fractured rebars |
| | | | No buckled or fractured rebars |
| | | | Fractured reinforcement |
| | | | Fractured vertical reinforcement |
| | | | Fracture horizontal reinforcement |

Table 6-2 Unreinforced masonry visual damage assessment affinity diagram. Level 1 presents the statements, which were extracted from the Chapter 7 of the FEMA 306 (1999) guideline.

| Unreinforced Masonry | | | |
|-----------------------------|----------------|--|---|
| Level 4 | Level 3 | Level 2 | Level 1 (Statements extracted from FEMA 306) |
| Crack properties | | | |
| | | Point property of cracks with different types | |
| | | Size of cracks | |
| | | Diagonal cracks upto ½” at upper portions of the wall | |
| | | Diagonal crack width < ¼” | |
| | | Cracks widen to 1/8” | |
| | | Cracks mostly close due to the confinement of the frame | |
| | | Diagonal cracks in pier with crack widths over ¼” | |
| | | Size of opening of head joints | |
| | | Stair stepped diagonal crack where head joints open and close to allow movement of bed joints | |
| | | Opening of head joints upto ½” creating a stair-stepped pattern | |
| | | Opening of head joints upto ¼” | |
| | | Opening of head joints upto ¼” | |
| | | Staggered hairline cracks / spalled mortar in head and bed joints | |
| | | Is there sliding/opening of bed joints? | |
| | | Hairline cracking / spalled mortar in bed joints within piers, but bed joints do not open | |
| | | Stair stepped joint sliding at upper portions of the wall | |
| | | Bed joints sliding at corners of infill | |
| | | Movements occur along bed joints in the form of diagonal cracking or horizontal cracking or horizontal bed joint sliding | |
| | | Horizontal cracks / spalled mortar on bed joints indicating in plane offset | |
| | | Horizontal cracks/ spalled mortar at bed joints | |
| | | Sliding occurs on bed joints | |
| | | Sliding along bed joints | |
| | | Sliding occurs on bed joints in the central portion of the pier | |
| | | Horizontal bed joint cracks near the base of the wall upto ½” | |
| | | Sliding along a horizontal bed joint near the base of the wall | |
| | | Excessive sliding | |
| | | Significant residual set | |
| | | Continuity of cracks | |
| | | Continuity of horizontal cracks | |
| | | Crack plane or stair stepping is not continuous across the pier | |

Unreinforced Masonry

| Level 4 | Level 3 | Level 2 | Level 1 (Statements extracted from FEMA 306) |
|---------|---------|---------|---|
| | | | Crack plane is not continuous across the pier |
| | | | Continuity of diagonal cracks |
| | | | Hairline cracks fully extend along diagonals (stairstep or though bricks) |
| | | | Severe corner-to-corner cracking |
| | | | Types of damage along crack paths |
| | | | Is there spalling and unit damage along cracks? |
| | | | Crushing/spalling at crack locations |
| | | | Crushing and/or 'walking out' of mortar along cracks |
| | | | Mortar and masonry units at the crack locations can be degraded |
| | | | Spalling and rounding edges of units along crack plane |
| | | | Degradation of cracking |
| | | | Significant sliding and/or deterioration of units |
| | | | Cracks at floor/roof lines and midheight of stories may have mortar spalls upto full depth of joint |
| | | | Spalling of mortar along cracks at midheight or floor/roof lines |
| | | | Mortar spalling in cracs at midheight or roof/floor lines upto full depth of joint |
| | | | Do cracks go through units? |
| | | | No cracks in units |
| | | | No cracks in units |
| | | | No cracks in masonry units |
| | | | No cracks in masonry units |
| | | | No cracks in masonry units |
| | | | Crushing/cracking of bricks |
| | | | Diagonal blocks pass through blocks |
| | | | Diagonal cracks in pier many of which go through masonry |
| | | | Diagonal cracks that propagate through the units |
| | | | Is there sliding off supporting bricks along crack? |
| | | | Upper bricks have slid off their supporting bricks |
| | | | Upper bricks have slid off their supporting brick |
| | | | Sliding of an upper brick off a lower unit |
| | | | Amount of offset along cracks |
| | | | Concurrent in-plane damage evidenced by extensive X crack |
| | | | Significant residual set |
| | | | Minor movement along or across crack plane |
| | | | Residual offset can occur at the crack plane |
| | | | No offset along the crack |
| | | | No offset along the crack |

Unreinforced Masonry

| Level 4 | Level 3 | Level 2 | Level 1 (Statements extracted from FEMA 306) |
|--|---------|---------|---|
| | | | <p>Significant movement or rotation along the crack plane</p> <p>Triangles above and below the crack separate</p> <p>Staggered hairline cracks/ spalled mortar at the end of the spandrel in head and bed joints indicating offset</p> <p>Staggered hairline cracks/ spalled mortar at the end of the spandrel in head and bed joints indicating offset</p> <p>Offset along the horizontal crack at the center portion</p> <p>Some offset along the horizontal crack in the central portion of the wall</p> <p>Out of plane offsets along cracks of upto ½"</p> |
| Properties of patterns of cracks | | | |
| Patterns of cracks | | | |
| <p>Multiple cracks stepping in each direction</p> <p>Hairline X cracks in the middle</p> <p>Significant stair-stepped movement</p> <p>Hairline cracks/spalled mortar on a horizontal plane or in stair-stepped fashion</p> <p>Steep inclined crack propagating upward from the toe</p> <p>Secondary cracking at an angle of 45-60° to the horizontal</p> <p>Diagonal cracks at the toe of the wall extend upwards several courses</p> <p>Diagonal stair-stepped cracks which propagate in head and bed joints</p> <p>Diagonally oriented cracks at the toe of the wall extend upwards several courses</p> <p>Diagonal stair step cracking at corners of infill</p> | | | |
| Location of concentrated cracks | | | |
| <p>Hairline cracking on diagonals concentrated in the center region</p> <p>Cracking concentrated within center region of panel</p> <p>Extensive spalling at the toe of the wall</p> | | | |
| Type of concentrated cracks | | | |
| <p>Predominantly vertical cracks/spalled mortar across the full depth</p> <p>Predominantly vertical cracks/spalled mortar through no more than one unit at the ends of the spandrel</p> | | | |
| Type and number of cracks in a region | | | |
| <p>More than one diagonal cracking</p> <p>Horizontal cracking on 1-3 cracks in the central portion</p> <p>Horizontal cracking on 1-3 cracks in the central portion</p> <p>Horizontal cracking on 1 or more cracks in the central portion</p> | | | |
| Amount of cracked courses in units | | | |
| Cracks have propagated into a significant number of | | | |

Unreinforced Masonry

| Level 4 | Level 3 | Level 2 | Level 1 (Statements extracted from FEMA 306) |
|---------------------------------------|-----------------|---|--|
| | | | courses of units In over 1/3 of the courses cracks go through the masonry units 5% of the courses or fewer have cracks in masonry units 5% of the courses or fewer have cracks in masonry units Hairline diagonal cracks in masonry units in fewer than 5% of courses Cracking of blocks near corners of infill |
| Properties of other damage indicators | | | |
| | Damage Location | | |
| | | Location of brick crushing | |
| | | Crushing of units at the corners Crushed/spalled bricks at corners of piers Crushing at corners Significant crushing spalling at corners of piers Significant toe crushing Spalling and crushing of the units at the toe Crushing of the toes No crushing or spalling of pier corners Minor crushing/spalling of pier corners Deterioration of units at bottom ends of spandrel Deterioration of units at bottom ends f spandrel Compression splitting in corner blocks | |
| | | Location of mortar crushing | |
| | | Location of cracking of bed joints and spalling | |
| | | Hairline cracks / spalled mortar in bed joints at top and bottom Hairline cracking in mortar bed at midheight of infill Hairline cracks / spalled mortar within pier Some hairline cracks along mortar courses Hairline cracking / spalled mortar in bed joints within piers Hairline cracks / spalled mortar in bed joints at top and bottom of pier Flexural cracking in the mortar beds around perimeter Horizontal hairline cracks in bed joints at the heel of the wall Horizontal cracks in bed joints at the heel of the wall Horizontal hairline cracks in bed joints at the heel of | |

Unreinforced Masonry

| Level 4 | Level 3 | Level 2 | Level 1 (Statements extracted from FEMA 306) |
|---------|---------|---------|--|
| | | | the wall |
| | | | Horizontal cracks / spalled mortar at or near the base of the wall upto 1/4" |
| | | | Horizontal cracks in bed joints |
| | | | Hairline cracks / spalled mortar in head and bed joints |
| | | | Location of cracks with various orientations |
| | | | Large diagonal or vertical cracks form at the upper corners of the wall |
| | | | Diagonal cracks form at the toe of the wall |
| | | | Small cracking may occur within the pier |
| | | | Diagonal cracking at the toe of the wall |
| | | | Large vertical or diagonal cracks at upper portions of the wall |
| | | | Diagonal cracking at the toe of the wall |
| | | | Horizontal cracks at floor/roof lines |
| | | | Series of horizontal cracks above the heel |
| | | | Horizontal flexural cracks at the top and bottom of piers |
| | | | Flexural cracking at the base of the wall |
| | | | Horizontal cracks at the top, bottom and middle of the pier |
| | | | Horizontal cracks directly below the wall diaphragm ties |
| | | | Cracks at floor/roof line and mid height |
| | | | Horizontal crack at mid-height |
| | | | Diagonally oriented cracks and minor spalling at the toe of the wall |
| | | | Diagonally oriented cracks at the upper portions of the wall |
| | | | Diagonally oriented cracks at the toe of the wall |
| | | | Flexural cracking at the heel of the wall |
| | | | Diagonally oriented cracks and spalling at the toe of the wall |
| | | | Vertical cracks at the ends of the spandrel |
| | | | Location of regional crushing |
| | | | Crushing at the corner of the infill |
| | | | Toe crushing |
| | | | Toes disintegrate |
| | | | Corner crushing in infill |
| | | | Toe crushing |
| | | | Location of falling masonry |
| | | | Portions of masonry at the edges of the pier have begun or about to fall |
| | | | Portions of masonry at the edges of the pier have begun or about to fall |

Unreinforced Masonry

| Level 4 | Level 3 | Level 2 | Level 1 (Statements extracted from FEMA 306) |
|---------|---------|---|---|
| | | | Portions of masonry at the edges of the pier have begun or about to fall |
| | | Location of spalling of face shells | Loss of corner blocks through complete spalling of face shells Faceshells spall off across a critical shear plane at midheight of infill and at corners |
| | | Location of movement of face shells | Lateral movement of face shells near corners Lateral movement of face shells near corners of infills |
| | | Mortar separation around perimeter | Separation of mortar around frame Separation of mortar around the perimeter of the panel |
| | | Crushing of mortar and bricks around perimeter | Crushing of mortar around perimeter of the frame Crushing of mortar and cracking of bricks extend over larger zones adjacent to beam and column Significant crushing of mortar and bricks along the height of the column |
| | | Movement modes of components | |
| | | Type and existence of total walking of piers | Significant out-of-plane or in-plane movement at top and bottom of piers Out-of-plane or in-plane movement at top and bottom of piers Significant out-of-plane or in-plane movement at top and bottom of piers Softening can occur due to cracking and the pier may begin to walk out of plane at top and bottom |
| | | Existence of total movement of spandrels | Some out of plane dislodgment of masonry No vertical slip of the spandrel No vertical offset of spandrel Spandrel has slipped vertically Out of plane of spandrel |
| | | Existence of partial out-of-plane movement of walls | Portions of the entire wall may walk out of plane |
| | | Existence of partial rotation of component | Spandrel rotation with respect to the pier Triangular portion of the wall above the crack rotates off the crack |

Table 6-3 Infilled frame visual damage assessment affinity diagram. Level 1 presents the statements, which were extracted from the Chapter 8 of the FEMA 306 (1999) guideline.

| Infilled Frames | | | |
|------------------------|----------------|---------------------------------------|---|
| Level 4 | Level 3 | Level 2 | Level 1 (Statements extracted from FEMA 306) |
| | | Crack properties | |
| | | Crack location | |
| | | | X-cracks in beam-column joint |
| | | | Flexural cracks at floor level (concrete columns) |
| | | | Vertical cracks at floor level |
| | | | Tensile flexural cracks at floor slab level |
| | | | Longitudinal splitting cracks around the splice |
| | | | Cracking in columns |
| | | | Flexural cracks in columns near top corner of infill |
| | | Size and extent of X-cracking | |
| | | | Column cracking over a length equal to two member widths is severe and a sign of low frame shear capacity |
| | | | Severe cracking at column ends (X-shaped) |
| | | | X-cracks in joint become more extensive and widen to 1/8" |
| | | | X-cracks in joint widen to 1/4" |
| | | | Extensive cracking in beam&column hinge zones |
| | | | Shear X cracks over a short length near column end (generally over 2 column widths) |
| | | Properties of other damage indicators | |
| | | Spalling extent and location | |
| | | | Spalling of side cover at beam-column joints |
| | | | Spalling from back of joint at exterior joints |
| | | | Cover mostly spalled around one member width away from column end |
| | | | Spalling of cover near column end |
| | | | Spalling of cover in plastic hinge of beams and columns of the frame |
| | | Fractured rebar location | |
| | | | Fractured transverse bars about one member width away from column end (middle of X crack) |
| | | Crushing location | |
| | | | Toe crushing (concrete column) over the bottom 1/2" |
| | | | Crushing of infill near the top of the column |

Appendix B. User Studies for Exploring the Differences in the Engineering Judgment for Damage Assessment

1 Introduction

This section presents the results of the user performed with researchers and engineers on rapid assessment and engineering analysis of reinforced concrete buildings. The study has three sections:

1. Rapid assessment: A virtual environment, which contains the structural walls and the damages observed on the walls were provided. The users were asked to walk inside the virtual environment and make a rapid assessment. Then they were asked to answer a set of questions, which were taken from the ATC-20 rapid assessment guideline. Participants were given 15 minutes to complete the assessment and the related questions.
2. The users were given the description of a reinforced concrete wall and they were asked to determine the damage severity of the wall. They were presented with the 18 damage parameters. This part progressed in steps:
 - a. In each step users were asked to select and view the values of 3 new parameters, which they think is the most important for determining damage severity.
 - b. After each selection they were asked to make an assessment of the damage severity.

- c. They were allowed to request new parameters until they were satisfied with their assessment.
 - d. If, after seeing a new parameter, they changed their assessment they were asked to designate the reason of the change of assessment.
 - e. They were asked to make an assessment using minimal total number of parameters.
3. The users were given the damage sketches of a solid wall and a wall with openings. They were asked to determine the potential damage modes and severities of the components.

All of the examples were adopted from the example application in Chapter 7 of FEMA 307 (1999).

2 General Information About the Participants

In order obtain information about the backgrounds and experience of the participants on damage assessment a list was provided to the users and the activities the users performed related to damage assessment was queried.

2.1 Which of the followings have you performed before?

| | | |
|---|----------|---------|
| Rapid assessment following an actual earthquake | 4 | 22 % |
| Laboratory studies on earthquake behavior of structures | 4 | 22 % |
| Analytical studies on earthquake behavior of structures | 5 | 28 % |
| Analysis and design of reinforced concrete structures | 3 | 17 % |

| | | |
|---|---|------|
| Post-earthquake damage evaluation certification (please specify in the Other box) | 2 | 11 % |
| Other | 0 | 0% |

2.2 Experience of the users

In this question, the experience of the users on damage assessment standards were asked. The users were provided with a list of available standards and asked to select the standards that they have used in the past.

2.2.1 Rapid assessment procedures

ATC21 ATC-20

2.2.2 Detailed engineering evaluation guidelines

ASCE41 FEMA 306 ASCE 41 FEMA 306, ASCE 41

2.2.3 Design guidelines

ACI 318 ts500/dbyyhy'07 TS500/DBYYHY'07 ACI 318, AISC 360, ACI 349

3 Rapid assessment

In this section, the users were provided with a virtual environment produced in a 3D modeling program. The virtual environment contained the 3D model of the case study building, which was used for validating the second and third research questions. The damages, which were obtained from hand sketched produced during the professionally performed damage assessment were superimposed on the components. Users were given 15 minutes and asked to perform a rapid assessment on the building. The results of the rapid assessment for all participants are summarized in the following sections.

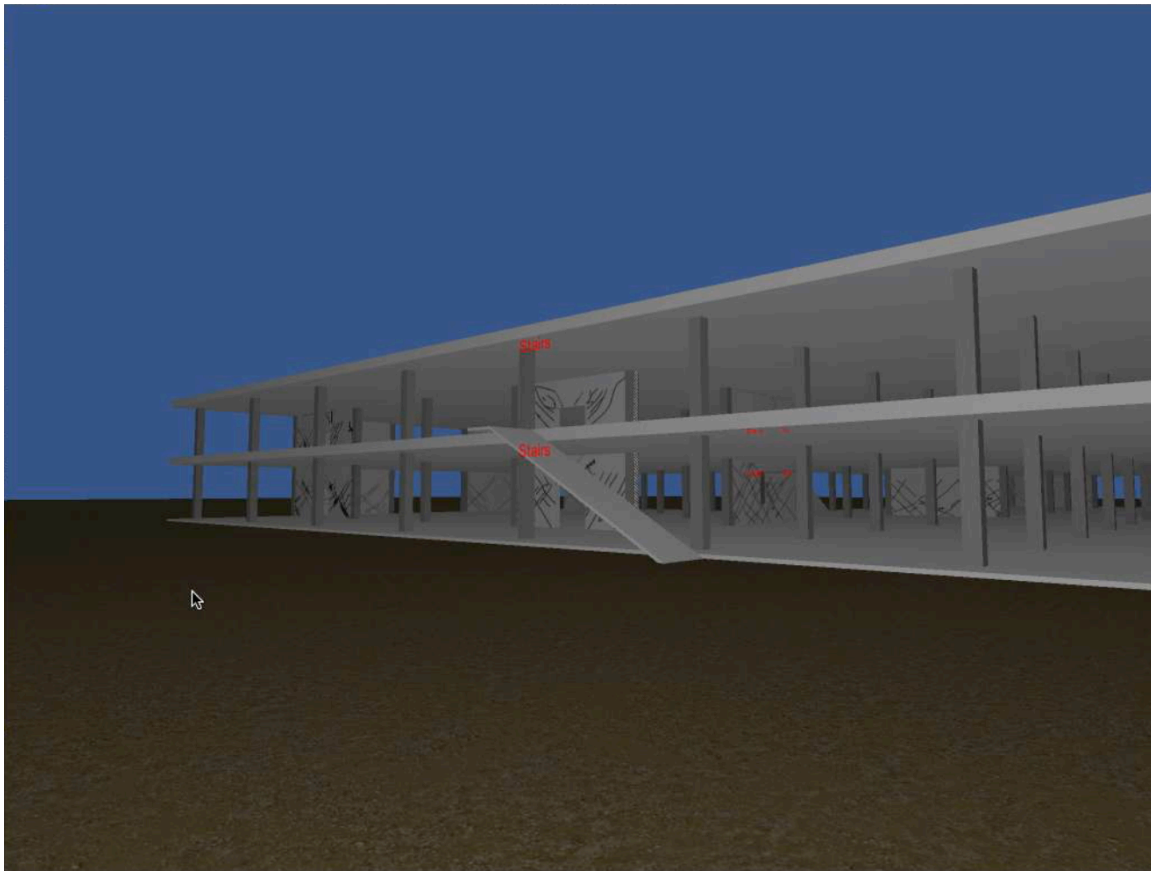


Figure 6-1 The users were given a virtual environment, where they can walk around a damaged building. The example was adopted from the example application in Chapter 7 of FEMA 307 (1999).

3.1 Building Information

3.1.1 Approximate footprint area (square meter or square feet)

The answers of the four participants out five total. One participant did not answer the question.
5440 3000 6600 m2 300 m2

3.2 Hazards

3.2.1 Collapse or Partial collapse

| | | |
|------------|---|-----|
| Minor/None | 4 | 80% |
| Moderate | 1 | 20% |
| Severe | 0 | 0% |

3.2.2 Building or Story leaning

| | | |
|------------|---|-----|
| Minor/None | 3 | 60% |
| Moderate | 2 | 40% |

Severe **0** 0%

3.2.3 Walls Damage

Minor/None **0** 0%

Moderate **2** 40%

Severe **3** 60%

Other: None

3.3 Posting

3.3.1 Estimated building damage

None **0** 0%

0-1% **0** 0%

1-10% **1** 20%

10-30% **2** 40%

30-60% **2** 40%

60-100% **0** 0%

3.3.2 Final Posting

Inspected and Safe (Green Placard) **0** 0%

Restricted Use (Yellow Placard) **3** 60%

Unsafe (Red Placard) **2** 40%

3.3.3 Entry restrictions (If the posting is Restricted)

Three participants suggested the following postings on the building.

- Can enter to conduct repairs on the walls. Not suitable for occupancy.
- Short term entry for content removal. Immediate remedy for shear cracks needs to be made.
- A possible aftershock may cause out of plane collapse of nonstructural masonry walls which all of them have moderate cracks.

4 Rapid assessments without visuals

In this section, the users were asked to perform a visual assessment without seeing the hand sketches or photographs of the damages. The goal was to evaluate the efficacy of the information requirements for representing damage, which were identified in the second research question.

The participants were given a list of damage parameters, with the values initially hidden. The users were then asked to select exactly three damage parameters, which they think are the most important. After each selected the users were shown the values of the selected parameters and asked to make an assessment. The same procedure (select parameters and make an assessment) was repeated until the participants came to a final conclusion about the severity.

Section 2 - Rapid damage assessment without the visual information

This part of the study aims at testing the effectiveness of certain damage parameters in representing the visual information, which is normally recorded using hand sketches or photographs. You will be given 18 damage parameters, which describe the damage state of a two-story flanged pier similar to the ones you evaluated earlier.

This part will progress in steps:

- * In each step you are asked to select and view the values of 3 new parameters, which you think is the most important for determining damage severity.
- * After each selection you will be asked to make an assessment of the damage severity.
- * Please keep requesting new parameters until you are satisfied with your assessment.
- * If, after seeing a new parameter, you change your assessment you will be asked to designate the reason of your change of assessment.

Please try to make an assessment using minimal total number of parameters.

When you are done with this section, click Finish & Submit and go back to the original survey for the last part.

Engin Anil - PhD Candidate, Carnegie Mellon University

Please enter your id to start (required)

yanbasan

Start

| Parameter | Value |
|---|-------------------|
| <input checked="" type="checkbox"/> Maximum Shear Crack Width | 1.02 mm |
| <input checked="" type="checkbox"/> Maximum Flexural Crack Width | < 0.8 mm |
| <input checked="" type="checkbox"/> Maximum Vertical Crack Width | No Vertical Crack |
| <input type="checkbox"/> Is there spalling? | |
| <input type="checkbox"/> Is there vertical cracking in the toe/heel of the wall? | |
| <input type="checkbox"/> What is the severity of the spalling in the web? | |
| <input type="checkbox"/> What is the severity of the spalling in the toe/heel? | |
| <input type="checkbox"/> What is the severity of sliding in the critical plane (if there is any)? | |
| <input type="checkbox"/> Is there spalling in the toe/heel? | |
| <input type="checkbox"/> Is there rebar damage in the boundary? | |
| <input type="checkbox"/> Is there crushing in the boundary? | |
| <input type="checkbox"/> Is there rebar damage? | |
| <input type="checkbox"/> What is the severity of the residual displacement? | |
| <input type="checkbox"/> Maximum shear crack width in the toe/heel | |
| <input type="checkbox"/> Maximum shear crack width in the web | |
| <input type="checkbox"/> Is there spalling in the web? | |
| <input type="checkbox"/> Is there concentrated shear cracks? | |
| <input type="checkbox"/> Is there concentrated flexural cracks? | |

[Show Selected Values](#)

^ You can move the window by holding the top bar ^

Decision time:

Based on the information you selected, please try determining the damage severity of the wall.

You can update your assessment if the new information has changed your previous decision. You can change it as many times as you want.

Click Submit when you are satisfied with your decision.

☒ Minor/None
☐ Moderate
☐ Severe
☐ No decision, yet

[Submit](#)

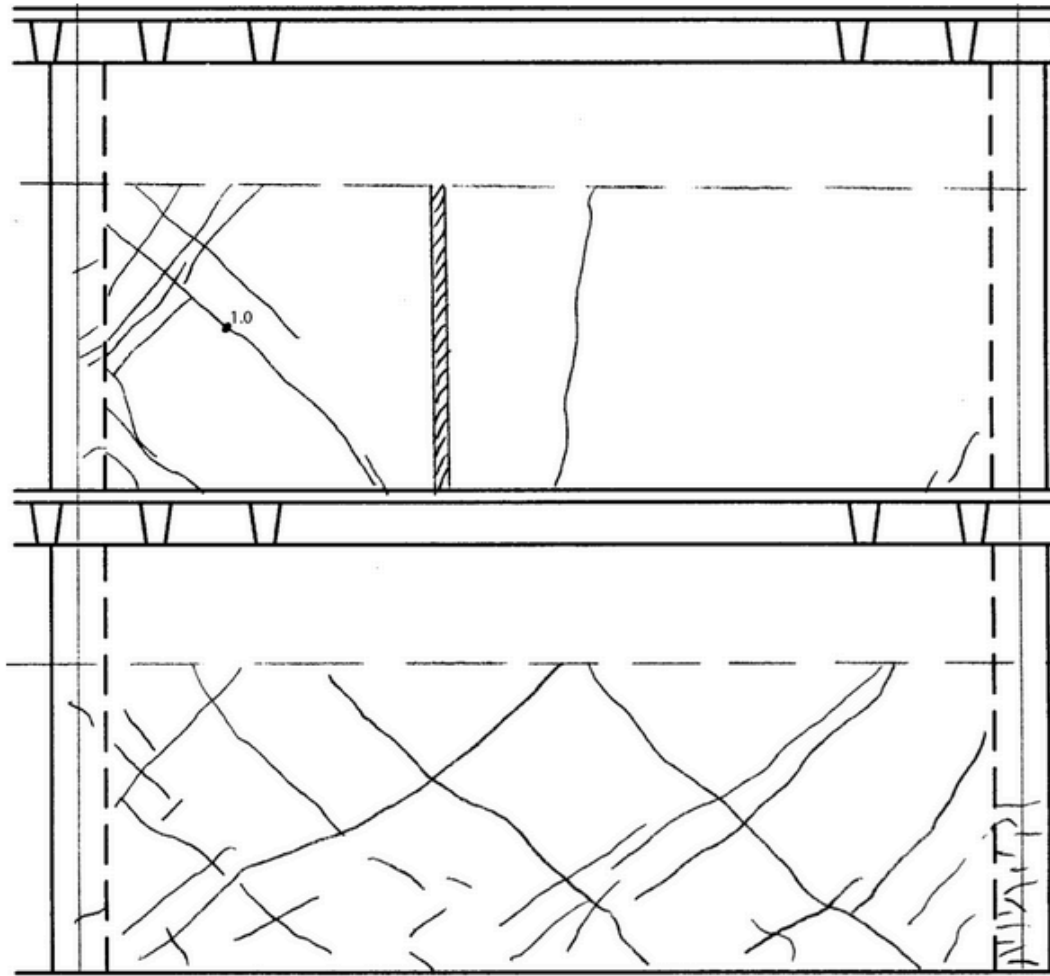
Figure 6-2 The snapshot of the user interaction window. The window first presents the 18 damage parameters without showing the values to the user and asks the user to select exactly three parameters. Upon selection, the values of the parameters are shown and the user is asked to make a decision about the severity of the damage. The user keeps asking for parameters, three at a time, until he/she is satisfied. The parameters, which affected the decision are recorded.

Table 6-4 The table shows the order in which the users asked to see the damage parameters. For example, 1 means that the corresponding parameter was seen first and 0 means that the parameter was never seen before deciding on the damage severity. The last column shows if the user changed his/her decision after seeing a certain parameter.

| Damage Parameters | User 1 | User 2 | User 3 | User 4 | User 5 | User 6 | Number of times changed the decision |
|--|----------------|---------------|---------------|----------------|---------------|---------------|---|
| Maximum Shear Crack Width, | 1 | 0 | 1 | 1 | 1 | 2 | 0 |
| Maximum Flexural Crack Width | 0 | 0 | 1 | 0 | 0 | 2 | 0 |
| Maximum Vertical Crack Width | 0 | 0 | 0 | 0 | 0 | 2 | 0 |
| Is there spalling? | 3 | 0 | 1 | 0 | 0 | 3 | 0 |
| Is there vertical cracking in the toe/heel of the wall? | 1 | 0 | 0 | 0 | 0 | 0 | 0 |
| What is the severity of the spalling in the web? | 2 | 0 | 2 | 0 | 2 | 0 | 1 |
| What is the severity of the spalling in the toe/heel? | 0 | 0 | 2 | 1 | 0 | 0 | 0 |
| What is the severity of sliding in the critical plane (if there is any)? | 0 | 1 | 2 | 2 | 0 | 0 | 0 |
| Is there spalling in the toe/heel? | 3 | 0 | 0 | 0 | 1 | 0 | 0 |
| Is there rebar damage in the boundary? | 2 | 1 | 0 | 1 | 0 | 3 | 1 |
| Is there crushing in the boundary? | 0 | 1 | 0 | 2 | 0 | 1 | 0 |
| Is there rebar damage? | 3 | 0 | 3 | 2 | 2 | 3 | 0 |
| What is the severity of the residual displacement? | 1 | 0 | 0 | 0 | 0 | 4 | 0 |
| Maximum shear crack width in the toe/heel | 0 | 0 | 0 | 0 | 0 | 4 | 0 |
| Maximum shear crack width in the web | 2 | 0 | 0 | 0 | 0 | 4 | 1 |
| Is there spalling in the web? | 0 | 0 | 3 | 0 | 1 | 0 | 1 |
| Is there concentrated shear cracks? | 0 | 0 | 3 | 0 | 0 | 1 | 0 |
| Is there concentrated flexural cracks? | 0 | 0 | 0 | 0 | 2 | 1 | 1 |
| Final decision | Minor/ None | Severe | Moderate | Minor/ None | Moderate | Moderate | |

5 Detailed Analysis of Solid Wall

In this section the participants were given a wall with openings and a solid wall. Both walls are damaged. They were asked to identify the potential damage modes and damage severities of the components (i.e., piers and spandrels) using the hand sketches. The users were provided with a list of seven damage modes and severities. They were asked to select the applicable modes and corresponding severities.



Legend:

— Crack

0.8 — Crack Width in mm

X X Crack previously filled with epoxy



Crack at pre-existing surface patch



Spall

*Widths of cracks, which are narrower than 0.8 mm are not shown

Figure 6-3 Users have been given a sketch of the damages on a solid wall and asked to determine the severities of the potential damage modes.

5.8.1 Ductile flexure [Potential damage modes]

| | | |
|----------------|---|-----|
| Not Applicable | 1 | 20% |
| Insignificant | 2 | 40% |
| Slight | 2 | 40% |
| Moderate | 0 | 0% |
| Heavy | 0 | 0% |
| Extreme | 0 | 0% |

5.8.2 Flexure/diagonal tension [Potential damage modes]

| | | |
|----------------|---|-----|
| Not Applicable | 0 | 0% |
| Insignificant | 0 | 0% |
| Slight | 2 | 40% |
| Moderate | 0 | 0% |
| Heavy | 2 | 40% |
| Extreme | 1 | 20% |

5.8.3 Flexure/diagonal compression [Potential damage modes]

| | | |
|----------------|---|-----|
| Not Applicable | 2 | 40% |
| Insignificant | 0 | 0% |
| Slight | 2 | 40% |
| Moderate | 0 | 0% |
| Heavy | 0 | 0% |
| Extreme | 1 | 20% |

5.8.4 Flexure/sliding shear [Potential damage modes]

| | | |
|----------------|---|-----|
| Not Applicable | 2 | 40% |
| Insignificant | 2 | 40% |
| Slight | 1 | 20% |
| Moderate | 0 | 0% |
| Heavy | 0 | 0% |

| | | |
|---------|---|----|
| Extreme | 0 | 0% |
|---------|---|----|

5.8.5 Flexure/boundary compression [Potential damage modes]

| | | |
|----------------|---|-----|
| Not Applicable | 1 | 20% |
| Insignificant | 3 | 60% |
| Slight | 0 | 0% |
| Moderate | 1 | 20% |
| Heavy | 0 | 0% |
| Extreme | 0 | 0% |

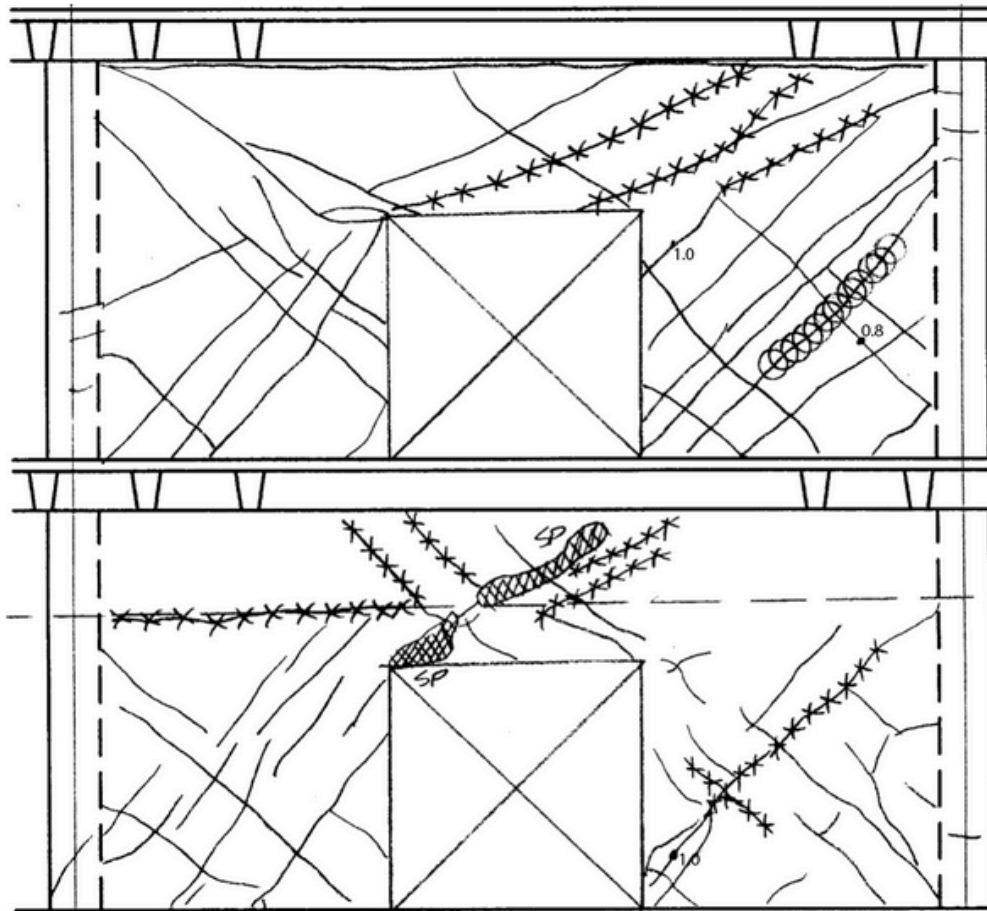
5.8.6 Pre-emptive shear [Potential damage modes]

| | | |
|----------------|---|-----|
| Not Applicable | 0 | 0% |
| Insignificant | 0 | 0% |
| Slight | 2 | 40% |
| Moderate | 1 | 20% |
| Heavy | 1 | 20% |
| Extreme | 1 | 20% |

5.8.7 Foundation rocking [Potential damage modes]

| | | |
|----------------|---|-----|
| Not Applicable | 3 | 60% |
| Insignificant | 2 | 40% |
| Slight | 0 | 0% |
| Moderate | 0 | 0% |
| Heavy | 0 | 0% |
| Extreme | 0 | 0% |

5.9 Detailed Assessment of a wall with openings



Legend:

- Crack
- 0.8 — Crack Width in mm
- ✕ ✕ Crack previously filled with epoxy
- ⊗ Crack at pre-existing surface patch
- SP Spall
- * Widths of cracks, which are narrower than 0.8 mm are not shown

Figure 6-4 The users have been given the damage sketches on a wall with openings and asked to assess the severities of potential damage modes of the piers and the coupling beams.

5.9.1 Non-linear mechanism

| | | |
|-----------------|---|-----|
| Strong Coupling | 1 | 20% |
| Weak Coupling | 4 | 80% |

5.9.2 Ductile flexure [Left Pier]

| | | |
|----------------|---|-----|
| Not Applicable | 2 | 40% |
| Insignificant | 2 | 40% |
| Slight | 1 | 20% |
| Moderate | 0 | 0% |
| Heavy | 0 | 0% |
| Extreme | 0 | 0% |

5.9.3 Flexure/diagonal tension [Left Pier]

| | | |
|----------------|---|-----|
| Not Applicable | 0 | 0% |
| Insignificant | 0 | 0% |
| Slight | 1 | 20% |
| Moderate | 1 | 20% |
| Heavy | 3 | 60% |
| Extreme | 0 | 0% |

5.9.4 Flexure/diagonal compression [Left Pier]

| | | |
|----------------|---|-----|
| Not Applicable | 1 | 20% |
| Insignificant | 0 | 0% |
| Slight | 2 | 40% |
| Moderate | 1 | 20% |
| Heavy | 1 | 20% |
| Extreme | 0 | 0% |

5.9.5 Flexure/sliding shear [Left Pier]

| | | |
|----------------|---|-----|
| Not Applicable | 2 | 40% |
| Insignificant | 2 | 40% |

| | | |
|----------|---|-----|
| Slight | 0 | 0% |
| Moderate | 1 | 20% |
| Heavy | 0 | 0% |
| Extreme | 0 | 0% |

5.9.6 Flexure/boundary compression [Left Pier]

| | | |
|----------------|---|-----|
| Not Applicable | 2 | 40% |
| Insignificant | 1 | 20% |
| Slight | 1 | 20% |
| Moderate | 0 | 0% |
| Heavy | 1 | 20% |
| Extreme | 0 | 0% |

5.9.7 Pre-emptive shear [Left Pier]

| | | |
|----------------|---|-----|
| Not Applicable | 0 | 0% |
| Insignificant | 0 | 0% |
| Slight | 1 | 20% |
| Moderate | 2 | 40% |
| Heavy | 2 | 40% |
| Extreme | 0 | 0% |

5.9.8 Foundation rocking [Left Pier]

| | | |
|----------------|---|-----|
| Not Applicable | 2 | 40% |
| Insignificant | 3 | 60% |
| Slight | 0 | 0% |
| Moderate | 0 | 0% |
| Heavy | 0 | 0% |
| Extreme | 0 | 0% |

5.9.9 Ductile flexure [Right Pier]

| | | |
|----------------|---|-----|
| Not Applicable | 2 | 40% |
| Insignificant | 3 | 60% |

| | | |
|----------|---|----|
| Slight | 0 | 0% |
| Moderate | 0 | 0% |
| Heavy | 0 | 0% |
| Extreme | 0 | 0% |

5.9.10 Flexure/diagonal tension [Right Pier]

| | | |
|----------------|---|-----|
| Not Applicable | 0 | 0% |
| Insignificant | 0 | 0% |
| Slight | 1 | 20% |
| Moderate | 1 | 20% |
| Heavy | 1 | 20% |
| Extreme | 2 | 40% |

5.9.11 Flexure/diagonal compression [Right Pier]

| | | |
|----------------|---|-----|
| Not Applicable | 1 | 20% |
| Insignificant | 1 | 20% |
| Slight | 1 | 20% |
| Moderate | 0 | 0% |
| Heavy | 1 | 20% |
| Extreme | 1 | 20% |

5.9.12 Flexure/sliding shear [Right Pier]

| | | |
|----------------|---|-----|
| Not Applicable | 2 | 40% |
| Insignificant | 2 | 40% |
| Slight | 1 | 20% |
| Moderate | 0 | 0% |
| Heavy | 0 | 0% |
| Extreme | 0 | 0% |

5.9.13 Flexure/boundary compression [Right Pier]

| | | |
|----------------|---|-----|
| Not Applicable | 2 | 40% |
| Insignificant | 2 | 40% |

| | | |
|----------|---|-----|
| Slight | 0 | 0% |
| Moderate | 0 | 0% |
| Heavy | 1 | 20% |
| Extreme | 0 | 0% |

5.9.14 Pre-emptive shear [Right Pier]

| | | |
|----------------|---|-----|
| Not Applicable | 0 | 0% |
| Insignificant | 0 | 0% |
| Slight | 1 | 20% |
| Moderate | 1 | 20% |
| Heavy | 2 | 40% |
| Extreme | 1 | 20% |

5.9.15 Foundation rocking [Right Pier]

| | | |
|----------------|---|-----|
| Not Applicable | 2 | 40% |
| Insignificant | 3 | 60% |
| Slight | 0 | 0% |
| Moderate | 0 | 0% |
| Heavy | 0 | 0% |
| Extreme | 0 | 0% |

5.9.16 Ductile flexure [Beam on the first floor]

| | | |
|----------------|---|-----|
| Not Applicable | 3 | 60% |
| Insignificant | 1 | 20% |
| Slight | 1 | 20% |
| Moderate | 0 | 0% |
| Heavy | 0 | 0% |
| Extreme | 0 | 0% |

5.9.17 Flexure/diagonal tension [Beam on the first floor]

| | | |
|----------------|---|-----|
| Not Applicable | 1 | 20% |
| Insignificant | 1 | 20% |

| | | |
|----------|---|-----|
| Slight | 0 | 0% |
| Moderate | 1 | 20% |
| Heavy | 1 | 20% |
| Extreme | 1 | 20% |

5.9.18 Flexure/diagonal compression [Beam on the first floor]

| | | |
|----------------|---|-----|
| Not Applicable | 1 | 20% |
| Insignificant | 1 | 20% |
| Slight | 0 | 0% |
| Moderate | 1 | 20% |
| Heavy | 1 | 20% |
| Extreme | 1 | 20% |

5.9.19 Flexure/sliding shear [Beam on the first floor]

| | | |
|----------------|---|-----|
| Not Applicable | 3 | 60% |
| Insignificant | 1 | 20% |
| Slight | 0 | 0% |
| Moderate | 1 | 20% |
| Heavy | 0 | 0% |
| Extreme | 0 | 0% |

5.9.20 Flexure/boundary compression [Beam on the first floor]

| | | |
|----------------|---|-----|
| Not Applicable | 4 | 80% |
| Insignificant | 0 | 0% |
| Slight | 1 | 20% |
| Moderate | 0 | 0% |
| Heavy | 0 | 0% |
| Extreme | 0 | 0% |

5.9.21 Pre-emptive shear [Beam on the first floor]

| | | |
|----------------|---|-----|
| Not Applicable | 1 | 20% |
| Insignificant | 0 | 0% |

| | | |
|----------|---|-----|
| Slight | 1 | 20% |
| Moderate | 0 | 0% |
| Heavy | 2 | 40% |
| Extreme | 1 | 20% |

5.9.22 Foundation rocking [Beam on the first floor]

| | | |
|----------------|---|------|
| Not Applicable | 5 | 100% |
| Insignificant | 0 | 0% |
| Slight | 0 | 0% |
| Moderate | 0 | 0% |
| Heavy | 0 | 0% |
| Extreme | 0 | 0% |

5.9.23 Ductile flexure [Beam on the second floor]

| | | |
|----------------|---|-----|
| Not Applicable | 3 | 60% |
| Insignificant | 1 | 20% |
| Slight | 1 | 20% |
| Moderate | 0 | 0% |
| Heavy | 0 | 0% |
| Extreme | 0 | 0% |

5.9.24 Flexure/diagonal tension [Beam on the second floor]

| | | |
|----------------|---|-----|
| Not Applicable | 1 | 20% |
| Insignificant | 0 | 0% |
| Slight | 1 | 20% |
| Moderate | 1 | 20% |
| Heavy | 2 | 40% |
| Extreme | 0 | 0% |

5.9.25 Flexure/diagonal compression [Beam on the second floor]

| | | |
|----------------|---|-----|
| Not Applicable | 2 | 40% |
| Insignificant | 1 | 20% |

| | | |
|----------|---|-----|
| Slight | 1 | 20% |
| Moderate | 0 | 0% |
| Heavy | 1 | 20% |
| Extreme | 0 | 0% |

5.9.26 Flexure/sliding shear [Beam on the second floor]

| | | |
|----------------|---|-----|
| Not Applicable | 3 | 60% |
| Insignificant | 1 | 20% |
| Slight | 1 | 20% |
| Moderate | 0 | 0% |
| Heavy | 0 | 0% |
| Extreme | 0 | 0% |

5.9.27 Flexure/boundary compression [Beam on the second floor]

| | | |
|----------------|---|-----|
| Not Applicable | 3 | 60% |
| Insignificant | 2 | 40% |
| Slight | 0 | 0% |
| Moderate | 0 | 0% |
| Heavy | 0 | 0% |
| Extreme | 0 | 0% |

5.9.28 Pre-emptive shear [Beam on the second floor]

| | | |
|----------------|---|-----|
| Not Applicable | 1 | 20% |
| Insignificant | 0 | 0% |
| Slight | 1 | 20% |
| Moderate | 2 | 40% |
| Heavy | 1 | 20% |
| Extreme | 0 | 0% |

5.9.29 Foundation rocking [Beam on the second floor]

| | | |
|----------------|---|------|
| Not Applicable | 5 | 100% |
| Insignificant | 0 | 0% |

| | | |
|----------|----------|----|
| Slight | 0 | 0% |
| Moderate | 0 | 0% |
| Heavy | 0 | 0% |
| Extreme | 0 | 0% |

Institutional Review Board

Federalwide Assurance No: FWA00004206

IRB Registration No: IRB00000603

Certification of IRB Approval

IRB Protocol Number: HS14-264
Title: Automation of the Engineering Analysis Procedures for the Determination of Post-Earthquake Seismic Capacity of Structures
Investigators: James Garrett and Engin Anil
Department: Civil and Environmental Engineering
Date: May 19, 2014

Carnegie Mellon University Institutional Review Board (IRB) reviewed the above referenced research protocol in accordance with 45 CFR 46 and CMU's Federalwide Assurance. The research protocol has been given **APPROVAL as Exempt by the IRB on May 19, 2014, in accordance with 45 CFR 46.101(b)(2).**

This approval does not expire. However, if you wish to make modifications to this protocol, please contact the IRB regarding these changes prior to their implementation to ensure compliance with this designation.

The Investigator(s) listed above in conducting this protocol agree(s) to follow the recommendations of the IRB and the Office of the Provost of any conditions to or changes in procedure subsequent to this review. In undertaking the execution of the protocol, the investigator(s) further agree(s) to abide by all CMU research policies including, but not limited to the policies on responsible conduct research and conflict of interest.

Please call the Office of Research Integrity and Compliance at 412-268-7166 if you have any questions regarding this determination. Thank you.



David Danks, Ph.D., IRB, Chair

References

1. FEMA, *FEMA 306 - Evaluation of Earthquake Damaged Concrete and Masonry Wall Buildings: Basic Procedures Manual*. 1998, FEMA: Washington, D.C.
2. Engineering, N.Z.S.f.E., *Building Safety Evaluation During a State of Emergency - Guidelines for Territorial Authorities*. 2009, Department of Building and Housing: New Zealand.
3. Hirosawa, M., S. Sugano, and T. Kaminosono, *Seismic evaluation method and restoration techniques for existing and damaged buildings developed in Japan*, in *Intl. Symp. on Earthquake Disaster Reduction Technologies*. 1992: Tsukuba, Japan. p. 373-397.
4. Kempton, K., et al., *Surveyor variability in large-scale house condition surveys*. *Structural Survey*, 2001. **19**(4): p. 156-162.
5. Phares, B.M., et al., *Reliability of visual bridge inspections*. *Public Roads*, 2001. **64**(5).
6. Graybeal, B.J.P., B. M.; Rolander D. D.; Moore, M., *Visual Inspection of Highway Bridges*. *Journal of Nondestructive Testing*, 2002. **21**(3): p. 67-83.
7. Park, H.S., et al., *A new approach for health monitoring of structures: terrestrial laser scanning*. *Computer aided civil and infrastructure engineering*, 2007. **22**: p. 19-30.
8. Tang, P., D. Huber, and B. Akinci, *Characterization of Laser Scanners and Algorithms for Detecting Flatness Defects on Concrete Surfaces*. *Journal of Computing in Civil Engineering*, 2011. **25**(1): p. 31-31.
9. Olsen, M.J., et al., *Terrestrial Laser Scanning-Based Structural Damage Assessment*. *Journal of Computing in Civil Engineering*, 2009. **24**(3): p. 264-72.
10. Tang, P., et al., *Automatic reconstruction of as-built building information models from laser scanned point clouds: A review of related techniques*. *Automation in Construction*, 2010. **19**(7): p. 829-843.
11. Zeibak-Shini, R., R. Sacks, and S. Filin, *Toward generation of a building information model of a deformed structure using laser scanning technology*, in *ICCCBE*. 2012: Russia.
12. Anil, E.B., et al., *Representation of damage information for post-earthquake damage assessment of reinforced concrete frames*, in *ASCE International Workshop on Computing in Civil Engineering*. 2013: Los Angeles.
13. Anil, E.B., G. Unal, and O. Kurc, *Information requirements for design and detailing of reinforced concrete frames in multiuser environments*. *Journal of Computing in Civil Engineering*, 2012. **26**(4): p. 465-477.
14. Paul, N. and A. Borrmann, *Geometrical and topological approaches in building information modeling*. *ITCON*, 2009. **14**.
15. Tuley, J., N. Vandapel, and M. Hebert. *Analysis and Removal of Artifacts in 3-D LADAR Data*. in *IEEE International Conference on Robotics and Automation*. 2005.
16. Hebert, M. and E. Krotkov. *3D measurements from imaging laser radars: how good they are?* 1991. Osaka, Japan.
17. Tang, P., B. Akinci, and D. Huber, *Quantification of edge loss of laser scanned data at spatial discontinuities*. *Automation in Construction*, 2009. **18**(8): p. 1070-1083.
18. Lichti, D.D. and S. Jamtsho, *Angular resolution of terrestrial laser scanners*. *Photogrammetric Record*, 2006. **21**(114): p. 141-160.
19. Yasaka, A., et al., *The development of the reinforced-concrete structural model on IFC specification*, in *Joint International Conference on Computing and Decision Making in Civil and Building Engineering*. 2006: Montreal, Canada.
20. Weise, M.K., Peter; Liebich, Thomas; Sherer, Raimar J., *Structural analysis extension of the IFC modeling framework*. *ITCon*, 2003. **8**.
21. BuildingSmart, *Industry Foundation Classes (IFC)*. 2013.
22. Barak, R., et al., *Unique requirements of building information modeling for cast-in-place reinforced concrete*. *Journal of Computing in Civil Engineering*, 2009. **23**(2): p. 64-74.
23. Anil, E.B., et al., *Deviation analysis method for the assessment of the quality of the as-is Building Information Models generated from point cloud data*. *Automation in Construction*, 2013. **35**: p. 507-516.

24. Fischer, M., F. Aalamin, and R. Akbas, *Formalizing product model transformations: Case examples and applications*, in *Artificial Intelligence in Structural Engineering*, I. Smith, Editor. 1998, Springer Berlin Heidelberg. p. 113-132.
25. FEMA, *FEMA 307 - Evaluation of Earthquake Damaged Concrete and Masonry Wall Buildings: Technical Resources*. 1998, FEMA: Washington, D.C.
26. Menches, C.L., A.B. Markman, and R.J. Jones. *Innovative Method for Investigating the Facility Damage Assessment Process*. 2008. Denver, Colorado.
27. Abdel-Qader, I., O. Abudayyeh, and M.E. Kelly, *Analysis of edge-detection techniques for crack identification in bridges*. Journal of Computing in Civil Engineering, 2003. **17**(4): p. 255-263.
28. Yu, S.-N., J.-H. Jang, and C.-S. Han, *Auto inspection system using a mobile robot for detecting concrete cracks in a tunnel*. Automation in Construction, 2007. **16**: p. 255-261.
29. Mraz, A., M. Gunaratne, and A. Nazef, *Guidelines for performance assessment of digital imaging systems used in highway applications*. Journal of Transportation Engineering, 2005. **131**(6): p. 429-443.
30. Boehler, W. and A. Marbs. *Investigating Laser Scanner Accuracy*. 2003 [cited December 2, 2013; Available from: http://hds.leica-geosystems.com/hds/en/Investigating_Accuracy_Mintz_White_Paper.pdf.
31. Chen, L.-C., et al., *Measuring system for cracks in concrete using multitemporal images*. Journal of Surveying in Civil Engineering, 2006. **132**(2): p. 77-82.
32. Chen, Z.Q. and T.C. Hutchinson, *Image-based framework for concrete surface crack monitoring*. Advances in Civil Engineering, 2010: p. 18.
33. Laefer, D.F., et al., *Lateral image degradation in terrestrial laser scanning*. Structural engineering international, 2009. **19**(2): p. 184-189.
34. Laefer, D.F., J. Gannon, and E. Deely, *Reliability of Crack Detection Methods for Baseline Condition Assessments*. Journal of Infrastructure Systems, 2010. **16**(2): p. 129-129.
35. Lecompte, D., J. Vantomme, and H. Sol, *Crack detection in a concrete beam using two different camera techniques*. Structural Health Monitoring, 2006. **5**(1): p. 59-68.
36. Yamaguchi, T., et al., *Image-based crack detection for real concrete surfaces*. Transactions on electrical and electronic engineering IEEEJ, 2008. **3**: p. 128-135.
37. Zhu, Z. and I. Brilakis, *Concrete column recognition in images and video*. Journal of Computing in Civil Engineering, 2010. **24**(6): p. 478-487.
38. Zhu, Z., S. German, and I. Brilakis, *Visual retrieval of concrete crack properties for automated post-earthquake structural safety evaluation*. Automation in Construction, 2011. **20**: p. 874-883.
39. Kamat, V.R. and S. El-Tawil, *Evaluation of augmented reality for rapid assessment of earthquake-induced building damage*. Journal of Computing in Civil Engineering, 2007. **21**(5): p. 303-310.
40. Mehrabi, A., et al., *Experimental evaluation of masonry -infilled RC frames*. Journal of Structural Engineering, 1996. **122**(3): p. 228-237.
41. Reichenbach, S.E., S.K. Park, and R. Narayanswamy, *Characterizing digital image acquisition devices*. Optical Engineering, 1991. **30**(2): p. 170-177.
42. Park, S.K., R. Schowengerdt, and M.-A. Kaczynski, *Modulation-transfer-function analysis for sampled image systems*. Applied Optics, 1984. **23**(15): p. 2572-2582.
43. A., M.A.G.M.N., *Guidelines for performance assessment of digital imaging systems used in highway applications*. Journal of Transportation Engineering, 2005. **131**(6): p. 429-443.
44. Abdel-Qader, I.A., Osama; Kelly, Michael E., *Analysis of edge-detection techniques for crack identification in bridges*. Journal of Computing in Civil Engineering, 2003. **17**(4): p. 255-263.
45. Yamaguchi, T.N., Shingo; Saegusa, Ryo; Hashimoto, Shuji, *Image-based crack detection for real concrete surfaces*. Transactions on electrical and electronic engineering IEEEJ, 2008. **3**: p. 128-135.
46. Matthew M. Torok, M.G.-F., Kevin B. Kochersberger, *Image-based automated 3D crack detection for post-disaster building assessment*. Journal of Computing in Civil Engineering, 2013. **Accepted manuscript**.
47. Chen, L.-C.S., Yi-Chen; Jan, Huang-Hsiang; Huang, Chen-Wei; Tien, Yong-Ming, *Measuring system for cracks in concrete using multitemporal images*. Journal of Surveying in Civil Engineering, 2006. **132**(2): p. 77-82.

48. Chen, Z.H., Tara C., *Image-based framework for concrete surface crack monitoring*. Advances in Civil Engineering, 2010: p. 18.
49. Zhenhua Zhu, S.G., Ioannis Brilakis, *Visual retrieval of concrete crack properties for automated post-earthquake structural safety evaluation*. Automation in Construction, 2011. **20**: p. 874-883.
50. Eric K. Forkuo, B.K., *Automatic fusion of photogrammetric imagery and laser scanner point clouds*. International Archives of Photogrammetry and Remote Sensing vol. XXXV part B4, 2005: p. 921-926.
51. Goesele, M., C. Fuchs, and H.P. Seidel. *Accuracy of 3D range scanners by measurement of the slanted edge modulation transfer function*. 2003.
52. MacKinnon, D., et al. *Evaluating laser range scanner lateral resolution in 3D metrology*. 2009.
53. Lichti, D.D. and B.R. Harvey, *The effects of reflecting surface material properties on time-of-flight laser scanner measurements*, in *ISPRS Symposium on Geospatial Theory, Processing and Applications*. 2002: Ottawa.
54. Geosystems, L. *Leica Scan Station 2 Data Sheet*. 2007 [cited December 2, 2013; Available from: http://hds.leica-geosystems.com/en/Leica-ScanStation-2_62189.htm].
55. Zoller+Fröhlich, Z+F Imager 5003 Technical Specification. 2005.
56. Fischler, M. and R. Bolles, *Random sampling consensus: a paradigm for model fitting with applications to image analysis and automated cartography*. Communications of the ACM, 1981. **24**(6): p. 381-395.
57. Yi-Chang Tsai, C.J., Yuchun Jiang, *A multi-scale crack fundamental element model for real-world pavement crack classification*. Journal of Computing in Civil Engineering, 2012. **Accepted manuscript**.
58. H. N. Koutsopoulos, A.B.D., *Primitive-based classification of pavement cracking images*. Journal of Transportation Engineering, 1993. **119**(3): p. 402-418.
59. Rumbaugh, J., *Object-oriented modeling and design*. 1991: Prentice Hall.
60. ATC-20, *Procedures for postearthquake safety evaluations of buildings*. 1989, Applied Technology Council (ATC): Redwood City, CA.
61. ATC-21, *Rapid Visual Screening of Buildings for Potential Seismic Hazards: A Handbook*. 2002, Applied Technology Council (ATC): Redwood City, CA.
62. ASCE, *Seismic rehabilitation of existing buildings*. 2006, American Society of Civil Engineers: Reston, Virginia.
63. Anil, E.B., B. Akinci, and D. Huber, *Representation requirements of as-is building information models generated from laser scanned point cloud data*, in *ISARC 2011*. 2011: Seoul, S. Korea.
64. Melchor-Lucero, O. and C. Ferregut, *Earthquake damage assessment of reinforced concrete members using an expert system*, in *Eleventh World Conference on Earthquake Engineering*. 1996: Acapulco, Mexico.
65. Mackerle, J., *Object-oriented programming in FEM and BEM: a bibliography (1990-2003)*. Advances in Engineering Software, 2004. **35**(6): p. 325-336.
66. Celes, W., G.H. Paulino, and R. Espinha, *A compact adjacency-based topological data structure for finite element mesh representation*. International Journal for Numerical Methods in Engineering, 2005. **64**: p. 1529-1556.
67. Forde, B.W.R., R.O. Foschi, and S.F. Stierner, *Object-oriented finite element analysis*. Computers and Structures, 1990. **34**(3): p. 355-374.
68. Turk, Z., T. Isakovic, and M. Fischinger, *Object oriented modeling of design system for RC buildings*. Journal of Computing in Civil Engineering, 1994. **4**(4): p. 436-453.
69. Beyer, H.H., Karen, *Contextual design: Defining customer-centered systems*. 1998, San Francisco, CA: Morgan Kaufmann Publishers. 472.
70. FEMA, *FEMA 306 - Evaluation of Earthquake Damaged Concrete and Masonry Wall Buildings: Basic Procedures Manual*. 1998, Washington, D.C.: FEMA.
71. Mehrabi, A.S., Benson; Schuller, Michael; Noland, James L., *Experimental evaluation of masonry -infilled RC frames*. Journal of Structural Engineering, 1996. **122**(3): p. 228-237.
72. Pilakoutas, K.E., Amr, *Cyclic Behavior of Reinforced Concrete Cantilever Walls - Part I - Experimental Results*. ACI Structural Journal, 1995. **92**(3): p. 271-281.
73. Perera, R., *Performance evaluation of masonry-infilled RC frames using loading based on damage mechanics*. Engineering Structures, 2005. **27**: p. 1278-1288.

74. Anil, E.B., et al., *Characterization of laser scanners for detecting cracks for post-earthquake damage inspection*, in *ISARC 2013*. 2013: Montreal, Canada.
75. German, S., et al., *Machine vision enhanced post-earthquake inspection*. *Journal of Computing in Civil Engineering*, 2013. **Accepted Manuscript**.
76. Borrmann, A. and E. Rank, *Topological analysis of 3D Building Models using a Spatial Query Language*. *Advanced Engineering Informatics*, 2009. **23**(4): p. 370-385.
77. GSA, *BIM Guide for 3D Imaging*. 2009, General Services Administration.
78. Eastman, C.M., et al., *BIM Handbook: A Guide to Building Information Modeling for Owners, Managers, Designers, and Contractors*. 2008, Hoboken, NJ: John wilye and Sons, Inc.
79. Lee, G., C. Eastman, and R. Sacks, *Twelve design patterns for integrating and normalizing product model schemas*. *Computer aided civil and infrastructure engineering*, 2007. **22**.
80. (ACI), A.C.I., *ACI 318-11 Building code requirements for structural concrete and commentary*. 2011: Farmington Hills, MI, USA.
81. Beghini, L.L., et al., *An object-oriented framework for finite element analysis based on a compact topological data structure*. *Advances in Engineering Software*, 2014. **68**: p. 40-48.
82. Crowley, A.J. and A.S. Watson, *CIMsteel Integration Standards Release 2*. 2000: American Institute for Steel Construction.
83. Tauscher, E. and M. Theiler. *IFC Tools Project*. 2014 [cited December 2014; Available from: <http://www.ifctoolsproject.com>].